UC Irvine

UC Irvine Electronic Theses and Dissertations

Title

Catalytic Control of Cytochrome P450

Permalink

https://escholarship.org/uc/item/5hh6r2b1

Author

Gable, Jessica A

Publication Date

2023

Peer reviewed|Thesis/dissertation

eScholarship.org Powered by the California Digital Library
University of California

UNIVERSITY OF CALIFORNIA,
IRVINE

Catalytic Control of Cytochrome P450

DISSERTATION

Submitted in partial satisfaction of the requirements
for the degree of

DOCTOR OF PHILOSOPHY

in Chemistry

by

Jessica A. Gable

Dissertation Committee:
Professor Thomas L. Poulos, Chair
Professor Andrew S. Borovik
Professor Michael T. Green

2023

Chapter 2 © 2023 American Chemical Society
Chapter 3 © 2023 Elsevier Inc.
Chapter 6 © 2022 American Chemical Society
All other materials © 2023 Jessica A. Gable

DEDICATION

to my mom and Zookie

TABLE OF CONTENTS

	Page
LIST OF FIGURES	iv
LIST OF TABLES	vii
LIST OF SCHEMES	viii
LIST OF EQUATIONS	ix
ACKNOWLEDGEMENTS	x
VITA	xi
ABSTRACT OF THE DISSERTATION	xiii
CHAPTER 1: Introduction to Cytochrome P450	1
CHAPTER 2: Cooperative Substrate Binding Controls Catalysis in Bacterial Cytochrome P450terp (CYP108A1)	16
CHAPTER 3: Redox Partner Recognition and Selectivity of Cytochrome P450lin (CYP111A1)	65
CHAPTER 4: Redox Partner Recognition and Selectivity of Cytochrome P450terp (CYP108A1)	98
CHAPTER 5: Proximal Push of Proline in CYP158A2	116
CHAPTER 6: Structural Insights on the Conversion of Cytochrome P450 to P420	129
CHAPTER 7: Conclusion	138

LIST OF FIGURES

Page

Figure 1-1. UV-vis spectra of P450s 2

Figure 1-2. Overall P450 fold and structure 3

Figure 1-3. Open and close transition of P450cam 4

Figure 1-4. P450 catalysis 6

Figure 1-5. The flow of electrons in a Class I P450 system 7

Figure 1-6. Various structural conformations of P450cam 8

Figure 2-1. Crystal structure of P450terp 20

Figure 2-2. Active site of P450terp WT substrate free 21

Figure 2-3. Comparison of two molecules in active sites 23

Figure 2-4. Residues contacting substrate molecules 24

Figure 2-5. Rotation of F188 25

Figure 2-6. Active site mutations 26

Figure 2-7. Crystal structure of P450terp F188A 26

Figure 2-8. Absorbance spectra of P450terp variants 28

Figure 2-9. Absorbance spectra of P450terp F188A 29

Figure 2-10. Absorbance spectra of reduced and carbon monoxide bound P450terp variants 31

Figure 2-11. Spectral titration data expanded 35

Figure 2-12. Double reciprocal and logarithmic plots of spectral titration data 37

Figure 2-13. ITC data 39

Figure 2-14. ITC of P450terp F188A without the adjusted baseline 41

Figure 2-15. NADH consumption spectral traces 43

Figure 2-16. NADH coupling chromatograms with the 4 variants 44

Figure 2-17. Mass spectra of the NADH coupling assays 45

Figure 2-18. Differences in tubes for NADH coupling 46

Figure 2-19. Spectral change of P450terp upon addition of linalool 47

Figure 2-20. NADH consumption assay of P450terp with linalool 47

Figure 2-21. Linalool bound in the active site of P450terp 48

Figure 2-22. P450terp Asp270 55

Figure 3-1. Ferredoxin sequence alignment 68

Figure 3-2. NADH traces at 340 nm for the consumption assays 69

Figure 3-3. Chromatogram of DCM in plastic and extraction of reaction mixture in DCM in plastic 71

Figure 3-4. Chromatograms of reaction extractions 72

Figure 3-5. Mass spectra of camphor, linalool, and product from reaction mixtures 73

Figure 3-6. UV-vis spectra of the P450 spin-shift in the presence of redox partner 75

Figure 3-7. Stopped-flow kinetics of P450lin oxycomplex decay 78

Figure 3-8. Stopped-flow spectra and difference spectra 79

Figure 3-9. Structural alignment of P450cam and P450lin 82

Figure 3-10. Structural alignment of residues involved in ferredoxin binding 84

Figure 3-11. P450 sequence alignment 85

Figure 3-12. Crystals of P450lin 88

Figure 3-13. Sequence alignment of the P450lins from *Pseudomonad* and *Acinetobacter* 90

Figure 3-14. Sequence alignment of the Ldx from *Pseudomonad* and *Acinetobacter* 90

Figure 3-15. Sequence alignment of the LdRs from *Pseudomonad* and *Acinetobacter* 90

Figure 4-1. Sequence alignment of Arx, Pdx, and Tdx 99

Figure 4-2. NADH consumption traces of P450terp with various redox partners 101

Figure 4-3. NADH coupling chromatograms 103

Figure 4-4. Stopped-flow spectra and kinetics of oxycomplex decay of P450terp 104

Figure 4-5. Stopped-flow spectra and kinetics of oxycomplex decay of P450terp with Tdx 105

Figure 4-6. Stopped-flow spectra and kinetics of oxycomplex decay of P450terp with Tdx E39L 105

Figure 4-7. Stopped-flow spectra and kinetics of oxycomplex decay of P450terp with Arx 106

Figure 4-8. Stopped-flow spectra and kinetics of oxycomplex decay of P450terp with Pdx 106

Figure 4-9. Crystal structure of Tdx C44S 108

Figure 4-10. P450terp and Tdx docking results compared to the P450cam-Pdx complex 110

Figure 5-1. Proximal push in P450cam 117

Figure 5-2. Crystal structure of 158A2 P354L substrate-free 120

Figure 5-3. Crystal structure of 158A2 P354L substrate-bound 121

Figure 5-4. UV-vis spectra of CYP158A2 WT and P354L 122

Figure 5-5. Generation of Compound II in CYP158A2 123

Figure 5-6. Kinetics of Compound II formation in CYP158A2 124

Figure 6-1. Crystal structure of the P450cam-Pdx complex1 130

Figure 6-2. P450cam-Pdx complex1 bound to carbon monoxide 131

Figure 6-3. Comparison of complex1 and complex2 132

Figure 6-4. P450cam histidine residues 133

Figure 6-5. UV-vis spectra of P450cam WT and variants in the reduced-CO form 134

LIST OF TABLES

Page

Table 2-1. Crystallographic data collection and refinement statistics of P450terp 18

Table 2-2. Residues interactions with substrate molecules 24

Table 2-3. Table of K_s and maximal high spin percentages for the four P450terp variants 29

Table 2-4. Binding affinities of P450terp WT and F188A for α-terpineol 37

Table 2-5. NADH turnover rates and coupling efficiencies for P450terp variants 43

Table 2-6. Crystallographic data collection and refinement statistics of P450terp bound to linalool 49

Table 2-7. Primers for mutagenesis 57

Table 3-1. NADH consumption assay rates for P450lin and P450cam 68

Table 3-2. P450lin oxycomplex decay rates from stopped-flow kinetics 77

Table 4-1. NADH turnover rates and coupling efficiencies for P450terp with various ferredoxins 102

Table 4-2. P450terp oxycomplex decay rates from stopped-flow kinetics 106

Table 4-3. Statistics for data collection and refinement of Tdx C44S 107

Table 5-1. Crystallographic data collection and refinement statistics of CYP158A2 P354L substrate-free and substrate-bound 119

LIST OF SCHEMES

Page

Scheme 2-1. The net reaction of the P450terp system 18

Scheme 3-1. The hydroxylation of linalool to 8-oxo-linalool as catalyzed by the P450lin system 67

Scheme 3-2. Preparation and oxidation of the ferrous-O_2, oxycomplex 76

LIST OF EQUATIONS

Page

Equation 2-1. One-Site Binding Model 38

Equation 2-2. Two-Site Binding Model 38

Equation 2-3. Specific Binding Model with a Hill Coefficient 38

Equation 3-1. Monoexponential 77

Equation 3-2. Biexponential 77

ACKNOWLEDGEMENTS

The first person I want to thank is Professor Thomas L. Poulos, who has been an amazing advisor throughout the years. I was a late bloomer in grad school, but your support has been constant. I learned so much in your lab, and I feel prepared for whatever comes next.

I want to thank my committee members, Professors Andy Borovik and Michael Green. I learned so much in your classes, and the various ways in which I popped in and out of your labs.

It is not an understatement to say that I wouldn't be where I was without Alec Follmer. You trained me in the beginning on the basics of P450 research (although I will never do an ammonium sulfate fractionation again). You graduated, and I learned a few things in your absence. You returned, and now we can actually do an experiment correctly the first time! Amazing. Thank you so much for helping with the papers, which would have a struggle without you.

José, your time in the lab was brief but so impactful. You came in and immediately started helping out us clueless grad students. You showed me how to work the stopped-flow, which at the time scared me so much.

Christine, I love talking with you and how you bring a levelheadedness to the lab that is so refreshing. This is basically my first job, so I didn't know how anything is supposed to go, and it is so nice to get a grounded opinion on academia and industry work.

I want to thank Drs. Irina Sevrioukova and Huiying Li. You two basically kept the lab running after Joumana left and I'm sure there is more you have taken care of that I don't even know about.

I would also like to thank my advancement committee: Profs. Andy Borovik (again), Mike Green (again), Jenny Yang, Elizabeth Bess, and Reginald McNulty. Although not on my committee(s), I want to thank Celia Goulding for encouraging me to come to UCI in the first place and for always chit-chatting in the hallway.

Thank you to past and present Poulosians: Vidhi Murarka, Oanh Tran, Jenny Kim, Sayanna Are, Matt Lewis, and my undergrads Negar Mojgani and Christian Dela Cruz.

And now for the personal stuff... thank you so much to my mom, who put up with me complaining about stuff that didn't even make sense, for so many reasons. Thank you for taking care of my little, stupid dog (yeah yeah it worked out for the best or whatever).

Thank you to all of my various friend groups, both close and far. Josselyn, alive girl, I know how much you love being called that. We really gotta work on aligning our career paths so we are in the same city again. Emily and Vivian, thank you for all the serious conversations and dumb jokes over the years. Nalini, Maryam, and Marilynn – we've all come so far, and we will continue to go far (riding Nalini's coattails). Amy, Inji, and Cyrus, you three are the reason I gotta be careful when checking my phone. You keep me on my toes, and no matter what degree I get I know there will be people wittier than me. I want to thank horror movies, which was a surprising personal development, and they give me something to actually be scared of (and not scared of stopped-flow). Thank you to Andrew Hozier-Byrne, who I believe released his 3rd album just for me, as a reward for writing my thesis. If you are still reading this, go listen to Unreal Unearth – you're welcome.

Finally, I acknowledge the American Chemical Society and Elsevier Inc. for permission to include aspects of my published works in chapters 2, 3, and 6. Financial support was provided by NIH grant GM57353 (T.L.P.). Also, I would like to thank the staff at the Stanford Synchrotron Radiation Lightsource (SSRL) and Berkeley's Advanced Light Source (ALS) for their resources and assistance in carrying out crystallographic experiments.

VITA

EDUCATION

Massachusetts Institute of Technology (MIT) **Cambridge, MA**
Bachelor of Science in Chemistry and Literature June 9, 2017
Cumulative GPA: 4.7/5.0

University of California, Irvine **Irvine, CA**
Ph.D. Candidate in Chemistry September 2023
Cumulative GPA: 3.969/4.0

RESEARCH EXPERIENCE

Undergraduate Researcher **September 2014 – June 2017**
Drennan Lab MIT

- Learned the basics of protein expression and purification, and X-ray crystallography
- Focused on non-heme iron enzymes and cobalamin-containing metalloproteins

Graduate Student Researcher **September 2017 – September 2023**
Poulos Lab UCI

- Investigated several bacterial P450s, namely P450cam, P450terp, and P450lin
- Centered work around structure-function relationships between substrate, redox partner, and P450

SKILLS

Software: Phenix, Coot, Pymol, Prism, ProDataSX, Illustrator, Chromeleon, MATLAB
Benchwork: protein X-ray crystallography, stopped flow kinetics, UV-vis spectroscopy, mass spectrometry, protein expression and purification, mutagenesis

CONFERENCES AND PRESENTATIONS

SoCal Bioinorganic Chemistry Conference Caltech, CA; December 8, 2018

- Presented a poster about the interactions between P450terp and its natural ferredoxin redox partner, Tdx

West Coast Structural Biology Workshop Asilomar,CA; March 17-20, 2019

- Attended presentations and workshops

International Conference on Cytochrome P450 Washington D.C.; July 17-22,2022

- Gave a talk and presented a poster about the expanded interactions between P450terp, its natural substrate, and its redox partner Tdx

PUBLICATIONS

Structural Insights on the Conversion of Cytochrome P450 to P420
ACS Omega 2022, 7, 22, 18481–18485
doi: https://doi.org/10.1021/acsomega.2c00960

Cooperative Substrate Binding Controls Catalysis in Bacterial Cytochrome P450terp (CYP108A1)
J. Am. Chem. Soc. 2023, 145, 7, 4254–4265
doi: https://doi.org/10.1021/jacs.2c12388

Redox partner recognition and selectivity of cytochrome P450lin (CYP111A1)
J. Inorg. Biochem. 2023, 244, 112212,
doi: https://doi.org/10.1016/j.jinorgbio.2023.112212

MANUSCRIPTS IN PREPARATION

Gable, J. A., Follmer, A. H., Poulos, T. P. "Redox Partner Recognition and Selectivity of Cytochrome P450terp (CYP108A1)"

Gable, J. A., Follmer, A. H., Poulos, T. P. "Redox Partner Recognition and Selectivity of Cytochrome P450terp (CYP108A1) "Proximal Push of Proline in CYP158A2

TEACHING

Introduction to Chemical Biology Laboratory Techniques **Winter 2018**
Teaching Assistant UCI
Instructor: Jennifer Prescher

General Chemistry Laboratory **Spring 2018**
Teaching Assistant UCI
Instructor: Kimberly Edwards

General Chemistry Laboratory **Spring 2019**
Teaching Assistant UCI
Instructor: Kimberly Edwards

General Chemistry Laboratory **Spring 2021**
Teaching Assistant UCI
Instructor: Kimberly Edwards

ABSTRACT OF THE DISSERTATION

Catalytic Control of Cytochrome P450

By

Jessica A. Gable

Doctor of Philosophy in Chemistry

University of California, Irvine, 2023

Professor Thomas L. Poulos, Chair

Cytochromes P450 (P450s) are heme-containing monooxygenases that catalyze a variety of reactions, such as hydroxylation, epoxidation, and C–C bond breakage. Significant efforts have gone into the study of the catalytic cycle, in which high-valent intermediates are generated under physiological conditions to break unactivated C–H bonds. The various forms of regulation of the catalytic cycle required to ensure catalysis proceeds only under the appropriate physiological conditions are diverse and less well understood. For example, regulation is important in order to avoid wasting otherwise valuable reducing equivalents, preventing high-valent intermediates from degrading the protein, and/or preventing the release of reactive oxygen species. This thesis focuses on a few regulatory aspects of the catalytic cycle. One such aspect is substrate binding in a bacterial P450, named P450terp, after the substrate α-terpineol. The crystal structure of P450terp reveals a second substrate binding site. Substrate binding studies reveal that this second binding site is important for binding of substrate in the first binding site and turnover assays show that the second substrate binding site is necessary for efficient catalysis. Another aspect of regulation is the binding of the protein redox partner, in what has historically been called the effector role. I focus on *Pseudomonad* P450s, since their similar biological roles might lead to similar structure function relationships. Studies on P450terp and P450lin, named after the substrate linalool, reveal that they are promiscuous, able to turnover substrate with an exogenous

protein redox partner. While this marks a difference from the model *Pseudomonad* system, there is a consistency in the effector role of the protein redox partner that is shared by many P450s. In all P450s that utilize a protein redox partner studied thus far, binding of the redox partner results in structural changes in the P450, as evidenced by an increase in the decay of an intermediate in the catalytic cycle called the oxycomplex. Besides these two external forms of regulation, I also look into the effects of mutating residues in the active site. One such example is mutation of the residue immediately following the cysteine residue ligating the heme in an investigation into a "proximal push" that might mimic redox partner binding and possible effects on the stability of high-valent intermediates in the catalytic cycle. Another example is the mutation of certain residues in an investigation of the origin of the P420 species, which is considered to be an inactivated, damaged P450 incapable of performing catalysis. Together, all of these studies have advanced our understanding of regulation of the P450 catalytic cycle.

Chapter 1

Introduction to Cytochrome P450

Cytochromes P450 (P450s) are a class of heme-containing monooxygenases that catalyze a broad range of reactions, such as hydroxylation, C–C bond formation and cleavage, and epoxidation, to name a few.[1] P450s are ubiquitous thorough the biosphere and important in human health with 70-80% of drugs on the market interacting with a P450 in the liver, and about a third of those interact with one isoform.[2] The chemistry of P450s is powered by a heme cofactor that is attached to the protein through ligation to a thiolate of a cysteine amino acid residue (Figure 1-1A). Due to the thiolate-ligated heme cofactor, P450s have a unique UV-vis profile that provides a valuable spectroscopic handle (Figure 1-1B). In fact, P450 stands for pigment 450, which refers to the λ_{max} of the most intense feature, called the Soret, when the heme is bound to carbon monoxide (CO).[3] Historically, this band at 450 nm was important for the isolation and characterization of the enzyme because all other heme proteins at the time, when bound to CO, exhibited Soret maxima at 420 nm, and this difference is due to the thiolate ligand.[4]

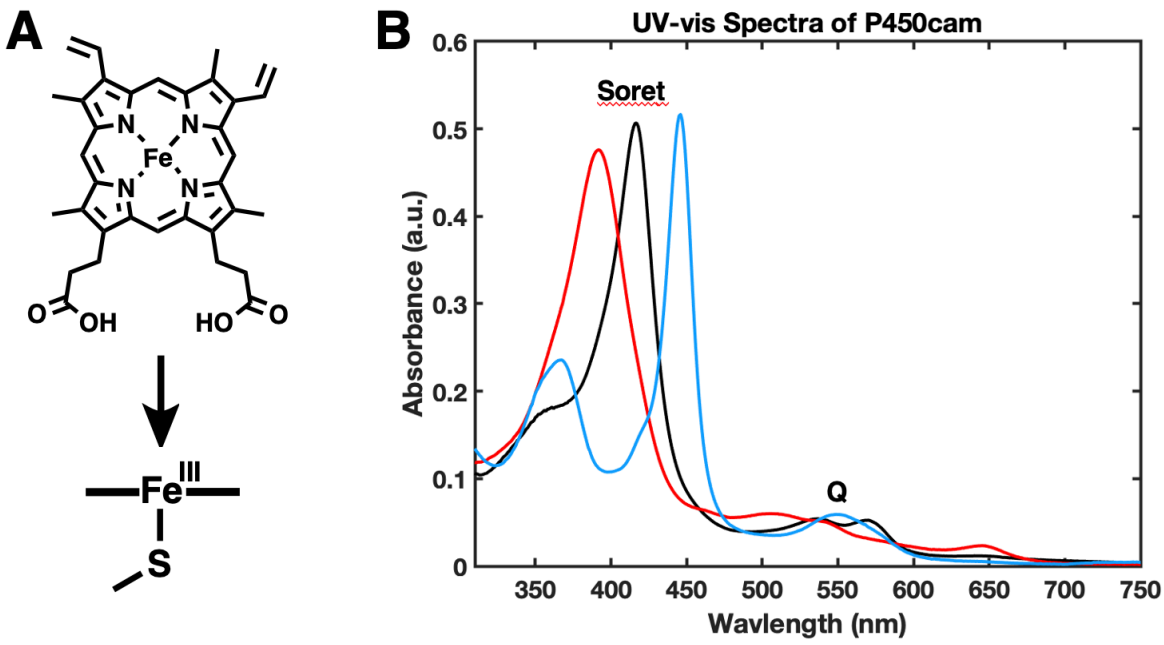

Figure 1-1. UV-vis spectra of P450s. (A) The heme cofactor involved in all P450s, which will be shown as the bottom representation through the thesis. (B) UV-vis spectra of P450cam, as an example of changes in the Soret. The black line is the Soret in the absence of substrate, at 417 nm. The red line shows the blue shift in Soret upon binding of substrate to 392 nm. The blue line is the titular 450 nm band after which P450s are named upon reduction and binding to CO.

P450s have a wide range of substrates and biological roles. Some examples of substrates are small terpenes, such as camphor, which are of particular interest in this thesis. In some cases, these P450s can oxidatively assimilate potentially toxic terpenes as a sole carbon and energy source.[5–9] Other examples are macrocycles, like cholesterol or phenobarbital, which are substrates for human P450s, whether in steroid biosynthesis or drug detoxification, respectively. As more P450s are discovered throughout nature, the substrate scope correspondingly increases.

Despite the large number of diverse substrates, various types of chemistry, and low sequence identity, P450s have a conserved triangular fold that makes structure-function relationships more broadly applicable (Figure 1-2A). The first P450 to have a crystal structure solved was P450cam, which is named after its substrate camphor. The crystal structure was solved in 1985, by Professor Thomas Poulos.[10] As such, P450cam serves as a cornerstone of

our lab, and a more detailed summary will be provided later. Shown in Figure 1-2 is the cartoon representation of the crystal structure of P450cam (PDB ID: 2CPP). The I helix is the longest helix of a P450, and thus can be thought of as the “backbone” of the enzyme structure. The F and G helices can play a role in substrate binding and can be involved in large structural changes. The cysteine residue that ligates the heme cofactor is closer to one side than another, and the closer side is called the proximal side (Figure 1-2B). The side that has the F and G helices and substrate access channel is called the distal side.

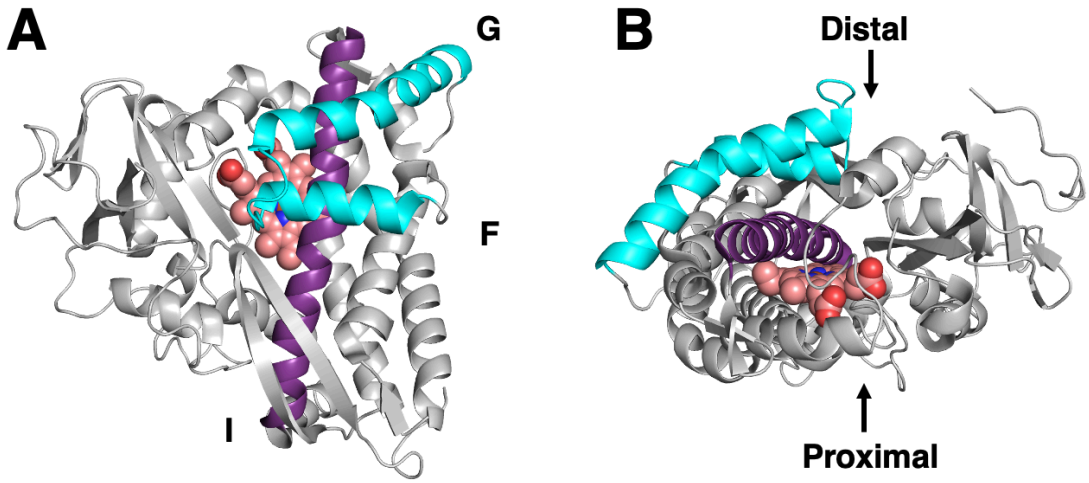

Figure 1-2. Overall P450 fold and structure. (A) A cartoon representation of P450cam (PDB ID: 2CPP) is shown. The heme is shown in pink-colored spheres. The I helix is highlighted in purple, and the F and G helices are shown in cyan. (B) An alternate view of P450cam shows the proximal and distal sides of a P450.

In addition to the common triangular fold, many P450s undergo conformational changes upon binding of substrate. These conformational changes mainly involve the F and G helices, which shift from an “open” conformation in the absence of substrate to a “closed” conformation in the presence of substrate (Figure 1-3). The open conformation has the F and G helices pulled away and back, which provides an access channel to the heme pocket. Substrate enters through

this channel and may result in movement of the F and G helices to cover this access channel. These structural changes often are accompanied by a change in the Soret (Figure 1-1B). The substrate-free, open form exhibits a Soret at 417 nm. Upon binding of substrate, the Soret shifts to 392 nm. Substrate binding is the first step of the catalytic cycle, which has been explored in detail over the years.

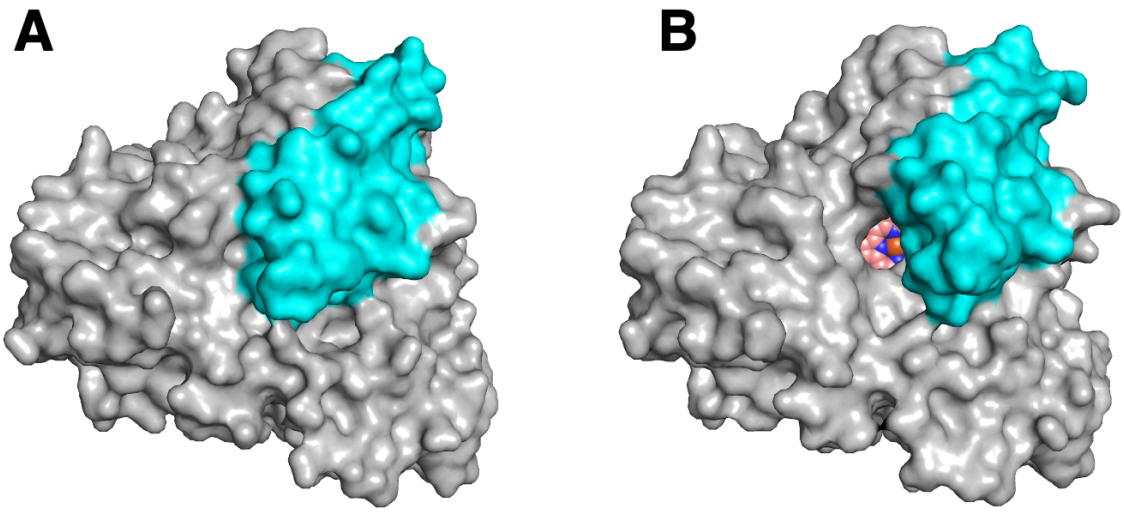

Figure 1-3. Open and close transition of P450cam. (A) The surface representation of P450cam (PDB ID: 2CPP) is shown in the closed conformation, where there is no access to the heme. (B) A surface representation of P450cam (PDB ID: 3L62) is shown in the open conformation, where there is an access channel to the heme. The difference between closed and open is due to presence or absence of the substrate, camphor, for P450cam. The acquisition of the open form was not trivial, and was obtained 25 years after the initial, closed form crystal structure.

The P450 catalytic cycle has remained an important topic over the years, as the powerful chemistry of P450s is able to break stable, unactivated C–H bonds under physiological conditions to form regio- and stereo-selective bonds (Figure 1-4). The catalytic cycle starts in the resting state with water ligated to the ferric iron in the heme. Substrate binding is the first step in starting the catalytic cycle. Substrate binds in the heme pocket, displacing the water ligand, but does not directly coordinate the heme. This displacement of the axial water ligand changes the heme iron from 6-coordinate to 5-coordinate, resulting in an increase in the reduction potential, allowing for

the first of two electrons to be delivered. The change in coordination of the iron also results in a change in the distribution of the electrons in the d orbitals of the iron. The 6-coordinate iron is called “low-spin”, as the 5 electrons of the ferric iron are maximally paired, resulting in a spin state of S = 1/2. The 5-coordinate iron is called “high-spin”, as the 5 electrons now maximally unpaired resulting in a spin state of S = 5/2. These spin shifts often are associated with changes in the UV-vis spectra (Figure 1-1B), with the low-spin species exhibiting the Soret around 417 nm and the high-spin species around 392 nm. After the binding of substrate, the first electron can now be delivered, resulting in ferrous heme, and oxygen can now bind, resulting in what is commonly referred to as the “oxycomplex”. Delivery of a second electron occurs in what is possibly a proton-coupled step,[11,12] and results in a hydroxyperoxo species. Another proton is delivered via a water-mediated proton network,[13–15] and the O–O bond heterolytically cleaves to release water and form Compound I, a Fe(IV)oxo species coupled to a radical species distributed over the porphyrin ring of the heme and sulfur of the thiolate ligand; this species is the catalytically competent intermediate in the catalytic cycle.[16] The abstraction of an H atom from the substrate results in a substrate radical and a Fe(IV)hydroxo species called Compound II.[17] In a radical rebound step, the hydroxyl group recombines with the substrate radical, and the catalytic cycle returns to resting state upon dissociation of product and return of a water molecule.

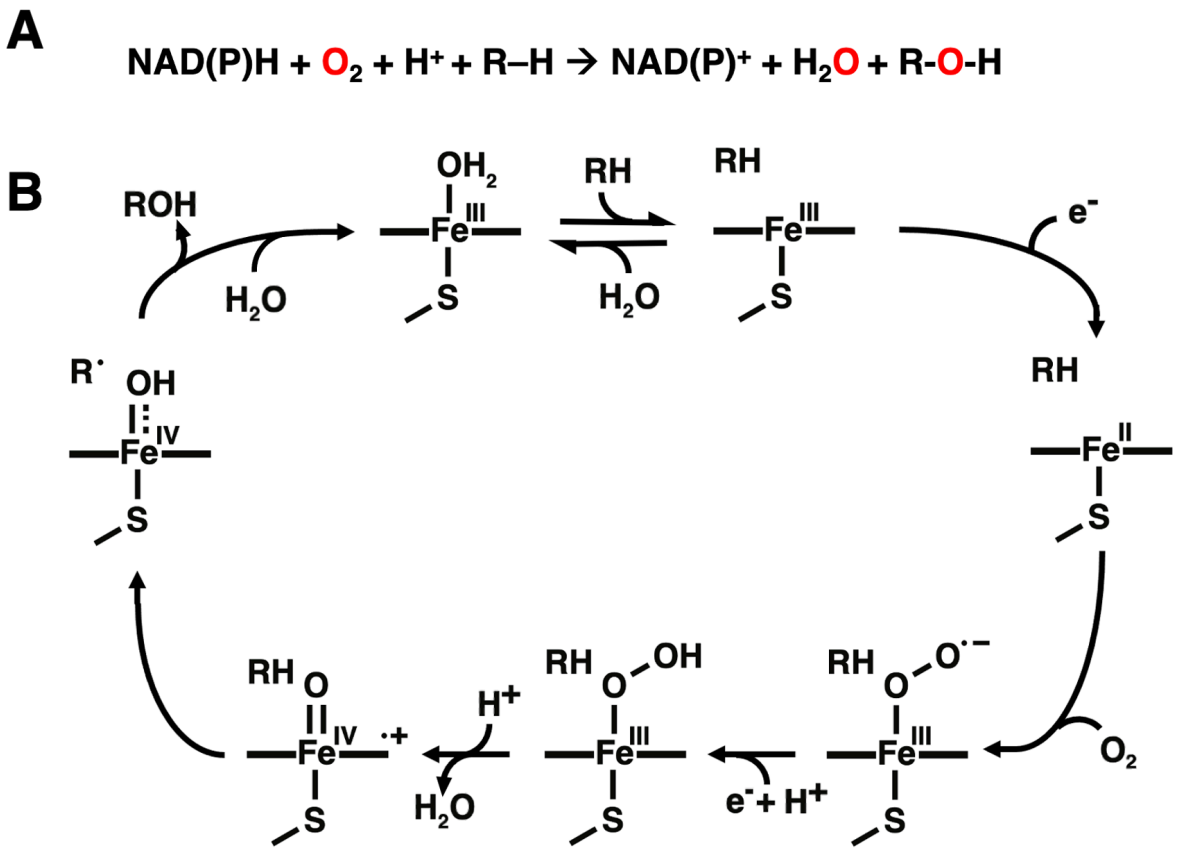

Figure 1-4. P450 catalysis. (A) Net reaction of P450s. (B) Catalytic cycle of P450s.

Despite the extensive investigations of the catalytic cycle, much less is known about the regulation of these steps in catalysis. Regulation is important because it is imperative that the catalytic cycle only occurs under the right circumstances; otherwise, valuable reducing equivalents will be wasted, high-valent intermediates could start degrading the protein, and/or reactive oxygen species could be released, which would be damaging to the cell. My thesis focuses on regulation of the catalytic cycle; in particular, substrate binding and the second electron transfer. Substrate binding is the most general form of regulation across all P450s. On the other hand, the second electron transfer is more nuanced, and depends on the particular P450 system. In most P450s, the second electron transfer can only be delivered by a protein redox partner. This is different from the first electron transfer, which can be delivered by any

biological or chemical reductant with an adequate reduction potential. The reliance of P450s on protein redox partners for the second electron transfer has historically been called the "effector role," and there are spectroscopic and structural data showing the influence of a redox partner on the P450.[18–21] The P450s that we mainly study in our lab are Class I P450s, which means that they require two protein redox partners (Figure 1-5). The redox partner that is important for interaction with the P450 is the Fe_2-S_2 ferredoxin in this system.

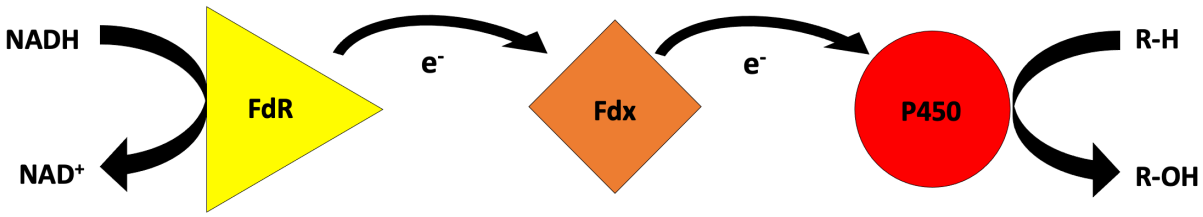

Figure 1-5. The flow of electrons in a Class I P450 system. A flavin adenine dinucleotide (FAD) containing reductase takes 2 electrons from NADH and transfers them one at a time to a Fe_2-S_2 containing ferredoxin, which then transfers them one at a time to the P450, where the oxidation of the substrate takes place.

As such, our lab is interested in the generality of structure function relationships in P450s and studying various isoforms to draw more general conclusions that are broadly applicable across all P450s. As I mentioned before, our lab has had a long-standing interest in P450cam, which is possibly the most well understood P450. Thus, much of our other P450 systems are chosen with P450cam in mind. A brief overview of P450cam is provided next to acquaint the reader with relevant information about P450cam.

P450cam

As previously mentioned, P450cam was the first P450 to have its crystal structure solved. It was discovered by selecting for *Psuedomonad* bacteria that could survive on camphor as a carbon source.[5,6] It was not the first P450 discovered, but its ease of expression, purification and

stability enabled generation of large amounts of protein for many experiments. Over the years, P450cam has run the gamut of experimentation, and is probably the most well-studied P450. However, recent studies have shown that even the most well understood P450 has new discoveries, and therefore underscores how much more there is to investigate as a whole.

P450cam is a bacterial Class I P450, which means it has two redox partner proteins necessary for catalysis. In particular, it requires a flavin adenine dinucleotide (FAD) containing reductase called putidaredoxin reductase (PdR) and a Fe_2-S_2 containing ferredoxin called putidaredoxin (Pdx). PdR removes a hydride from NADH and transfers the electrons to Pdx one at a time, which transfers an electron to P450cam. Redox partner interactions have been and is an active area of research in our lab and in the field.

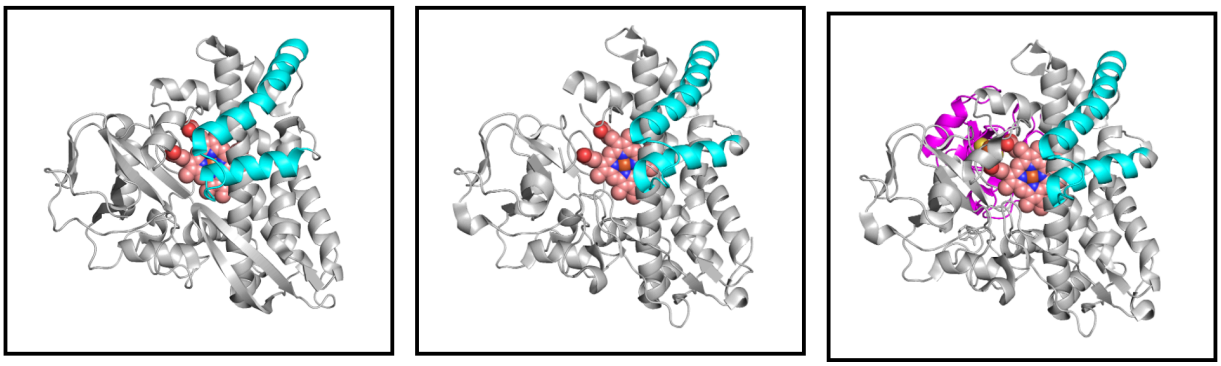

Figure 1-6. Various structural conformations of P450cam. (Left) The closed conformation of P450cam is shown (PDB ID: 2CPP). (Middle) The open conformation of P450cam is shown (PDB ID: 3L62). (Right) The covalently linked complex of P450cam and Pdx (magenta) is shown (PDB ID: 4JWU).

Recent focus in the lab has been on the interactions between the ferredoxin and the P450. There is a wealth of information about the interactions between Pdx and P450cam, which have come to be recognized as unique. P450cam is very specific for Pdx, and 2 residues in particular are very important – Asp38 and Trp106 of Pdx.[20,22] Both of these residues are required for catalysis, and alteration of either one results in a loss of a catalytically competent system. The

importance of these residues was clarified by the crystal structure of the covalently linked complex of P450cam to Pdx.[15] Pdx binding to P450cam pushes the P450 to resemble more of an open conformation and allows for the formation of a water-mediated proton network (Figure 1-6). In particular, Pdx binding frees up a critical residue, Asp251, from being locked in hydrogen bonds, and can now participate in the water-mediated proton network required for oxygen activation.[11,12] Before the crystal structure of the complex was solved, there were reports of P450cam spectral changes upon Pdx binding, including UV-vis, NMR, EPR, and Resonance Raman spectroscopy.[23–32] Pdx binding also increases the decay rate of the oxycomplex, thereby "activating" the P450.[31] All of these changes lead to the idea that Pdx may serve in an "effector role" of catalysis. Over the years it has become apparent that the P450cam and Pdx interaction may have unique characteristics. Thus, to test the generality of redox partner interactions, we turned to the closely related, homologous systems – P450terp and P450lin.

Homologous *Pseudomonad* P450 – P450terp and P450lin

P450terp and P450lin are some of the early P450s to be studied after P450cam, and they are Class I P450s that come from *Psuedomonad* bacteria and enable the bacteria to survive on a terpene substrate as a sole carbon source. There are some publications about both, but as many more, diverse P450s were uncovered, investigation into these two P450s stopped.

P450terp was discovered in 1992 in a swamp in Texas and was selected by testing which bacterial colonies could survive on α-terpineol as a sole carbon-source,[7] which was similar to the discovery process of P450cam. P450terp was the second ever P450 to have its crystal structure determined, almost 10 years after P450cam.[33,34] The crystal structure does not have substrate and resembled what we now refer to as an open conformation. There were a couple of other publications about P450terp, but they became limited after 1995.[35–38]

P450lin was the second bacterial P450 to be investigated alongside P450cam.[8] There is a report of preliminary crystal structure data, but no subsequent structure emerged.[39] There are some publications about substrate binding and discussion about P420 species with P450cam, but again publications involving the P450lin system paused after 2002.[40,41]

The relevance of using P450terp and P450lin is in their similarities to P450cam. They all are Class I Pseudomonad P450s that assimilate a terpene to enable their respective bacteria allowing them to live off the terpene as a sole carbon and energy source. Therefore, if their biological roles are similar, we expect their structure-function relationships to be similar as well. Thus, if what we know about P450cam holds true for P450terp and P450lin, this would indicate that these bacterial P450s share common regulatory mechanisms.

The structure-function relationships that we investigate are in the context of impact on regulation and catalysis. There has been many investigations into the importance of the thiolate ligand of P450s, and one such mutation was made in P450cam. This mutation was L358P in P450cam, and it mimics the some of the effects of Pdx binding in the absence of redox partner, like activating the P450 by increasing the rate of decay of the oxycomplex.[29,42] Both Pdx binding and the L358P mutation "push" on the proximal side of the heme and, given the similar effects of redox partner binding and the L358P mutation, this proximal push effect is very likely important for oxygen activation. This can be further explored by mutations and exploring the effect of redox partner binding in other P450s. There are different threads of investigation in this thesis, but overall, there is a common theme of how these subtle regulations influence catalysis.

Summary of Dissertation

This dissertation focuses on select forms of regulation of the P450 catalytic cycle. In the second chapter, I will discuss how cooperative substrate binding influences catalysis in P450terp. The substrate-bound crystal structure of P450terp reveals two substrate binding sites. Therefore,

a series of mutations were made to weaken both binding sites to investigate their roles in binding and catalysis. Binding studies reveal cooperativity in substrate binding, and the mutation of a particular residue, F188A, eliminates the substrate binding cooperativity. The crystal structure of the F188A variant reveals only one substrate in the active site. Turnover studies show that mutations vary the coupling efficiency, and it was found that the distant, second binding sight impacts both binding of the substrate in the first site, and “pins” it in place for productive catalysis.

The third and fourth chapters focus on the redox partner effector role on P450lin and P450terp. Both P450lin and P450terp are able to turnover substrate with a nonnative ferredoxin, Arx, which is the redox partner from the CYP101D1 system. Various mutations were made to Pdx to mimic the native ferredoxin redox partner proteins of P450terp and P450lin systems, to different degrees of change in turnover rate. However, in both systems, ferredoxins that were able to enable turnover also increased the decay rate of the oxycomplex. So far, all P450s studied have an increased rate of decay of the oxycomplex in the presence of redox partner, so this may be a common theme for all P450s.

The fifth chapter discusses the application of the P450cam L358P mutation to a P450 that was used to trap Compound II, CYP158A2. CYP158A2 is a natural “L358P” P450, as the WT has a proline immediately following the ligating cysteine. The proline is thought to push on the heme and activate it, as evidenced by the P450cam L358P mutation. The preliminary results indicate that the natural proline stabilizes Compound II.

The sixth chapter is a brief investigation into the development of the P420 species in P450cam. Historically, it has been regarded that P450s that exhibit a Soret at 420 nm when bound to CO instead of 450 nm were damaged and inactive. The source of what causes the change in Soret has been debated, and one such hypothesis is histidine ligation in place of cysteine, as many hemoproteins that naturally have P420 have histidine ligands. A series of mutations that alter the closest histidines to glutamines indicate that a histidine ligand is not necessary for

formation of P420. Thus, the formation of P420 is more nuanced and may be a result of a disturbance in the heme pocket, and not necessarily alteration of the heme ligand.

Overall, my thesis aims to understand some of the different forms of regulation of the catalytic cycle of P450s and to broaden our understanding of the diverse and ever-growing field of P450s.

References:

(1) Poulos, T. L. Heme Enzyme Structure and Function. *Chem. Rev.* **2014**, *114* (7), 3919–3962. https://doi.org/10.1021/cr400415k.

(2) Zanger, U. M.; Schwab, M. Cytochrome P450 Enzymes in Drug Metabolism: Regulation of Gene Expression, Enzyme Activities, and Impact of Genetic Variation. *Pharmacology & Therapeutics* **2013**, *138* (1), 103–141. https://doi.org/10.1016/j.pharmthera.2012.12.007.

(3) Omura, T.; Sato, R. A New Cytochrome in Liver Microsomes. *J Biol Chem* **1962**, *237*, 1375–1376.

(4) Hanson, L. K.; Eaton, W. A.; Sligar, S. G.; Gunsalus, I. C.; Gouterman, M.; Connell, C. R. Origin of the Anomalous Soret Spectra of Carboxycytochrome P-450. *J. Am. Chem. Soc.* **1976**, *98* (9), 2672–2674. https://doi.org/10.1021/ja00425a050.

(5) Katagiri, M.; Ganguli, B. N.; Gunsalus, I. C. A Soluble Cytochrome P-450 Functional in Methylene Hydroxylation. *Journal of Biological Chemistry* **1968**, *243* (12), 3543–3546. https://doi.org/10.1016/S0021-9258(18)93343-0.

(6) Gunsalus, I. C. A Soluble Methylene Hydroxylase System: Structure and Role of Cytochrome P-450 and Iron-Sulfur Protein Components. *Hoppe Seylers Z Physiol Chem* **1968**, *349* (11), 1610–1613.

(7) Peterson, J. A.; Lu, J. Y.; Geisselsoder, J.; Graham-Lorence, S.; Carmona, C.; Witney, F.; Lorence, M. C. Cytochrome P-450terp. Isolation and Purification of the Protein and Cloning and Sequencing of Its Operon. *Journal of Biological Chemistry* **1992**, *267* (20), 14193–14203. https://doi.org/10.1016/S0021-9258(19)49697-X.

(8) Ropp, J. D.; Gunsalus, I. C.; Sligar, S. G. Cloning and Expression of a Member of a New Cytochrome P-450 Family: Cytochrome P-450lin (CYP111) from Pseudomonas Incognita. *J Bacteriol* **1993**, *175* (18), 6028–6037. https://doi.org/10.1128/jb.175.18.6028-6037.1993.

(9) Tsang, H.-L.; Huang, J.-L.; Lin, Y.-H.; Huang, K.-F.; Lu, P.-L.; Lin, G.-H.; Khine, A. A.; Hu, A.; Chen, H.-P. Borneol Dehydrogenase from Pseudomonas Sp. Strain TCU-HL1 Catalyzes the Oxidation of (+)-Borneol and Its Isomers to Camphor. *Appl Environ Microbiol* **2016**, *82* (21), 6378–6385. https://doi.org/10.1128/AEM.01789-16.

(10) Poulos, T. L.; Finzel, B. C.; Gunsalus, I. C.; Wagner, G. C.; Kraut, J. The 2.6-A Crystal Structure of Pseudomonas Putida Cytochrome P-450. *J Biol Chem* **1985**, *260* (30), 16122–16130.

(11) Gerber, N. C.; Sligar, S. G. A Role for Asp-251 in Cytochrome P-450cam Oxygen Activation. *Journal of Biological Chemistry* **1994**, *269* (6), 4260–4266. https://doi.org/10.1016/S0021-9258(17)41772-8.

(12) Vidakovic, M.; Sligar, S. G.; Li, H.; Poulos, T. L. Understanding the Role of the Essential Asp251 in Cytochrome P450cam Using Site-Directed Mutagenesis, Crystallography, and

Kinetic Solvent Isotope Effect. *Biochemistry* **1998**, *37* (26), 9211–9219. https://doi.org/10.1021/bi980189f.
(13) Nagano, S.; Poulos, T. L. Crystallographic Study on the Dioxygen Complex of Wild-Type and Mutant Cytochrome P450cam. *Journal of Biological Chemistry* **2005**, *280* (36), 31659–31663. https://doi.org/10.1074/jbc.M505261200.
(14) Schlichting, I.; Berendzen, J.; Chu, K.; Stock, A. M.; Maves, S. A.; Benson, D. E.; Sweet, R. M.; Ringe, D.; Petsko, G. A.; Sligar, S. G. The Catalytic Pathway of Cytochrome P450cam at Atomic Resolution. *Science* **2000**, *287* (5458), 1615–1622. https://doi.org/10.1126/science.287.5458.1615.
(15) Tripathi, S.; Li, H.; Poulos, T. L. Structural Basis for Effector Control and Redox Partner Recognition in Cytochrome P450. *Science* **2013**, *340* (6137), 1227–1230. https://doi.org/10.1126/science.1235797.
(16) Rittle, J.; Green, M. T. Cytochrome P450 Compound I: Capture, Characterization, and C-H Bond Activation Kinetics. *Science* **2010**, *330* (6006), 933–937. https://doi.org/10.1126/science.1193478.
(17) Yosca, T. H.; Rittle, J.; Krest, C. M.; Onderko, E. L.; Silakov, A.; Calixto, J. C.; Behan, R. K.; Green, M. T. Iron(IV)Hydroxide p K_a and the Role of Thiolate Ligation in C–H Bond Activation by Cytochrome P450. *Science* **2013**, *342* (6160), 825–829. https://doi.org/10.1126/science.1244373.
(18) Tyson, C. A.; Lipscomb, J. D.; Gunsalus, I. C. The Role of Putidaredoxin and P450 Cam in Methylene Hydroxylation. *J Biol Chem* **1972**, *247* (18), 5777–5784.
(19) Gunsalus, I. C.; Lipscomb, J. D.; Meeks, J. R. CYTOCHROME P-450 $^{***}_{am}$ SUBSTRATE AND EFFECTOR INTERACTIONS. *Ann NY Acad Sci* **1973**, *212* (1 Multienzyme S), 107–121. https://doi.org/10.1111/j.1749-6632.1973.tb47590.x.
(20) Sligar, S. G.; Debrunner, P. G.; Lipscomb, J. D.; Namtvedt, M. J.; Gunsalus, I. C. A Role of the Putidaredoxin COOH-Terminus in *P* -450 $_{cam}$ (Cytochrome *m*) Hydroxylations. *Proc. Natl. Acad. Sci. U.S.A.* **1974**, *71* (10), 3906–3910. https://doi.org/10.1073/pnas.71.10.3906.
(21) Lipscomb, J. D.; Sligar, S. G.; Namtvedt, M. J.; Gunsalus, I. C. Autooxidation and Hydroxylation Reactions of Oxygenated Cytochrome P-450cam. *Journal of Biological Chemistry* **1976**, *251* (4), 1116–1124. https://doi.org/10.1016/S0021-9258(17)33808-5.
(22) Kuznetsov, V. Yu.; Poulos, T. L.; Sevrioukova, I. F. Putidaredoxin-to-Cytochrome P450cam Electron Transfer: Differences between the Two Reductive Steps Required for Catalysis. *Biochemistry* **2006**, *45* (39), 11934–11944. https://doi.org/10.1021/bi0611154.
(23) Lipscomb, J. D. Electron Paramagnetic Resonance Detectable States of Cytochrome P-450cam. *Biochemistry* **1980**, *19* (15), 3590–3599. https://doi.org/10.1021/bi00556a027.
(24) Unno, M.; Christian, J. F.; Sjodin, T.; Benson, D. E.; Macdonald, I. D. G.; Sligar, S. G.; Champion, P. M. Complex Formation of Cytochrome P450cam with Putidaredoxin. *Journal of Biological Chemistry* **2002**, *277* (4), 2547–2553. https://doi.org/10.1074/jbc.M108917200.
(25) Shiro, Y.; Iizuka, T.; Makino, R.; Ishimura, Y.; Morishima, I. Nitrogen-15 NMR Study on Cyanide (C15N-) Complex of Cytochrome P-450cam. Effects of d-Camphor and Putidaredoxin on the Iron-Ligand Structure. *J. Am. Chem. Soc.* **1989**, *111* (20), 7707–7711. https://doi.org/10.1021/ja00202a007.
(26) Shimada, H.; Nagano, S.; Hori, H.; Ishimura, Y. Putidaredoxin–Cytochrome P450cam Interaction. *Journal of Inorganic Biochemistry* **2001**, *83* (4), 255–260. https://doi.org/10.1016/S0162-0134(00)00173-2.
(27) Pochapsky, S. S.; Pochapsky, T. C.; Wei, J. W. A Model for Effector Activity in a Highly Specific Biological Electron Transfer Complex: The Cytochrome P450 $_{c\ am}$ –Putidaredoxin Couple $_{,}$. *Biochemistry* **2003**, *42* (19), 5649–5656. https://doi.org/10.1021/bi034263s.

(28) Nagano, S.; Shimada, H.; Tarumi, A.; Hishiki, T.; Kimata-Ariga, Y.; Egawa, T.; Suematsu, M.; Park, S.-Y.; Adachi, S.; Shiro, Y.; Ishimura, Y. Infrared Spectroscopic and Mutational Studies on Putidaredoxin-Induced Conformational Changes in Ferrous CO-P450cam ·. *Biochemistry* **2003**, *42* (49), 14507–14514. https://doi.org/10.1021/bi035410p.
(29) Tosha, T.; Yoshioka, S.; Ishimori, K.; Morishima, I. L358P Mutation on Cytochrome P450cam Simulates Structural Changes upon Putidaredoxin Binding. *Journal of Biological Chemistry* **2004**, *279* (41), 42836–42843. https://doi.org/10.1074/jbc.M404216200.
(30) Tosha, T.; Yoshioka, S.; Takahashi, S.; Ishimori, K.; Shimada, H.; Morishima, I. NMR Study on the Structural Changes of Cytochrome P450cam upon the Complex Formation with Putidaredoxin. *Journal of Biological Chemistry* **2003**, *278* (41), 39809–39821. https://doi.org/10.1074/jbc.M304265200.
(31) Glascock, M. C.; Ballou, D. P.; Dawson, J. H. Direct Observation of a Novel Perturbed Oxyferrous Catalytic Intermediate during Reduced Putidaredoxin-Initiated Turnover of Cytochrome P-450-CAM. *Journal of Biological Chemistry* **2005**, *280* (51), 42134–42141. https://doi.org/10.1074/jbc.M505426200.
(32) Zhang, W.; Pochapsky, S. S.; Pochapsky, T. C.; Jain, N. U. Solution NMR Structure of Putidaredoxin–Cytochrome P450cam Complex via a Combined Residual Dipolar Coupling–Spin Labeling Approach Suggests a Role for Trp106 of Putidaredoxin in Complex Formation. *Journal of Molecular Biology* **2008**, *384* (2), 349–363. https://doi.org/10.1016/j.jmb.2008.09.037.
(33) Hasemann, C. A.; Ravichandran, K. G.; Peterson, J. A.; Deisenhofer, J. Crystal Structure and Refinement of Cytochrome P450terp at 2·3 Å Resolution. *Journal of Molecular Biology* **1994**, *236* (4), 1169–1185. https://doi.org/10.1016/0022-2836(94)90019-1.
(34) Boddupalli, S. S.; Hasemann, C. A.; Ravichandran, K. G.; Lu, J. Y.; Goldsmith, E. J.; Deisenhofer, J.; Peterson, J. A. Crystallization and Preliminary X-Ray Diffraction Analysis of P450terp and the Hemoprotein Domain of P450BM-3, Enzymes Belonging to Two Distinct Classes of the Cytochrome P450 Superfamily. *Proc. Natl. Acad. Sci. U.S.A.* **1992**, *89* (12), 5567–5571. https://doi.org/10.1073/pnas.89.12.5567.
(35) Fruetel, J. A.; Mackman, R. L.; Peterson, J. A.; Ortiz de Montellano, P. R. Relationship of Active Site Topology to Substrate Specificity for Cytochrome P450terp (CYP108). *Journal of Biological Chemistry* **1994**, *269* (46), 28815–28821. https://doi.org/10.1016/S0021-9258(19)61979-4.
(36) Tuck, S. F.; Peterson, J. A.; Ortiz de Montellano, P. R. Active Site Topologies of Bacterial Cytochromes P450101 (P450cam), P450108 (P450terp), and P450102 (P450BM-3). In Situ Rearrangement of Their Phenyl-Iron Complexes. *Journal of Biological Chemistry* **1992**, *267* (8), 5614–5620. https://doi.org/10.1016/S0021-9258(18)42809-8.
(37) Hasemann, C. A.; Kurumbail, R. G.; Boddupalli, S. S.; Peterson, J. A.; Deisenhofer, J. Structure and Function of Cytochromes P450:A Comparative Analysis of Three Crystal Structures. *Structure* **1995**, *3* (1), 41–62. https://doi.org/10.1016/S0969-2126(01)00134-4.
(38) Sevrioukova, I. F.; Peterson, J. A. Reaction of Carbon-Monoxide and Molecular-Oxygen with P450terp (CYP108) and P450BM-3 (CYP102). *Archives of Biochemistry and Biophysics* **1995**, *317* (2), 397–404. https://doi.org/10.1006/abbi.1995.1180.
(39) Gunsalus, I. C.; Ghosh, D.; Gao, Y.-G.; Wang, A. H.-J. Cytochrome P450lin(P450111): Crystal Unit Cell, Tertiary Structure-Function Model. *Journal of Basic and Clinical Physiology and Pharmacology* **1992**, *3* (Supplement). https://doi.org/10.1515/JBCPP.1992.3.S1.55.
(40) Hui Bon Hoa, G.; Di Primo, C.; Dondaine, I.; Sligar, S. G.; Gunsalus, I. C.; Douzou, P. Conformational Changes of Cytochromes P-450cam and P-450lin Induced by High Pressure. *Biochemistry* **1989**, *28* (2), 651–656. https://doi.org/10.1021/bi00428a035.

(41) Deprez, E.; Gill, E.; Helms, V.; Wade, R. C.; Hui Bon Hoa, G. Specific and Non-Specific Effects of Potassium Cations on Substrate–Protein Interactions in Cytochromes P450cam and P450lin. *Journal of Inorganic Biochemistry* **2002**, *91* (4), 597–606. https://doi.org/10.1016/S0162-0134(02)00467-1.
(42) Nagano, S.; Tosha, T.; Ishimori, K.; Morishima, I.; Poulos, T. L. Crystal Structure of the Cytochrome P450cam Mutant That Exhibits the Same Spectral Perturbations Induced by Putidaredoxin Binding. *Journal of Biological Chemistry* **2004**, *279* (41), 42844–42849. https://doi.org/10.1074/jbc.M404217200.

Chapter 2

Cooperative Substrate Binding Controls Catalysis in Bacterial Cytochrome P450terp (CYP108A1)

Introduction

P450s generate highly oxidizing intermediates during the catalytic cycle, such as ferryl-oxo/hydroxo ($Por^{\bullet+}$-Fe^{IV}=O/Por- Fe^{IV}–OH) species, Compounds I and II, respectively.[1–3] While the catalytic cycle is well-studied, significantly less is known about the mechanisms by which these enzymes regulate the formation of their potent intermediates and prevent undesired oxidation of the protein scaffold.[4–6]

Despite these uncertainties, much more is known about the binding of substrate for the initiation of catalysis. Upon substrate binding, a change in spin-state is accompanied by an increase in the heme redox potential allowing an electron to be transferred from a redox partner protein. This substrate-dependent control of the first electron transfer ensures that dioxygen binding to the reduced ferrous state only occurs when substrate is bound minimizing the likelihood of unproductive dioxygen activation and generation of harmful radical oxygen species (ROS).[7]

Much of what is known about the molecular level details of P450s derives from studies with *Pseudomonas putida* P450cam (CYP101A1) which was the first P450 to be sequenced[8,9] and have a crystal structure solved.[10] Like many other bacterial P450s, P450cam belongs to a Class I system that requires two additional soluble electron transfer (ET) proteins to perform catalysis. Specifically, a FAD-containing protein, putidaredoxin reductase (PdR), shuttles electrons from NADH to the Fe_2S_2 ferredoxin, putidaredoxin (Pdx), where the subsequent reduction of the heme iron by Pdx enables O_2 binding and activation followed by substrate hydroxylation. As more P450s were discovered and the number of detailed mechanistic studies expanded, it became clear that P450cam exhibits some additional unusual regulatory properties.

The earliest unique feature of P450cam to be discovered was its strict requirement for its own redox partner[11] while many other P450s can be supported by foreign redox partners.[12–15] It now is known that Pdx binding to P450cam results in a Pdx-specific induced conformational change that triggers the formation of a proton relay network required for O_2 activation.[16–18] More recently, P450cam was found to have a second allosteric substrate binding site and undergoes complex and large structural changes in response to the binding of heme iron ligands.[17,19]

Using P450cam as a model system brings forth an important question: to what extent is the complexity of P450cam shared by other P450s? Given that P450cam is from *Pseudomonas putida*, which uses camphor as a sole carbon source, it is reasonable to expect that other Class I *Pseudomonad* P450s that also use a terpenoid natural product as a sole carbon source might share similar properties. One example is P450terp (CYP108A1), a P450 that begins the oxidative assimilation of α-terpineol as a carbon source by hydroxylation, forming 7-hydroxy-terpineol (Scheme 2-1). P450terp is co-expressed with two electron transfer proteins, an FAD-containing protein, terpredoxin reductase (TdR) and a Fe_2S_2 ferredoxin, terpredoxin (Tdx). CYP108A1 was the second *Pseudomonad* P450 to be characterized and have a crystal structure solved.[20–22] However, the available P450terp structure is substrate-free and enzymatic characterization is limited to a few publications.[23–27]

Here, the crystal structure of P450terp co-crystallized with its substrate α-terpineol is presented. Strikingly, this structure reveals two molecules of α-terpineol within the active site, which suggests that P450terp may exhibit homotropic allosteric control. This possibility was explored with mutagenesis, additional crystal structures, molecular dynamics simulations, and substrate binding using both spectroscopic titration and isothermal titration calorimetry. These studies reveal that P450terp does indeed exhibit substrate cooperativity and that the allosteric site is required for efficient catalysis. The results underscore how even the seemingly simplest cytochrome P450s can exhibit complex and diverse regulatory properties. Furthermore, these

results are discussed in the context of the biological roles that these P450s serve in the metabolism of unusual alternative carbon sources.

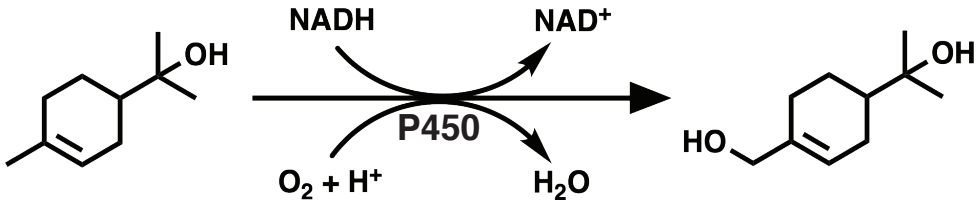

Scheme 2-1. The net reaction of the P450terp system where the FAD-containing TdR shuttles electrons from NADH to the Fe_2S_2-containing Tdx. Electrons are then transferred from Tdx to heme iron of P450terp for O_2 activation and hydroxylation α-terpineol.

Results

X-ray Crystallography

It was initially anticipated that P450terp would adopt a more closed conformation when substrate binds given how commonly "open-to-closed" transitions are observed in other P450s.[7] As such, P450terp was co-crystallized in the presence of substrate rather than soaking α-terpineol into substrate-free crystals as to avoid restrictions of a conformational change by any restraints imposed by the crystal lattice. Regardless, the substrate-P450 complex crystallized with the same space group and cell dimensions as the previously determined substrate-free structure (1CPT) and diffracted to a resolution of 2.0 Å (Table 2-1).

Table 2-1. Crystallographic data collection and refinement statistics of P450terp

	P450terp WT SB	**P450terp WT SF**	**P450terp F188A SB**
PDB entry	8EUH	8EUK	8EUL
Data Collection			
Resolution (Å)	2.00	1.98	2.24
Resolution range (Å)	58.5 - 2.0 (2.072 - 2.0)	59.52 - 1.984 (2.055 - 1.984)	38.06 - 2.244 (2.324 - 2.244)
Space group	P 61 2 2	P 61 2 2	P 61 2 2
Unit Cell	68.12 68.12 455.406 90 90 120	68.73 68.73 457.039 90 90 120	67.81 67.81 456.684 90 90 120
Total reflections	1009679 (100691)	927460 (75823)	538276 (61645)
Unique reflections	44104 (4262)	46098 (4465)	31395 (3015)

Multiplicity	22.9 (23.6)	20.1 (17.0)	17.1 (20.3)
Completeness (%)	99.84 (99.84)	99.92 (99.98)	99.74 (99.01)
Mean *I*/σ(*I*)	14.40 (2.61)	27.93 (11.55)	10.53 (3.42)
Wilson *B*-factor (Å^2)	32.53	27.62	31.91
R_{pim}	0.03164 (0.2775)	0.01765 (0.04957)	0.04543 (0.2297)
$CC_{1/2}$	0.997 (0.91)	0.998 (0.995)	0.996 (0.927)
CC*	0.999 (0.976)	0.999 (0.999)	0.999 (0.981)
Refinement			
Reflections used in refinement	44036 (4262)	46079 (4465)	31340 (3009)
Reflections used for R-free	2232 (188)	2383 (207)	1509 (147)
R_{work}	0.1785 (0.2494)	0.1798 (0.1926)	0.1995 (0.3513)
R_{free}	0.2096 (0.2586)	0.2065 (0.2231)	0.2235 (0.3230)
CC(work)	0.958 (0.897)	0.951 (0.900)	0.946 (0.773)
CC(free)	0.964 (0.925)	0.949 (0.817)	0.930 (0.729)
Number of non-hydrogen atoms	3609	3680	3523
Macromolecules	3301	3308	3266
Ligands	100	91	94
solvent	208	281	163
Protein residues	418	418	415
Root-mean-square deviation for bonds (Å)	0.015	0.011	0.009
Root-mean-square deviation for angles (deg)	1.59	1.35	1.26
Ramachandran favored (%)	97.1	97.83	97.57
Ramachandran allowed (%)	2.9	2.17	2.43
Ramachandran outliers (%)	0	0	0
Rotamer outliers (%)	0.56	0	0.86
Clashscore	1.65	2.38	2.86
Average B-factor (Å^2)	39.59	35.07	39.18
Macromolecules	39.46	34.74	39.1
Ligands	38.46	35.24	42.92

Solvent	42.25	38.96	38.7

Statistics for the highest-resolution shell are shown in parentheses. As R_{merge} tends to increase with high multiplicity, R_{pim} is reported, which better accounts for the increased redundancy multiplicity.[28]

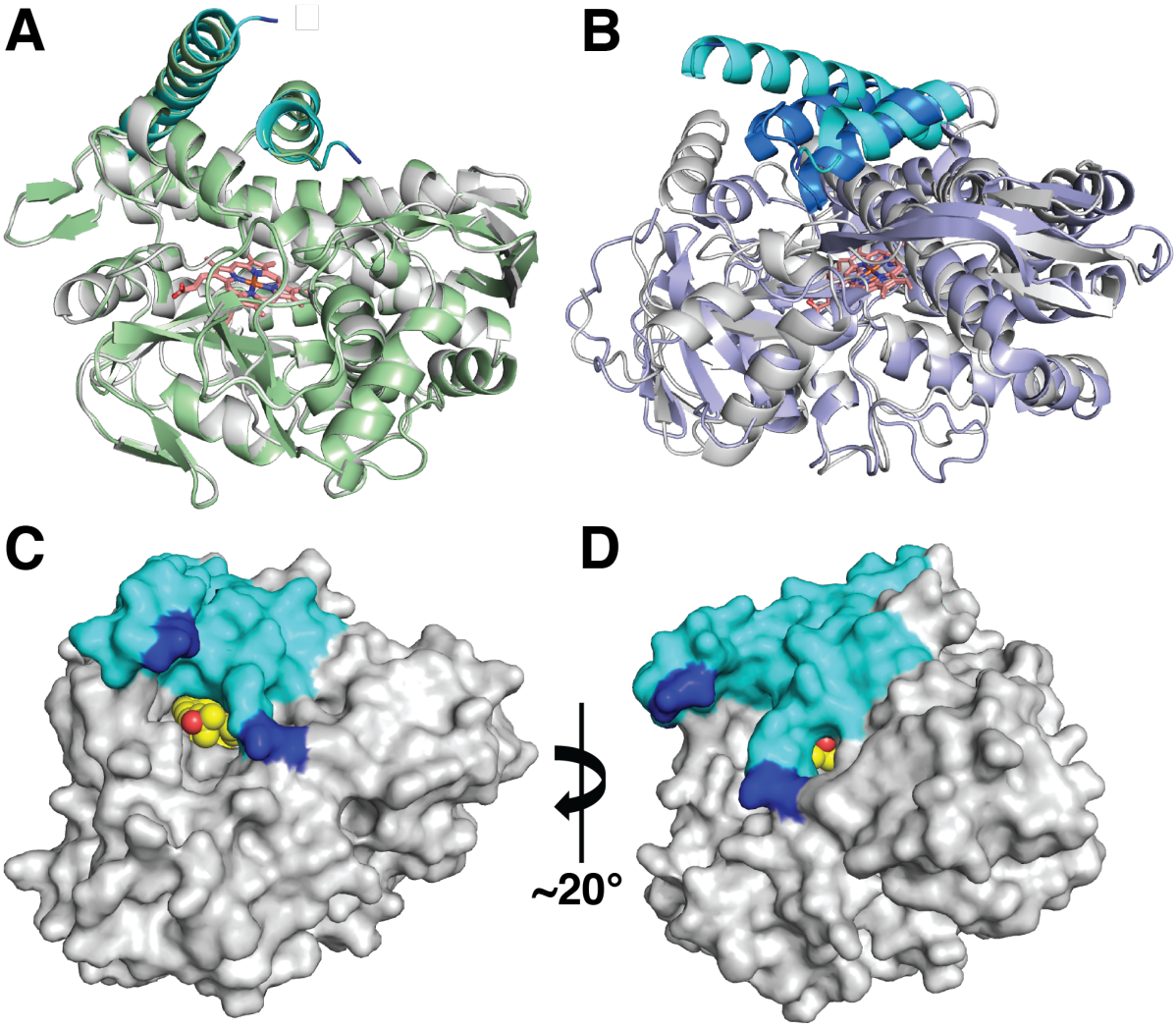

Figure 2-1. Crystal structure of P450terp. (A) Overlay of substrate-bound P450terp (grey) and substrate-free P450terp, 1CPT (green). The F and G helices of substrate-bound P450terp are shown in cyan and the end residues of the F and G loop are highlighted blue. The heme is shown in pink. Residues 191 – 206 cannot be modelled in substrate-free P450terp (1CPT) while residues 193-202 cannot be modeled in our structure of substrate-bound P450terp. (B) Overlay of substrate-bound P450terp (grey) and substrate-bound P450cam (purple). The F and G helices of P450terp are in cyan, and the F and G helices of P450cam are in blue. The heme is shown in pink. (C) Surface representation of substrate-bound P450terp and (D) rotated about 20°. The F and G helices are cyan, while the ends of the loop are blue. Substrate molecules are yellow spheres.

Alignment of the substrate-free and substrate-bound structures reveals minimal change of the overall protein conformation with a Cα-RMSD of 0.26 Å (Figure 2-1A). In both structures, the loop connecting the F and G helices is disordered, but a few more residues in the F-G loop were modeled that were not previously reported (Figure 2-1A). It was unclear whether this increase in ordered F-G loop density is due to substrate-binding, improved resolution, or advancements in data processing. Therefore, an α-terpineol-free P450terp structure was determined to 2.0 Å (Table 2-1) and both the substrate-free and substrate-bound structures have the same number of F/G loop residues, which suggests the newly ordered residues in the structure do not appear as a consequence of α-terpineol binding. However, the absence of substrate did not result in a vacant active site, but rather a molecule of ethylene glycol provided by the mother liquor fits well into residual density above the heme (Figure 2-2).

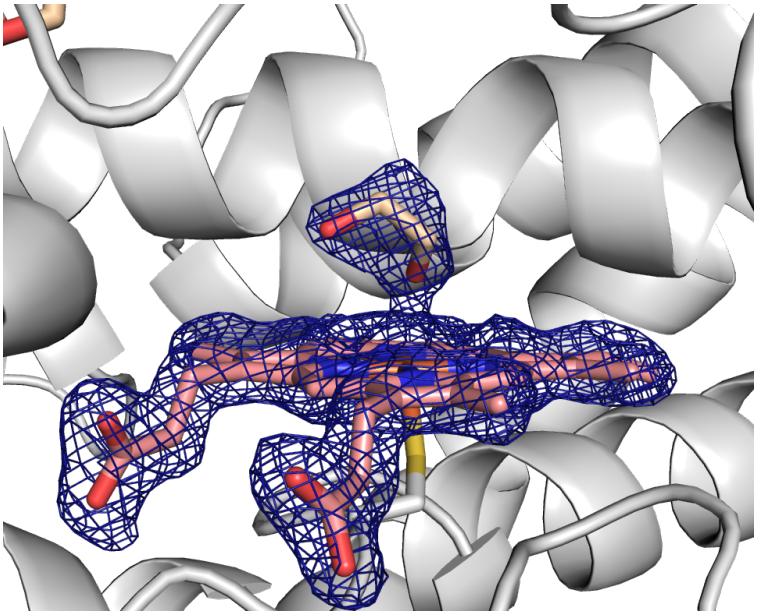

Figure 2-2. Active site of P450terp WT substrate free. Ethylene glycol is shown in wheat and the heme is in pink. Electron density for both is shown at 1σ of a $2F_O$-F_C map.

Compared to P450cam, substrate-bound P450terp displays a more open active site due to the F-G loop disorder and positioning of the G-helix (Figure 2-1B), suggesting P450terp may

not undergo the open/close motions observed in other P450s. In P450cam, these motions change inter-residue couplings throughout the enzyme that allow for the retention of regioselectivity even upon alteration of key interactions with substrate.[29] It is then natural to question how P450terp positions α-terpineol for hydroxylation and maintains its regioselectivity. Surprisingly, the substrate-bound structure exhibited two molecules of α-terpineol in the active site. A surface representation of the substrate-bound P450terp structure reveals two channels into the active site, each blocked by the second substrate (Figure 2-1C and 2-1D). While it is possible that disordered residues of the F-G loop cover the large channel between the two helices (Figure 2-1C), the number of unmodelled residues is insufficient to cover both channels simultaneously (Figure 2-1D).

Within the active site, electron density for the primary molecule of substrate (terp1), closest to the heme, is very well-defined and the carbon to be activated, C7, is positioned 4.2 Å from the heme iron (Fig 2-3A). In P450cam, the corresponding carbon atom of camphor, C5, is 4.0 Å from the iron.[10] The proximal substrate is held in place by key nonpolar contacts provided by Phe317 and Phe414 as well as hydrogen bonding interactions between the substrate hydroxyl group and the side chains of Ser101 and Thr103. Above terp1, large lobes of density were best modeled as a second substrate molecule (terp2) in two distinct but equally populated conformations refined to 49% and 51% occupancy (Figure 2-3C). Both conformations of terp2 clearly interact with the side chain of Phe188 with one conformation forming a hydrogen bond with the phenol sidechain of Tyr80. A Polder map of terp2 contoured at 5σ clearly shows the occupancy of a second molecule of substrate and supports the existence of two conformations. (Figure 2-3D). The closest distance between the two substrates is 4.0 Å, and there is minimal direct contact between the two molecules based on a space-filling model of the active site. A majority of the interaction between the two substrates is mediated by nonpolar contacts of the surrounding residues (Figure 2-4 and

Table 2-2). Phe188 undergoes a slight rotation to better interact with terp2 in the substrate-bound structure compared to the substrate-free structure (Figure 2-5).

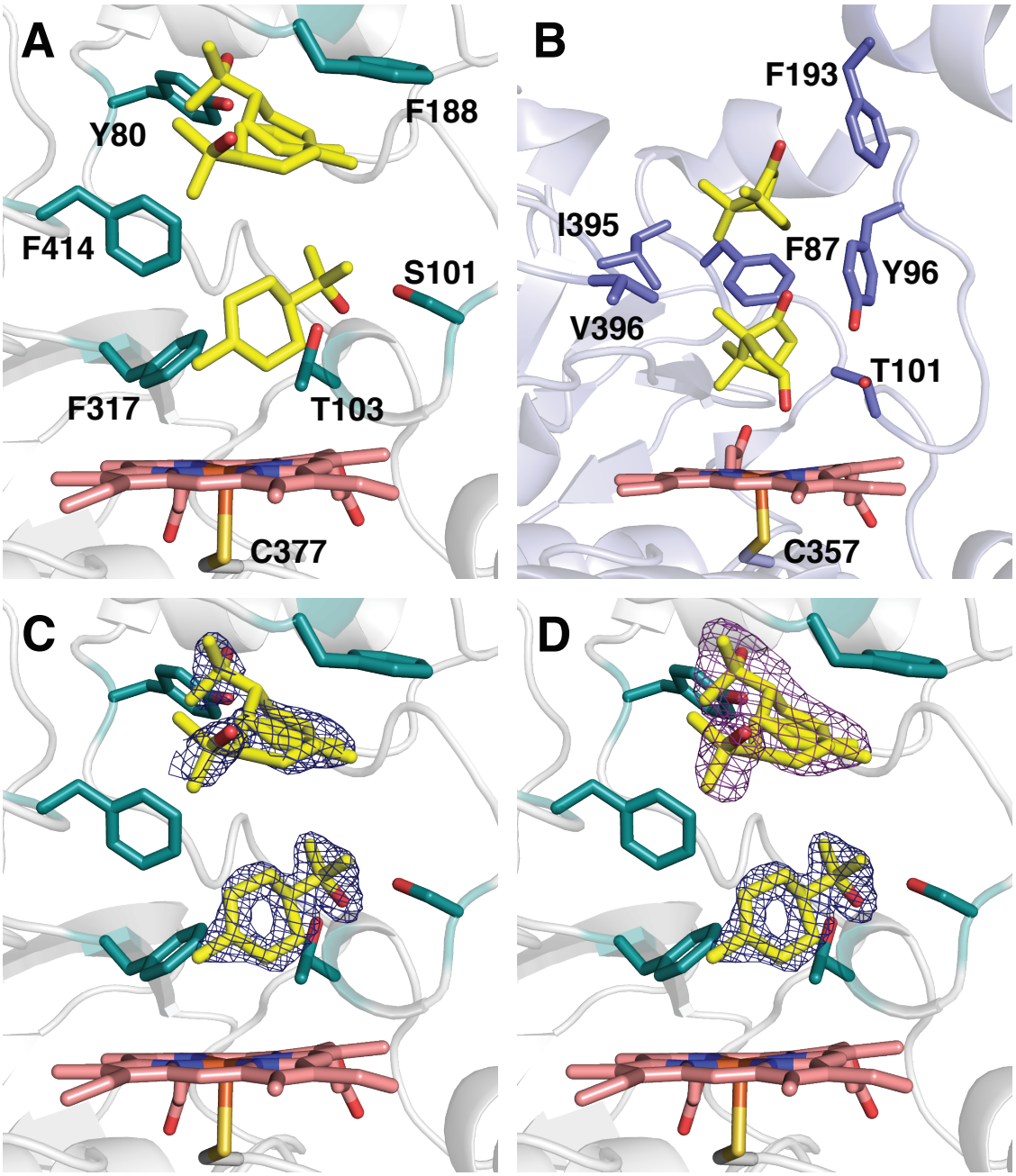

Figure 2-3. Comparison of two molecules in active sites. (A) Two molecules of α-terpineol are bound in our crystal structure of P450terp. Residues contacting these molecules are shown. The bottom substrate (terp1) has one conformation while the top substrate (terp2) has two alternate conformations. (B) Active site of P450cam in complex with Pdx is shown with one molecule of product, 5-*exo*-hydroxycamphor, in the active site, and one molecule of substrate, camphor, above it. The residues contacting these molecules are shown. (C) Electron density for the two molecules of α-terpineol is shown at 2σ for terp1 and 1σ for terp2 of a $2F_O$-F_C map. (D) Polder map for the second substrate is shown in dark purple at 5σ.

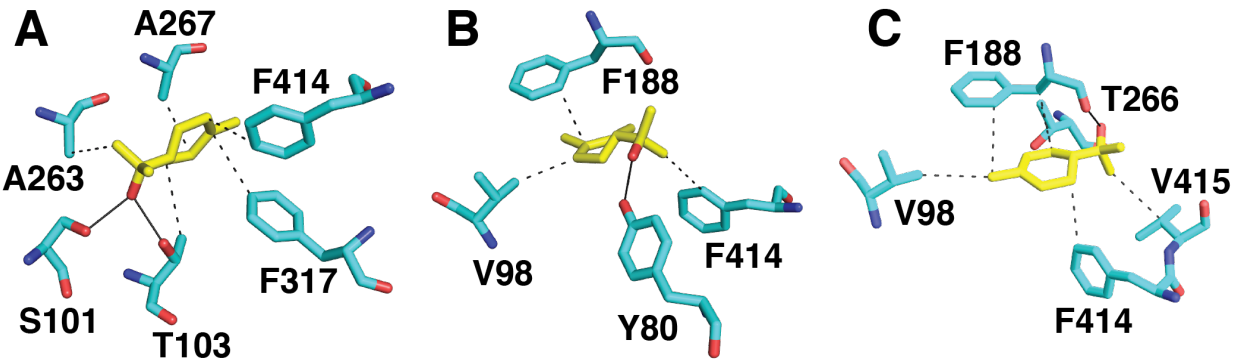

Figure 2-4. Residues contacting substrate molecules. (A) The residue environment around terp1. (B) The residue environment around a conformation of terp2, referred to as terp2a in Table 2-2. (C) The residue environment around a conformation of terp2, referred to as terp2b in Table 2-2. Solid lines represent hydrogen bonds, and dashed lines indicate nonpolar interactions.

Table 2-2. Residues interactions with substrate molecules. terp1 is the substrate molecule in the primary binding site, and the two conformations of terp2 are split into terp2a and terp2b.

		Residue #	Amino Acid	Distance (Å)
terp1	Nonpolar	103	Thr	3.87
		263	Ala	3.88
		267	Ala	3.59
		317	Phe	3.87
		414	Phe	3.81
	Hydrogen bonds	101	Ser	2.85
		103	Thr	2.75
terp2a	Nonpolar	98	Val	3.56
		188	Phe	3.55
		414	Phe	3.92
	Hydrogen bonds	80	Tyr	2.34
terp2b	Nonpolar	98	Thr	3.92
		188	Phe	3.62
		266	Thr	3.76
		414	Phe	3.57
		415	Val	3.83
	Hydrogen bonds	188	Phe (backbone)	2.90

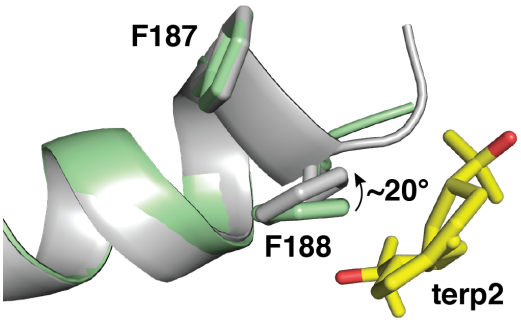

Figure 2-5. Rotation of F188. Substrate free (green) (1CPT) and substrate bound (grey) structures were aligned to F187. F188 is rotated ~20° relative to the plane of the phenyl ring in the substrate free structure to better contact terp2.

Guided by this structure and the hypothesis that the second substrate stabilizes the active site enabling efficient catalysis, several active site mutants were generated: a single mutant F188A to weaken binding of the secondary molecule, a double mutant S101A/T103A to disrupt the primary, and a triple mutant S101A/T103A/F188A to perturb both sites (Figure 2-6). The structure of the single mutant F188A co-crystallized with substrate using the same conditions as those for WT was determined to 2.2 Å (Table 2-1). While the Cα-RMSD between WT and the F188A variant is 0.09 Å and terp1 remains similarly positioned within the active site, there is no electron density in the corresponding secondary site of F188A for substrate or any other small molecule (Figure 2-7B). Additionally, albeit at slightly lower resolution, the B-factor for terp1 in F188A also increases to 65.9 $Å^2$ from 35.2 $Å^2$ in WT consistent with the hypothesis that the second substrate molecule serves to stabilize the primary molecule for hydroxylation (Figure 2-7A). Upon reprocessing the WT structure at a lower, comparable resolution of 2.2 Å, the B-factor remains essentially unchanged at 35.3 $Å^2$, which supports the conclusion that the higher B-factor in the F188A structure results from the loss of the second α-terpineol.

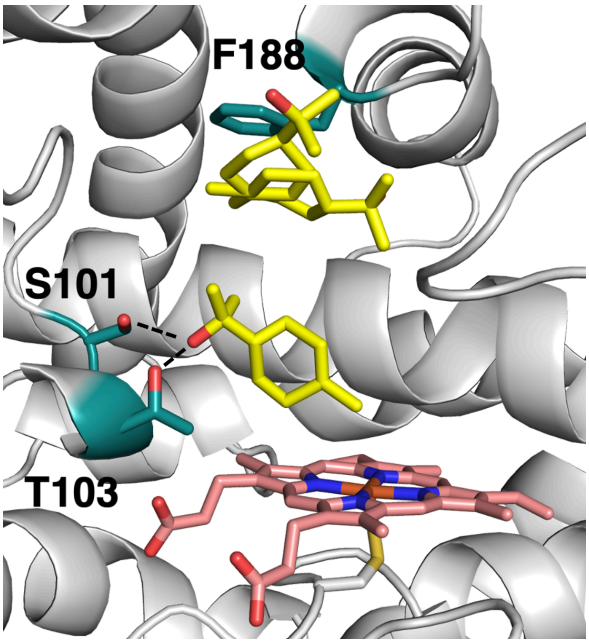

Figure 2-6. Active site mutations. Mutated residues of P450terp are shown in teal. Heme is in pink, and substrates, α-terpineol, in yellow. Each residue was mutated to alanine. The side chain oxygen of T103 is 2.7 Å from the oxygen of the first substrate. The side chain oxygen of S101A is 2.8 Å from the oxygen of the first substrate. There were 3 variants made of P450terp: S101A T103A, F188A, and S101A T103A F188A. The F188A variant expressed just as well as WT, but the variants with S101A and T103A expressed rather poorly. Thr103 makes an H-bond with Glu77 of the B loop, so in mutating it to alanine, the absence of the H-bond may destabilize the heme pocket.

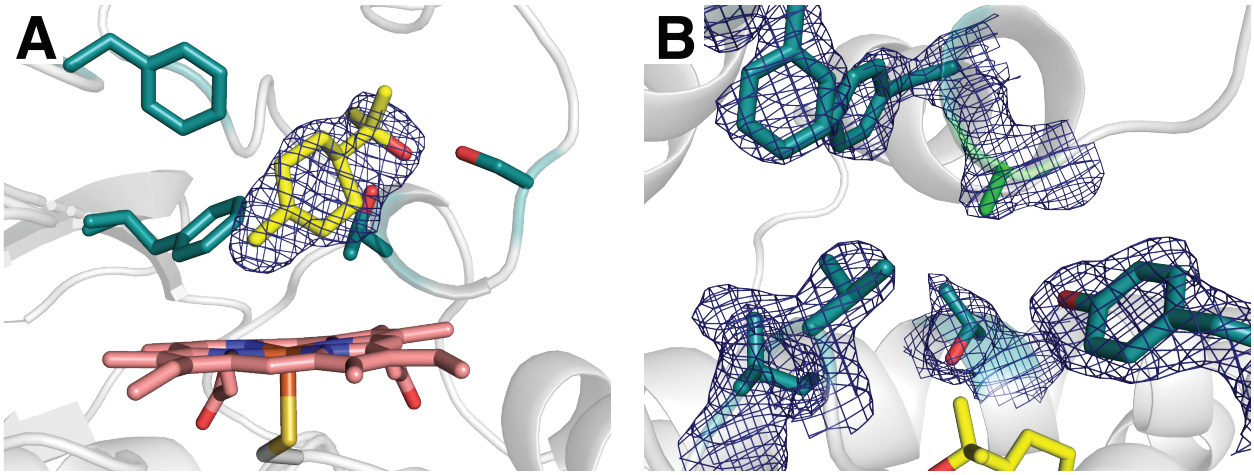

Figure 2-7. Crystal structure of P450terp F188A. (A) Electron density for terp1 is shown at 1σ of a $2F_O$-F_C map. (B) The second substrate site is shown with electron density at 1σ. The mutation of Phe188 to Ala is shown in green. No density is observed in the second site.

Substrate Binding

In the absence of substrate, the UV-vis spectra of all four variants are nearly identical, displaying similar Soret maxima and Q-band profiles (Figure 2-8A). However, in the presence of 1 mM α-terpineol (~300-fold excess), the variants show substantially different distributions of Soret intensities corresponding to different populations of their nominal low- (418 nm) and high-spin (396 nm) states. The origin of the differences in the relative low-spin and high-spin populations is challenging to interpret, and may be due to changes in the substrate dissociation constant, presence of an axial ligand, spin-state equilibria, or some combination of these factors. As one may expect, wild-type (WT) displays a complete shift to its respective high-spin species similar to WT P450cam, indicating a complete occupation of the active site by α-terpineol. The single mutant F188A, which was designed to disrupt the secondary site, exhibits an incomplete shift, ~70% (Figure 2-8B), where even at high substrate concentrations (10 mM), the Soret band does not fully convert to the substrate-bound spectrum (Figure 2-9). Since spectral changes of the Soret band directly report on perturbations to the heme cofactor upon substrate binding, the decrease in the high-spin state formation reflects a decrease in the occupancy and/or greater mobility of the primary substrate position compared to WT. Furthermore, from the X-ray crystal structure, it is known that mutation of Phe188 weakens the binding of α-terpineol in the second position, which in combination with the incomplete spin-shift, suggests that the binding ability of terp2 directly impacts the binding ability of terp1. The S101A/T103A variant displays a smaller Soret shift than the F188A mutant. Presumably, the elimination of hydrogen bonding interactions with the primary substrate molecule greatly decreases the affinity for the first site. Based on the crystal structure of substrate-bound WT P450terp, interactions with several hydrophobic residues nearby, Phe414 and Phe317, help retain some favorable interactions along with an unperturbed secondary site, which serves to entrap terp1 and leads to the observed partial binding. As expected, the S101A/T103A/F188A variant displays the smallest high spin shift as critical contacts

for both sites are eliminated (Figure 2-8C). Table 2-3 lists the maximal high spin percentages of each of the variants.

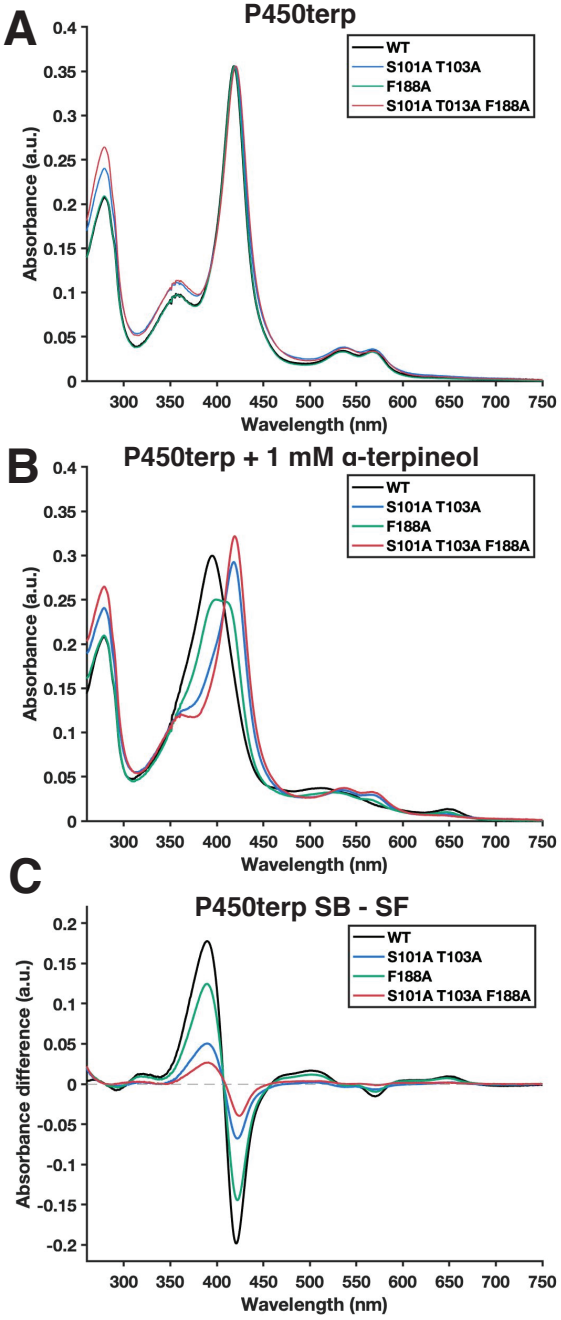

Figure 2-8. Absorbance spectra of P450terp variants in the (A) absence and (B) presence of 1 mM α-terpineol in 50 mM KPi pH 7.4. (C) Difference spectra of P450terp variants of substrate-bound (SB) minus substrate-free (SF).

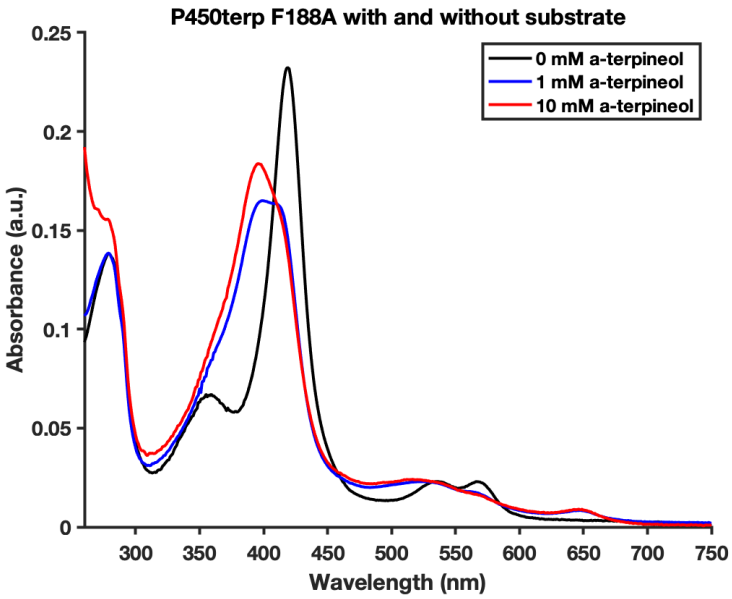

Figure 2-9. Absorbance spectra of P450terp F188A in the presence of 0 mM, 1 mM, and 10 mM α-terpineol. The increase of absorbance around 260-280nm is due to the increase of α-terpineol. Even in the presence of ~300 fold excess α-terpineol, P450terp F188A does not shift completely to high spin. Instead, it shifts ~87% relative to WT. Allowing time for the P450 and substrate to equilibrate did not increase the extent of the spin shift. In general, time did not play a role in the observed spin shifts of any of the variants or WT.

Table 2-3. Table of K_S and maximal high spin percentages for the four P450terp variants. "–" denotes no experiment for K_S was performed as the spectral shift is not high enough for reasonable calculations.

P450terp	**K_S**	**Maximal HS**
WT	2.67 ± 0.18	100%
S101A T103A	–	28.3%
F188A	36.1 ±1.4	70.1%
S101A T103A F188A	–	14.9%

Another important point of comparison is the differences between the UV-vis absorption spectra of the different variants. The Soret maxima of WT and F188A remain identical at 418 nm in the absence of substrate, while the variants containing S101A and T103A display shifted maxima at 419 and 421 nm in the double and triple mutants, respectively, indicating a change in their ground state electronic structure. Moreover, in the canonical carbon monoxide bound (CO-bound) P450 spectra, P450terp WT and the F188A variant exhibit P450-type spectra while the

S101A/T103A/F188A variant displays the “inactive” P420-type spectrum (Figure 2-10). In the presence of substrate, the S101A/T103A variant is P450-type, and in the absence of substrate is P420. As the S101 and T103 residues are directly adjacent to the heme, it is likely that mutation of these residues does not only perturb substrate binding but also affects the stability, and therefore electronic structure, of the heme. It seems that binding of substrate in this case helps to stabilize the heme pocket in the S101A/T103A variant. This is further evidenced upon examination of the spectra of the reduced species prior to CO binding where the Soret band of the S101A/T103A variant and triple mutant red-shifts to ~425 nm and the Q-bands are sharp and distinct from the broad profiles displayed by WT and F188A (Figure 2-10A and 2-10B). Both the shift in the Soret as well as the sharp α and β bands at 528 and 560 nm, respectively, of the double and triple mutants are consistent with spectral features observed for pressure-inactivated ferrous P450 (P420) species as well as low-spin ferrous 6-coordinate cytochromes *c* and b_5.[30–32] This similarity supports the assignment of the reduced state of these P450terp variants as low-spin and/or hexacoordinate. It is also, therefore, interesting to note that these results are consistent with previous work that demonstrates that a histidine ligand is not necessary for formation of the “inactivated” P420 species.[33]

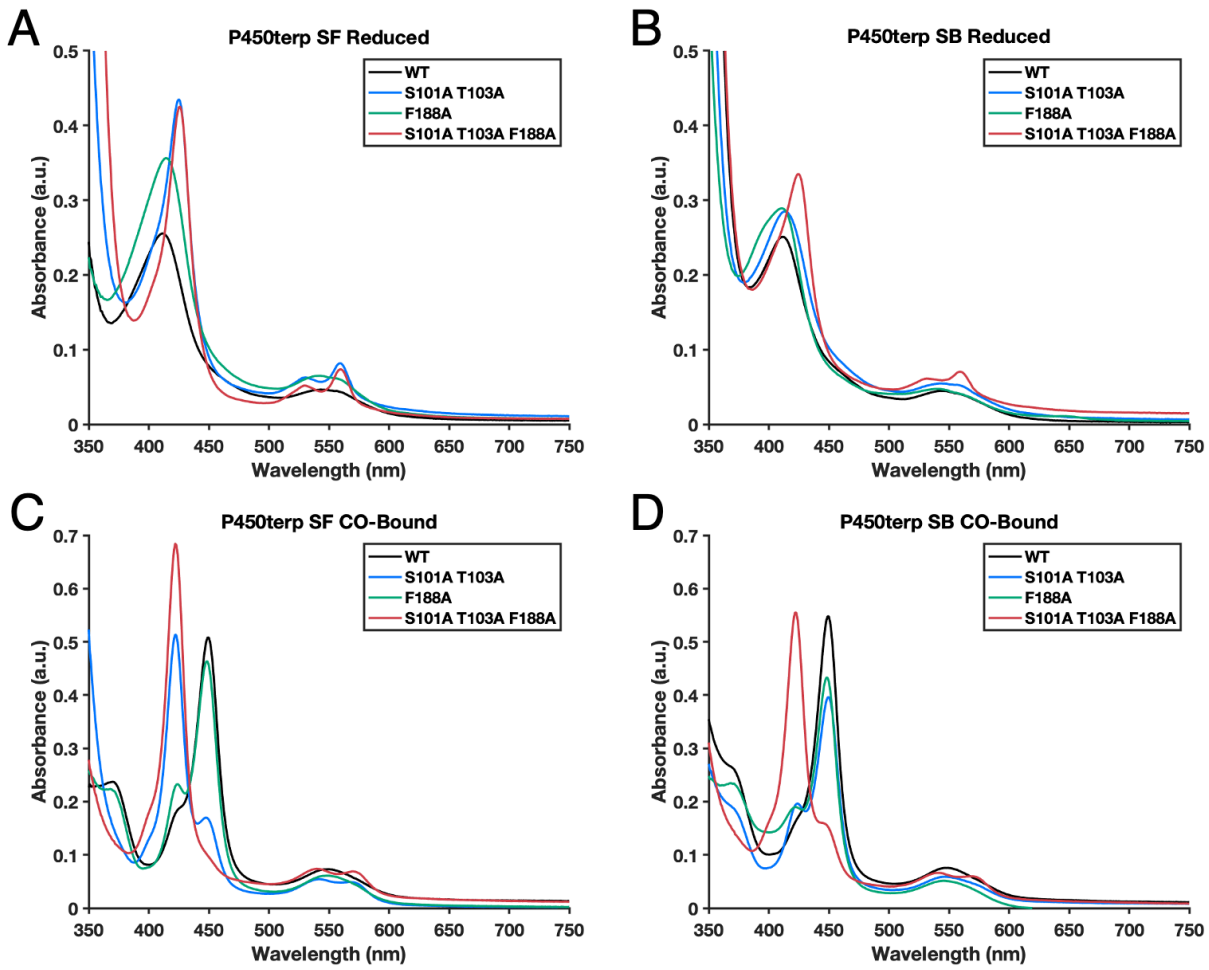

Figure 2-10. Absorbance spectra of reduced and carbon monoxide bound (CO-bound) P450terp variants. P450terp in the (A) absence and (B) presence of 1 mM α-terpineol plus an excess of dithionite. WT is 3.0 µM, F188A is 4.1 µM, S101A T103A is 4.0 µM, S101A T103A F188A is 3.3 µM in the reduced spectra. P450terp in the (C) absence and (D) presence of 1 mM α-terpineol plus an excess of dithionite in CO-bubbled buffer to generate the CO-bound P450. WT is 4.6 µM, F188A is 4.5 µM, S101A T103A is 3.8 µM, S101A T103A F188A is 4.0 µM in the CO-bound spectra.

For the substrate free spectra (Figure 2-8), WT and F188A exhibit a Soret maxima at 418 nm, while S101A T103A and S101A T103A F188A display Soret maxima at 419 nm and 421 nm, respectively. Thr103 H-bonds with Glu77 on the B loop, so it is logical that the T103A mutation results in a perturbation of the heme pocket. Even in the substrate bound spectra, the variants with altered heme pockets containing S101A and T103A, the Soret maxima shifts to 418 nm in

the presence of substrate. It appears that the destabilization of those mutations might be somewhat stabilized by substrate ordering of the active site.

The reduced spectra of P450terp clearly show a difference between the variants with and without the mutations of S101A and T103A (Figure 2-10A and 2-10B). The Soret maxima are around 410 nm for WT and F188A, while they are around 420 nm for S101A T103A with and without F188A. The Q bands of the variants with S101A and T103A suggest reduction has indeed occurred. These data suggest that the S101A and T103A mutations alter the heme pocket in some capacity. These sharp Q-band features and the ratio of the α/ β bands is observed in other reduced heme-proteins like cytochrome c. However, in the presence of substrate, the spectra of the variants with the S101A and T103 mutations become different upon reduction. The Soret maxima of the S101A T103A variant is ~410 nm and displays broad Q bands, while the S101A T103A F188A variant has changed much less and resembles the substrate free spectra, supporting the assignment that this species lacks the ability to bind substrate binding. The difference of the F188A mutation suggests that the second substrate helps to order the heme pocket, as the reduced spectra have changed.

The CO-bound spectra exhibit a similar pattern where WT and the F188A variant are mostly P450, while the variants with the S101A and T103 mutations are mostly P420 in the absence of substrate. These changes again can be attributed to changes in the heme pocket. The exact origin of P420 remains debated, but a recent paper by our group demonstrates that P420 can be generated without the requirement of a histidine ligand to replace the thiolate ligand of the heme and this more likely do to disordering of the heme pocket.[33] This is supported by the fact that in the presence of substrate, the S101A T103A variant is mostly P450 while the S101A T103A F188A variant remains P420, suggesting that the second substrate might help to order the heme pocket.

These spectra also corroborate our coupling efficiency data, as WT, F188A, and S101A T103A variants all had appreciable coupling, and are mostly P450 in the presence of substrate. The S101A T103A F188A variant had almost nonexistent coupling and is mostly P420.

Binding Affinities of α-Terpineol

To test the hypothesis that substrates act cooperatively in the P450terp active site, the binding affinities of α-terpineol to WT and F188A were measured by UV-vis spectral titrations and isothermal titration calorimetry (ITC). From the spectral titrations, a spectral binding constant, K_S, was determined to be 2.67 μM for WT and 36.1 μM for the F188A variant (Figure 2-11 and Table 2-4). More importantly, however, the data for WT were not well represented by a one- or two-site binding model (Equations 2-1 and 2-2), which contain the underlying assumption that each site exhibits a fixed and invariant affinity, where B_{max} is the maximum specific binding, and K_D is the equilibrium dissociation constant, Y is fraction of sites occupied by the substrate, and X is the concentration of substrate. Double-reciprocal plots of the data made this inadequacy obvious as the substrate dependency of the WT was not linear and displayed an upward concavity (Figure 2-12). The data were instead best-fit to a binding site model utilizing a Hill-coefficient that accounts for cooperative interaction between multiple substrates (Equation 2-3), where B_{max} is the maximum specific binding, K_D is the equilibrium dissociation constant, h is the Hill coefficient, Y is fraction of sites occupied by the substrate, and X is the concentration of substrate. The fit of WT P450terp exhibited a Hill-coefficient of 1.41, where a value >1 indicates positive cooperativity, consistent with our hypothesis (Fig. 2-11G). The assumptions underlying the Hill-coefficient equation are not the most microscopically accurate representation of the binding modes occurring here. However, comparison to the F188A spectral titration still provide semi-quantitative and significant insight, as data for the mutant fit well to a one binding site model: 36.1 μM with Hill-coefficient of 1.01, indicating a lack of cooperativity (Fig. 2-11H). As previously mentioned, since

spectral titrations report on the status of the heme environment, it is therefore reasonably assumed that the obtained binding affinity of 36.1 μM reflects the diminished affinity of α-terpineol for the primary binding site, as the secondary binding site has likely been impaired.

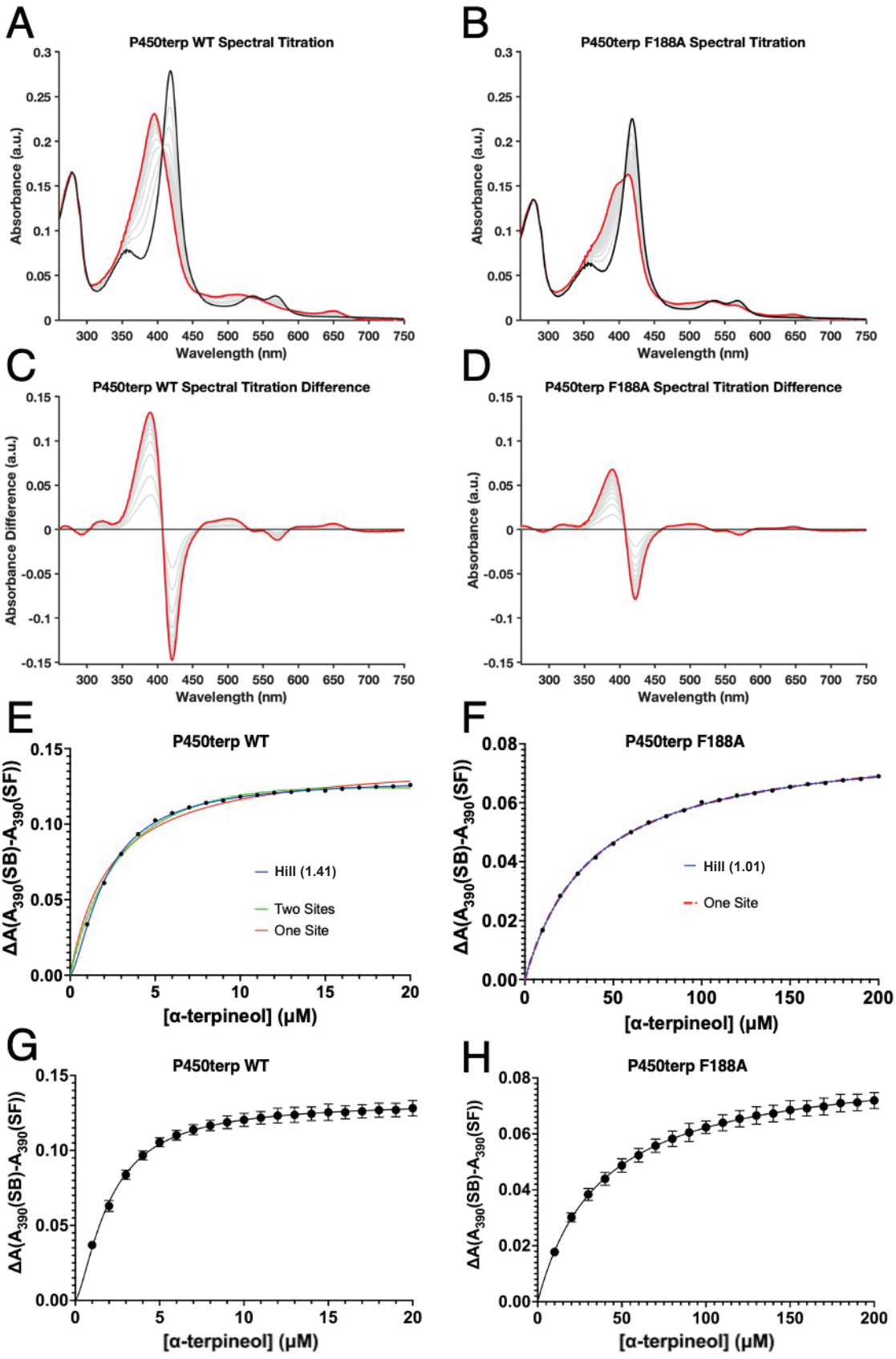
A
P450terp WT Spectral Titration
Absorbance (a.u.)
Wavelength (nm)
B
P450terp F188A Spectral Titration
Absorbance (a.u.)
Wavelength (nm)
C
P450terp WT Spectral Titration Difference
Absorbance Difference (a.u.)
Wavelength (nm)
D
P450terp F188A Spectral Titration Difference
Absorbance (a.u.)
Wavelength (nm)
E
P450terp WT
ΔA(A390(SB)-A390(SF))
Hill (1.41)
Two Sites
One Site
[α-terpineol] (μM)
F
P450terp F188A
ΔA(A390(SB)-A390(SF))
Hill (1.01)
One Site
[α-terpineol] (μM)
G
P450terp WT
ΔA(A390(SB)-A390(SF))
[α-terpineol] (μM)
H
P450terp F188A
ΔA(A390(SB)-A390(SF))
[α-terpineol] (μM)

Figure 2-11. Spectral titration data expanded. Left column: Absolute spectra of the titrations of P450terp (A) WT and (B) F188A. Black is starting, substrate free; red is final, substrate bound; grey are the intermediate titrations. Difference spectra of substrate free subtracted from each titration step of P450 (C) WT and (D) F188A. Black is starting, substrate free; red is final, substrate bound; grey are the intermediate titrations. Curves for different fits are shown for P450terp (E) WT and (F) F188A. The final curves for P450terp (G) WT substrate binding with a Hill coefficient and (H) F188A with one binding site are shown with error bars. Fits were performed in Prism. P450terp WT demonstrates a complete shift to high spin after the titration, while P450terp F188A has an incomplete shift. Even at the end of the F188A titration, the final spectrum does not fully resemble the substrate bound spectrum of the F188A variant in 1 mM α-terpineol. However, the maximum solubility of α-terpineol has different reports, but to err on the side of caution, we chose not to go above 10 mM α-terpineol. Although the data did not fully converge, P450terp WT is best fit with a Hill coefficient greater than 1, suggesting positive cooperativity. P450terp F188A gave the same results for one site binding and specific binding with a Hill coefficient, showing that there is no cooperative binding with the alteration of the second substrate binding site.

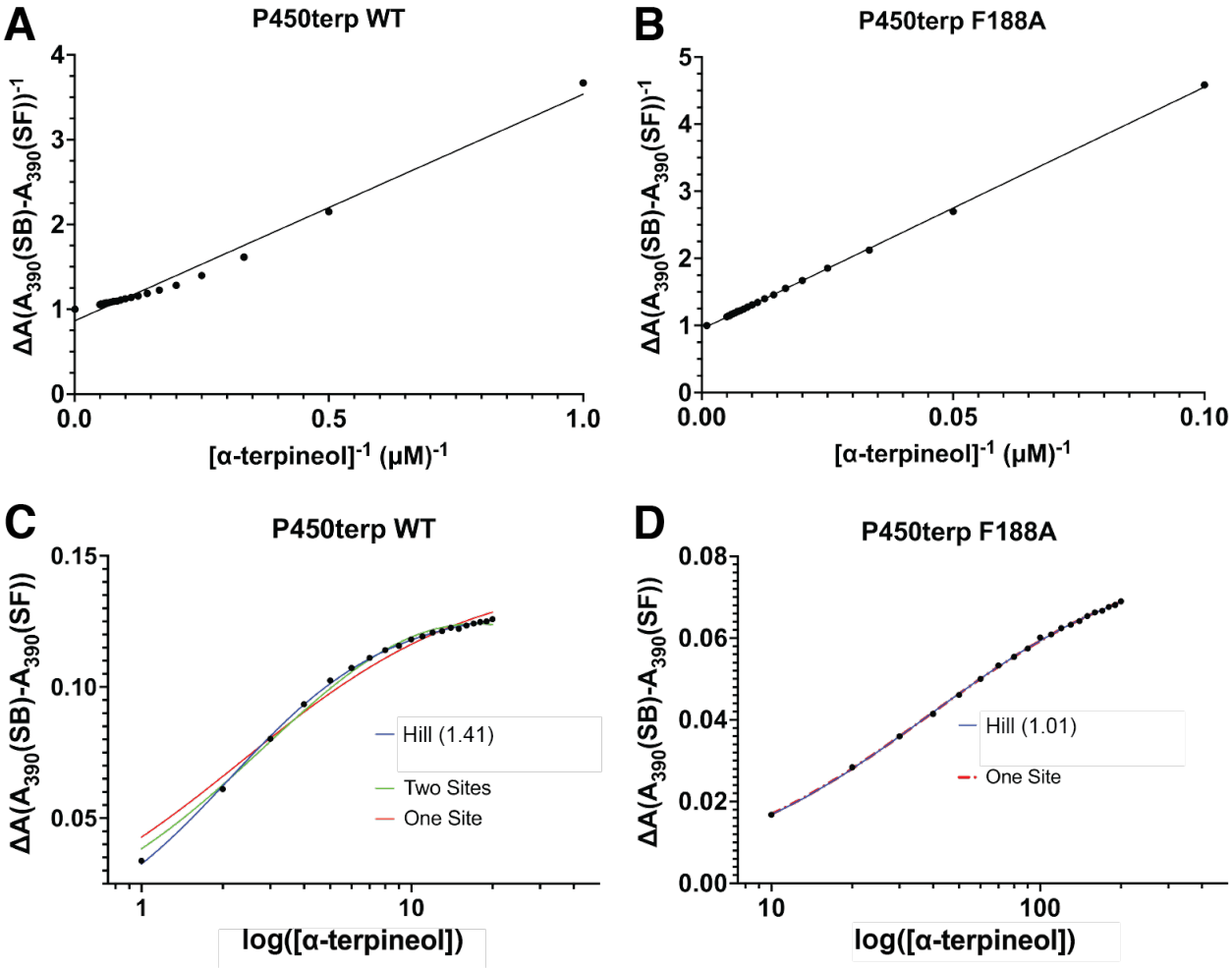

Figure 2-12. Double reciprocal and logarithmic plots of spectral titration data. (A) Double reciprocal plot of the spectral titration of P450terp WT shown with a line of best fit highlighting the upward concavity. (B) Double reciprocal plot of the spectral titration of P450terp F188A shown with a line of best fit. (C) Logarithmic plot of the spectral titration of P450terp WT fit to a one site binding model (red), two site binding model (green), and binding with Hill coefficient of 1.41 (blue). (D) Logarithmic plot of the spectral titration of P450terp F188A fit to a one site binding model (red) and specific binding with Hill coefficient of 1.01 (blue).

Table 2-4. Binding affinities of P450terp WT and F188A for α-terpineol.

P450terp	K_S (μM)	Hill Coefficient	K_{D1} (μM)	N_1 (sites)	K_{D2} (μM)	N_2 (sites)
WT	2.67 ± 0.18	1.41	1.19 ± 0.09	1.18 ± 0.06	31.2 ± 3.7	0.931 ± 0.075
F188A	36.1 ±1.4	1.01	33.6 ± 4.1	0.941 ± 0.011	–	–

$$Y = \frac{B_{max} * X}{(K_D + X)}$$

Equation 2-1. One-Site Binding Model

$$Y = \frac{B_{max1} * X}{(K_{D1} + X)} + \frac{B_{max2} * X}{(K_{D2} + X)}$$

Equation 2-2. Two-Site Binding Model

$$Y = \frac{B_{max} * X^h}{({K_D}^h + X^h)}$$

Equation 2-3. Specific Binding Model with a Hill Coefficient

Corroboration for these observations was obtained by ITC where the thermodynamic binding profiles lead to similar conclusions. The titration of WT P450terp with α-terpineol was enthalpically driven, indicated by the negative heats of enthalpy in the binding curve (Figure 2-13A). This observation contrasts with homologous P450 systems investigated by our lab, such as P450cam[34] and CYP101D1[35], that display entropically driven bindings of substrate. Additionally, each titration exhibited an unusual slow recovery to equilibrium in comparison to previous work. The data for WT were best fit to a two-site binding model with dissociation constants, K_D, of 1.19 μM and 31.2 μM, and site occupancies of 1.18 and 0.931, respectively (Figure 2-13C and Table 2-4). Again, recognizing that the assumptions of a two-site model are inadequate for a precise description of the affinities for these sites, the data were also fit to a single binding site model which provides similar results with a slightly higher error. This fit resulted in a K_D of 2.69 μM, which is consistent with our spectrally determined binding constant (2.67 μM).

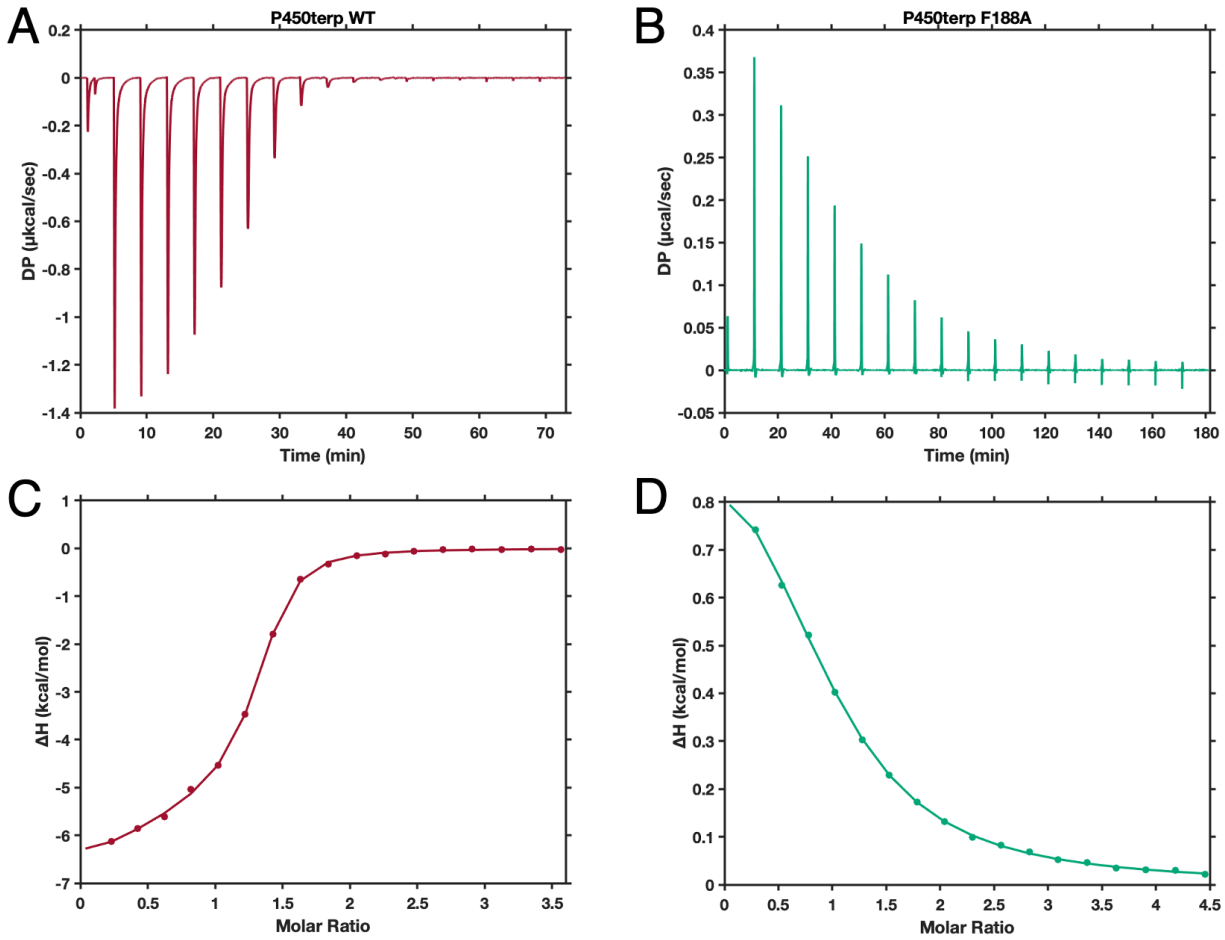

Figure 2-13. ITC data. (A) Raw heat of injections for P450terp WT with α-terpineol. (B) Raw heat of injections for P450terp F188A with α-terpineol. (C) The fit of a two-site binding model to the data of P450terp WT. (D) The fit of a one-site binding model to the data of P450terp F188A. Substrate binding in P450terp WT is enthalpically driven which is not typical of other P450s previously investigated. The F188A mutation alters the second site and removes cooperativity and as a result the data now fit well to a one-site binding model. Additionally, the binding becomes inverted (i.e. entropically driven). The data for WT were fit with both one-site binding (Equation 2-1) and two-site binding (Equation 2-2). Both yielded good fits, but two-site binding was determined to be a better fit due to a lower χ^2. The data for F188A were fit with both one-site binding (Equation 2-1) and two-site binding (Equation 2-2). However, convergence was only achieved with the one-site binding model.

ITC titrations were performed with the F188A variant, and the data became rather complicated. With a reduced affinity for the second site, it was observed that substrate binding becomes apparently entropically driven (Figure 2-13B). Entropically driven binding modes are generally attributed to desolvation of hydrophobic substrates as they enter the active site which is to be expected of terpenoid compounds like camphor and α-terpineol.[36] Alteration of the second

site exposes features associated with the affinity of a weakened active site. However, complication in the data interpretation arises upon inspection of the baseline recovery of the titration. The F188A variant displays an enthalpic slow recovery phase post-injection similar to WT (Figure 2-14). This slow re-equilibration phase caused difficulty in peak integration and proper assignment of a baseline for the titration. Inclusion of this slow feature into the background results in a well-defined binding curve that is best fit to a single binding site model with a K_D of 33.6 μM (Figure 2-13D and Table 2-4) matching the K_S of 36.1 μM for F188A. The reasoning for this inclusion is based on the assumption about the mechanism of binding and the origin of the slow re-equilibration phase. It is assumed that binding to the primary site is observed as the positive feature followed by the enthalpic stabilization of the primary site upon a cooperatively enhanced affinity for a debilitated second site. Therefore, subtraction of this enthalpic contribution reveals a binding constant for the active site in accordance with a K_S that reports directly on interaction with heme.

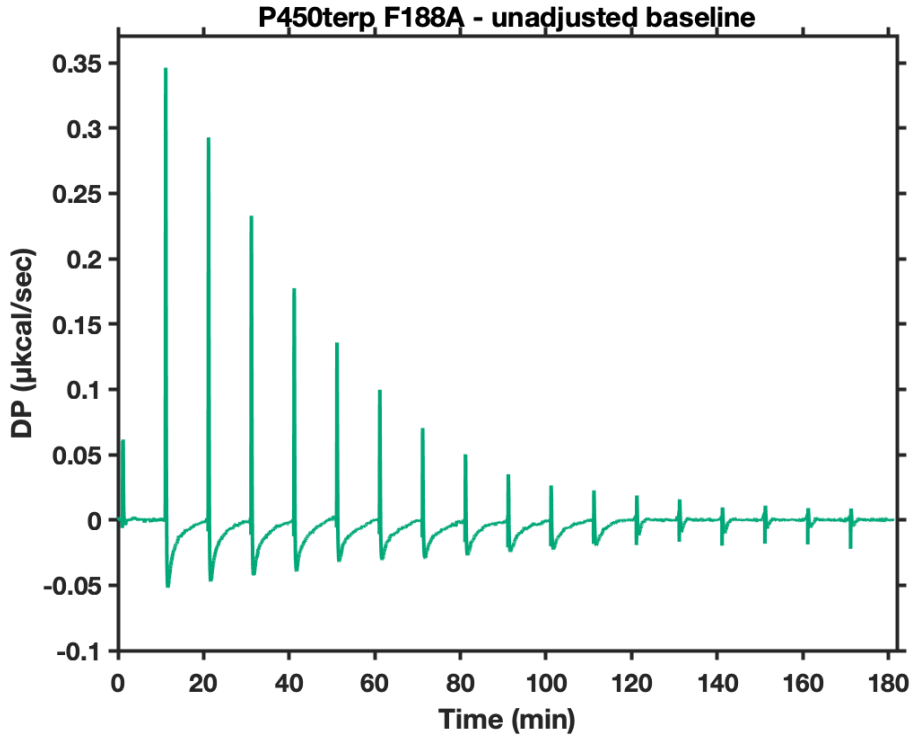

Figure 2-14. ITC of P450terp F188A without the adjusted baseline. There is an enthalpic relaxation phase after each injection. This same injection phase can be seen in WT (Figure 2-14) and is presumably part of the protein. An explanation for why the baseline was adjusted can be found in the main text.

Turnover and Coupling Efficiency

The structural and spectral/thermodynamic binding studies demonstrated the existence and impact of the second substrate site on active site stabilization. It is therefore reasonable to ask whether there is any influence of the secondary molecule on turnover performance. As discussed in the introduction, Class I P450 systems require the shuttling of electrons from a molecule of NADH to and between three independent soluble proteins for turnover. As the rate limiting step of P450 catalysis is the first electron transfer,[37] NADH consumption assays provide an indirect but simple measure of activity (Scheme 2-1). Further, the ratio of NADH molecules consumed to the amount of product formed allows for the coupling efficiency to be determined and related to the rate of reactivity from the consumption assays. P450cam displays a rapid rate of NADH consumption, ≈1000 min^{-1}, and an exemplary coupling efficiency of near 95%.[38,34] Due

to the nearly complete shift to high-spin upon camphor binding in P450cam, it is tempting suggest a relationship between the degree of high-spin shift and coupling efficiency of enzyme turnover. However, it is important to keep in mind that systems such as CYP101D1 display a similar NADH consumption rate and coupling efficiency to P450cam, but does not demonstrate a complete high-spin shift.[39]

P450terp WT has a high turnover rate of 670 min^{-1} comparable to that of P450cam and CYP101D1.[39] The coupling efficiency of P450terp was determined by substrate depletion monitored by GC/MS (Figures 2-15, 2-16, 2-17, 2-18), revealing that WT is also almost perfectly coupled at 96.9%, which may be expected as both P450cam and P450terp fulfill the same biological role. Additionally, as expected, the S101A/T103A/F188A variant exhibited negligible activity, 0.193 min^{-1} and accordingly is nearly completely uncoupled at 3.7% (Table 2-5).

Intriguingly, both the S101A/T103A and F188A variants showed moderate rates of NADH consumption. However, interpretation of their rates is complicated as they do not exhibit simple zero order kinetics possibly indicating a change in the rate-limiting step (Figure 2-15). Due to the complexities of determining the origin of this change, I report the qualitative observation that both rates are slow compared to WT, and the S101A/T103A variant is faster than the F188A variant. The S101A/T103A variant displays a coupling efficiency of 70.6% while F188A remains 51.2% coupled. The increased coupling efficiency of S101A/T103A compared to F188A highlights the importance of the secondary binding site for not only substrate binding but also for catalytic efficiency.

Table 2-5. NADH turnover rates and coupling efficiencies for P450terp variants. The S101A T103A and F188A variants display complicated kinetics for NADH consumption, so their rates are not reported. Examples of these kinetics can be found in Figure 2-16.

P450terp	NADH Turnover (min^{-1})	Coupling Efficiency (%)
WT	676 ± 27	97 ± 1
S101A T103A	–	71 ± 1
F188A	–	51 ± 1
S101A T103A F188A	0.193 ± 0.045	3.7 ± 1.1

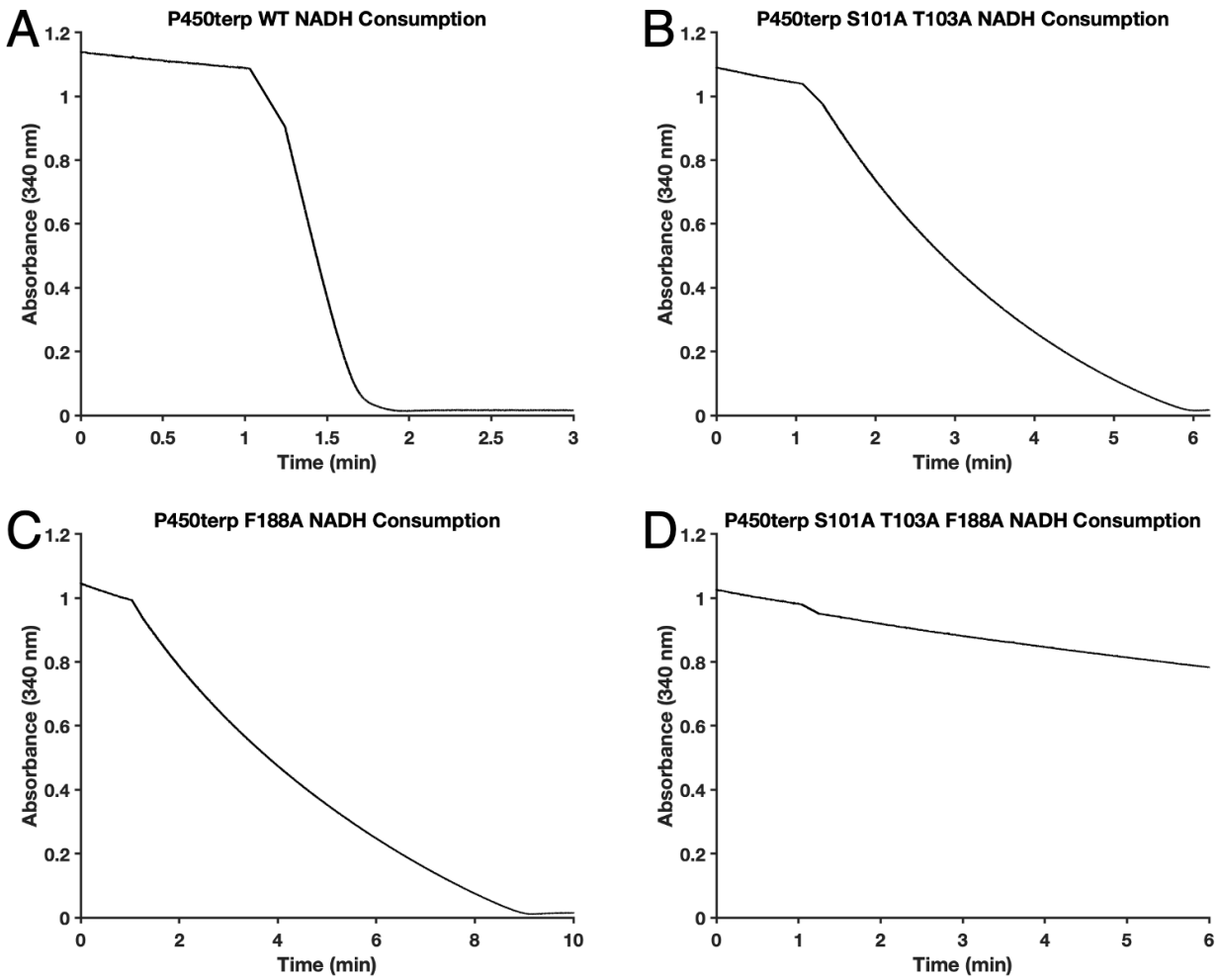

Figure 2-15. NADH consumption spectral traces. Absorbance traces at 340nm, monitoring the consumption of NADH with the P450terp (A) WT, (B) S101A/T103A, (C) F188A, and (D) S101A/T103A/F188A variants. The rates for WT and S101A/T103A/F188A can be fit to zero order, but not S101A/T103A and F188A.

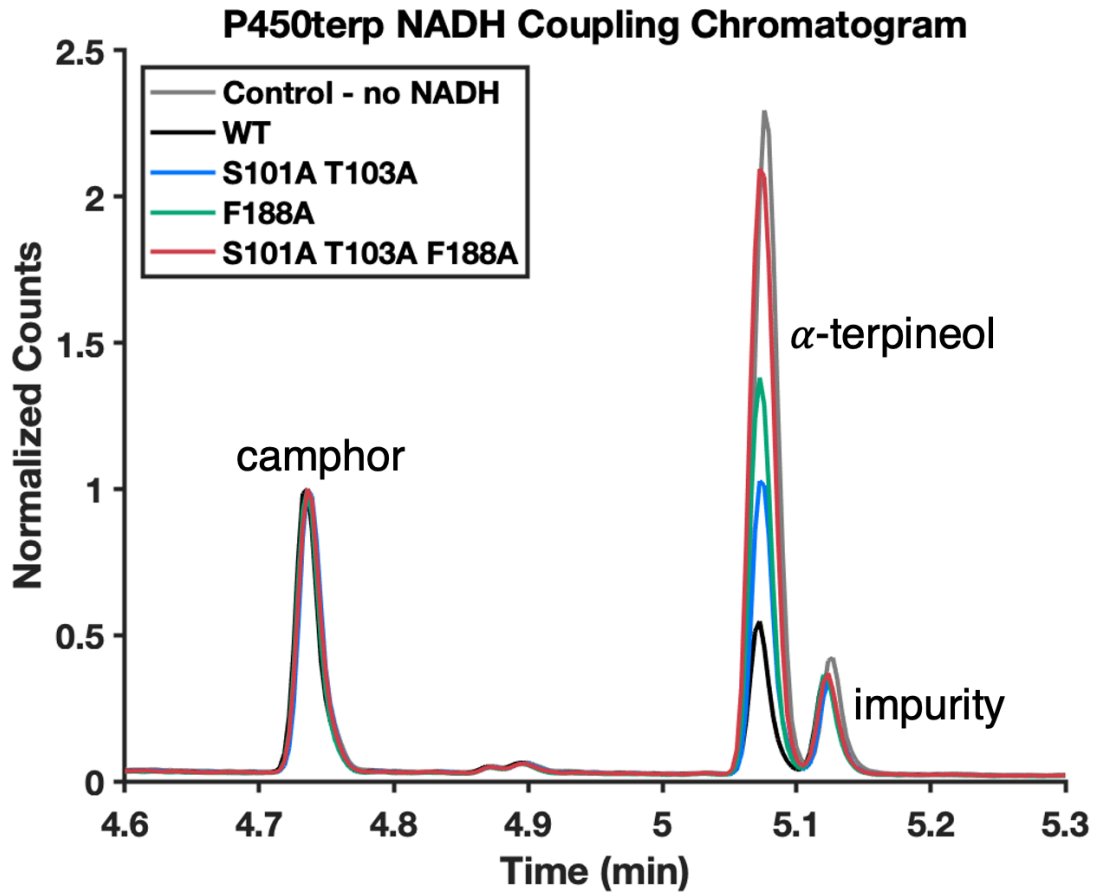

Figure 2-16. NADH coupling chromatograms with the 4 variants. All chromatograms are normalized to the camphor peak employed as an internal standard. Additionally, there is an impurity in the α-terpineol source. This impurity is noted by the manufacturer with a purity of 84% α-terpineol. The impurity peak is indeed about 16% of the total area of the control α-terpineol peak. A search of the NIST mass spectra database for the impurity peak (Figure 2-18) does not yield an exact match but does return isomers of α-terpineol. Throughout the reactions, the impurity peak area remains unaffected, indicating that the impurity or isomers of α-terpineol are not being metabolized by P450terp during the turnover assays.

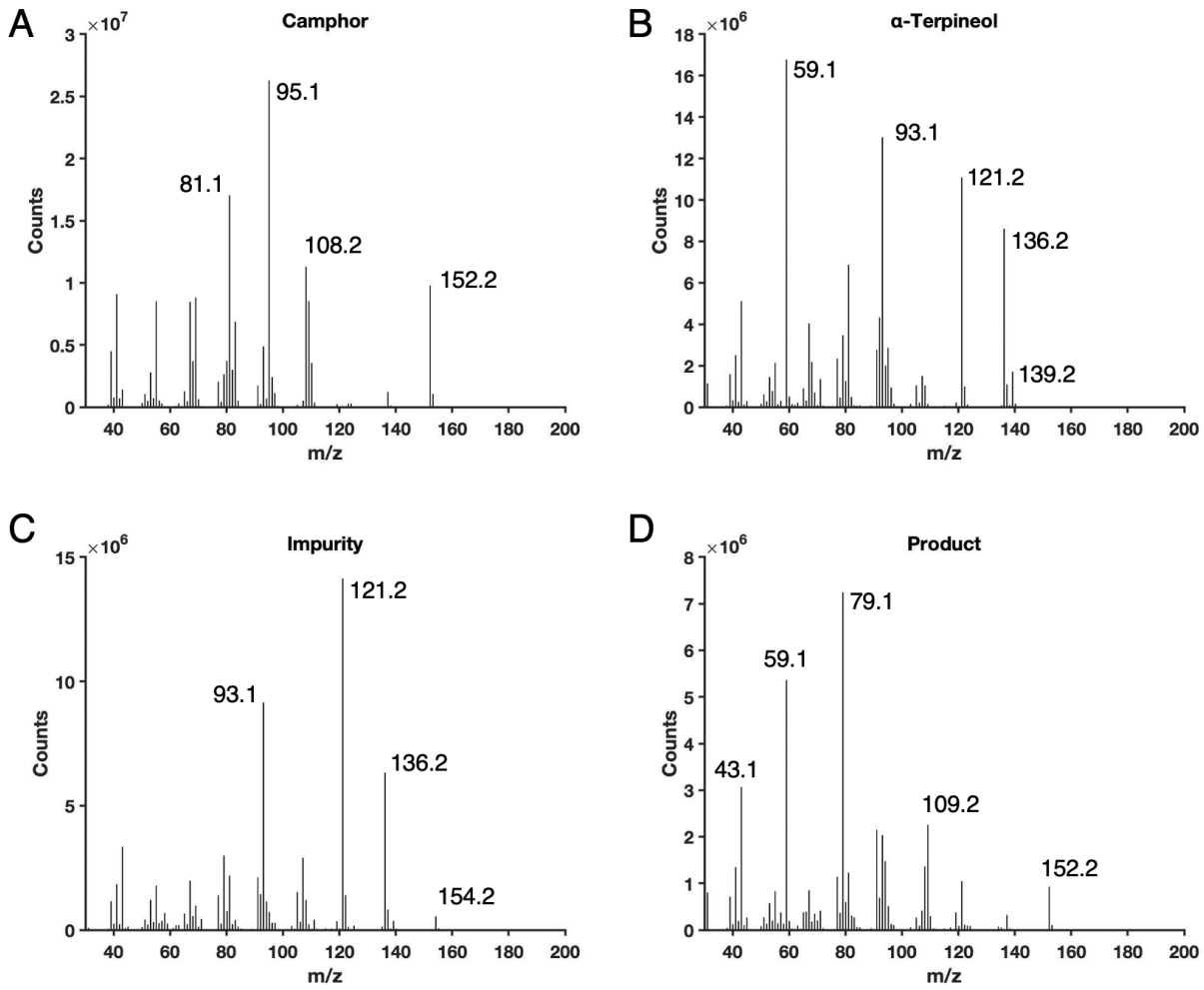

Figure 2-17. Mass spectra of the NADH coupling assays. These are the 4 mass spectra of the corresponding 4 peaks that emerge from the chromatograms: (A) camphor, (B) α-terpineol, (C) impurity, and (D) product. The masses of relevant fragmentations are shown. The camphor and α-terpineol spectra match well with their respective NIST database mass spectra reports. As previously mentioned, the impurity closely matches isomers of α-terpineol, but its exact identity is unknown. Additionally, in cases where the product peak could be identified, isomers are found of 7-hydroxy-terpineol but its identity is not definitive by its mass spectrum alone, and while library searches reveal isomers of the product with similar masses, they exhibit different fragmentation patterns.

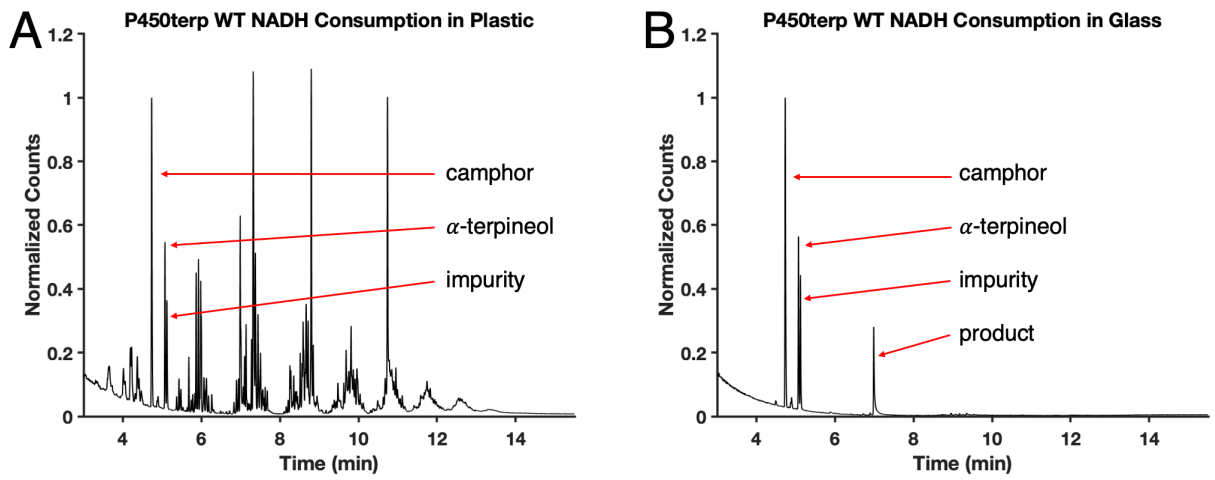

Figure 2-18. Differences in tubes for NADH coupling. The full chromatograms of NADH coupling assay are shown in (A) plastic and (B) glass. Product emerges at about 7 minutes. Plastic microcentrifuge tubes were used due to better separation by centrifugation of the aqueous and organic layers. However, glass tubes were used in several cases and as controls and were not able to be rapidly centrifuged, and therefore did not result in a good separation of layers in the extraction. Importantly, spectra of the chromatograms derived from experiments performed in glass demonstrate that there are only 4 chemicals in the reaction mixture. Further, due to the multiple hydroxyl groups of the product, solubility in DCM may also be affected and reduce extraction efficiency.

Interactions with Linalool

Given that our lab has worked with a number of P450s that use terpenes as substrates, I wanted to see if P450terp could possibly bind or turnover other terpene molecules. The two terpenes I tested were camphor and linalool, which are used in the P450cam and P450lin systems, respectively. The addition of camphor to P450terp did not cause a spectral shift, but the addition of linalool did induce an almost complete conversion to high-spin (Figure 2-19). The shift to high-spin indicates that linalool is indeed binding in the active site of P450terp. Linalool is a more flexible terpene, and thus it is reasonable to think that it could better fit into the open active site of P450terp.

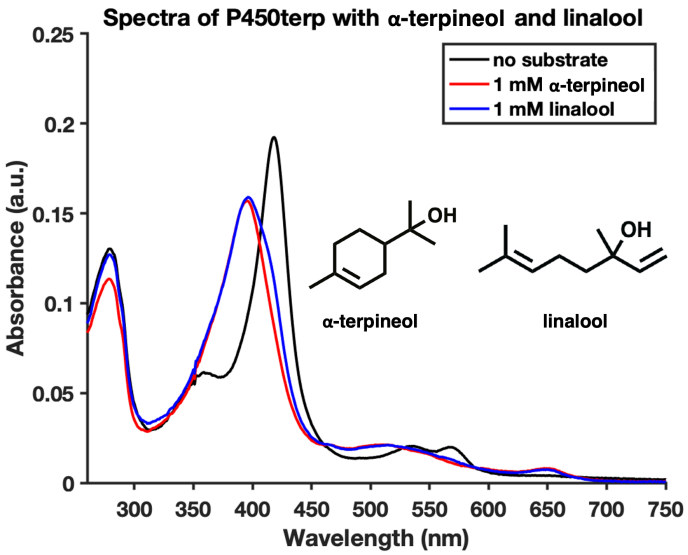

Figure 2-19. Spectral change of P450terp upon addition of linalool. P450terp was added to 50 mM KPi pH 7.4 to a concentration of 1.6 µM.

Given that P450terp could bind linalool in some capacity, I wanted to test if NADH consumption was possible with linalool as a substrate. The NADH consumption was carried out as previously done, and P450terp could indeed turnover linalool (Figure 2-20) at a rate of 577 min^{-1}, which is very close to the rate for turnover of α-terpineol (670 min^{-1}). The kinetics were best fit as zero order, which suggests there was no change in the rate limiting step.

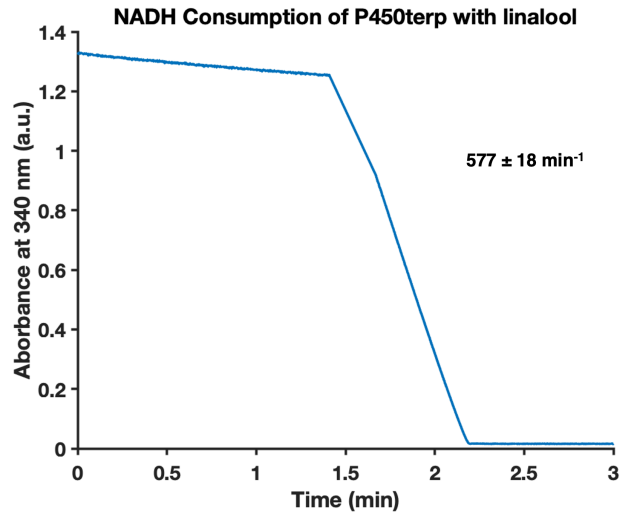

Figure 2-20. NADH consumption assay of P450terp with linalool. The consumption of NADH was monitored at 340 nm. The reaction mixture contained 0.5 µM P450terp, 5 µM Tdx, and 0.5 µM TdR in 50 mM KPi at room temperature. 2 µL of 185 mM NADH was added to a final concentration of 370 µM to collect the background rate. 20 uL of 10 mM linalool was added to initialize turnover.

Given that linalool induced a near-complete shift to high-spin in P450terp, I wanted to see whether or not linalool is bound in the second site, as α-terpineol does. Thus, a crystal structure of P450terp co-crystallized with linalool was solved to 2.36 Å (Figure 2-21 and Table 2-6). There was only one molecule of linalool bound in the active site, and there was no density for any molecule, linalool or water, near F188 in the second substrate binding site. However, even with the apparent lack of linalool in the second site, the NADH consumption trace looks similar to that of P450terp WT with α-terpineol, and not like that of P450terp F188A with α-terpineol. The kinetics of NADH consumption remain pseudo-zero order. Perhaps P450terp WT with an intact second site is better equipped to handle substrates, even non-native ones, than the weakened F188A variant. As a whole, the crystal structure of P450terp bound to linalool was still open, and there were not any major changes in the rest of the structure. The positioning of F188 resembled that of the substrate-free structure, and not was not rotated like in the α-terpineol-bound structure (Figure 2-5). Since it seems that P450terp exhibits an open structure and thus has a more open active site, P450terp can accommodate other exogenous terpenes. P450terp might be a better target for bioengineering enzymes as it might have a broader substrate range.

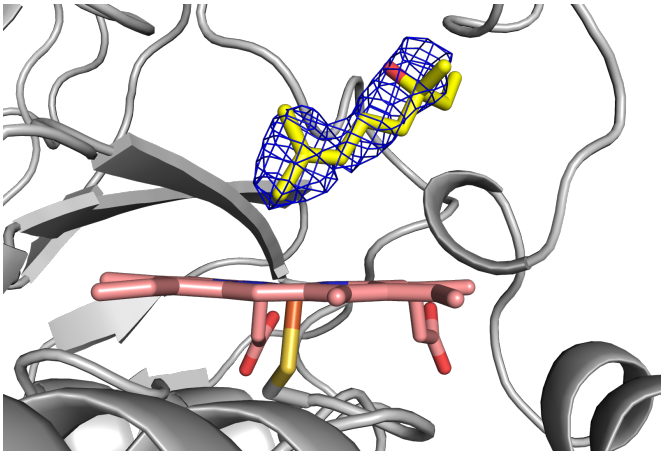

Figure 2-21. Linalool bound in the active site of P450terp. Linalool is shown in yellow, the heme is shown in salmon, and the protein backbone of P450terp is shown in grey. The electron density for linalool both is shown at 1σ of a $2F_O$-F_C map in blue mesh.

Table 2-6. Crystallographic data collection and refinement statistics of P450terp bound to linalool.

	P450terp WT linalool-bound
Resolution range	43.82 - 2.36 (2.444 - 2.36)
Space group	P 61 2 2
Unit cell	68.11 68.11 458.194 90 90 120
Total reflections	429682 (45674)
Unique reflections	27442 (2630)
Multiplicity	15.7 (17.3)
Completeness (%)	98.87 (99.81)
Mean I/sigma(I)	8.66 (2.33)
Wilson B-factor	48.86
R-merge	0.1876 (1.339)
R-meas	0.1941 (1.38)
R-pim	0.04842 (0.328)
CC1/2	0.989 (0.932)
CC*	0.997 (0.982)
Reflections used in refinement	27143 (2632)
Reflections used for R-free	1305 (120)
R-work	0.2070 (0.2985)
R-free	0.2295 (0.3604)
CC(work)	0.927 (0.818)
CC(free)	0.944 (0.560)
Number of non-hydrogen atoms	3421
macromolecules	3285
ligands	74
solvent	62
Protein residues	416
RMS(bonds)	0.009
RMS(angles)	1.15
Ramachandran favored (%)	97.57
Ramachandran allowed (%)	1.94
Ramachandran outliers (%)	0.49
Rotamer outliers (%)	0.57
Clashscore	2.72
Average B-factor	55.1
macromolecules	55.2
ligands	57.61
solvent	46.64

Discussion

The importance of allosteric interactions in the regulation of cytochromes P450 chemistry is well-recognized although the types of cooperativities exhibited by these systems are P450- and substrate-dependent, complex, and far from well-understood.[4,5] In this study, it was demonstrated how cytochrome P450terp (CYP108A1) simultaneously and cooperatively binds two molecules of its substrate, α-terpineol. This type of allostery demonstrated by P450terp where the binding of multiple copies of the same substrate enhances the relative affinities of one another is referred to as positive homotropic allostery. In particular, the direct interaction of both substrate molecules within the same active site reflects a special type of positive homotropic cooperativity that is common amongst several P450s.[4,5] Positive homotropy is often discussed in the context of the most abundant P450 in humans, CYP3A4, which exhibits an extremely broad substrate profile and is responsible for the majority of xenobiotic metabolism.[40] In fact, owing to its critical biological role, much of what is known about allosteric interactions in P450s originates from studies of the CYP3A4 isoform.[52] However, CYP108A1 (P450terp) serves a very different biological function than CYP3A4 and represents the first Class I bacterial P450 displaying positive homotropic allostery with its natural substrate that mediates catalytic efficiency.

This type of regulation represents an important concept in P450s that serve the biological role of oxidative assimilation of unusual carbon sources for energy. Several bacterial P450s have been shown to act as the first step in the oxidative metabolism of their substrates as sole carbon sources including P450cam,[42,43] P450terp,[20,44] P450lin,[45,46] P450cin[47] and others.[48,49] Regulation of biodegradative P450 activity has been shown at the organismal,[50] genetic,[51–53] and protein levels.[19,54] Bacterial P450s of this type represent important targets in the development of whole-cell and enzymatic biocatalysts.[55] Descriptions of the regulatory mechanisms like those presented here for P450terp are, therefore, critical not only for the understanding regulatory mechanisms in

bacterial metabolism but also for the design of systems that perform desired oxidative biotransformations.

Despite cytochrome P450terp originating from a plasmid-borne Class I *Pseudomonad* system like P450cam, it does not display many of the characteristic features associated with substrate binding including a large rearrangement of the F/G helices from an “open” to “closed” form or a shift of the I-helix. Instead, P450terp utilizes its second molecule of substrate to confer stability to the α-terpineol proximal to the heme center. This lack of a global conformational change upon substrate binding puts P450terp into a special category. In fact, historically it was debated whether this type of interaction truly constitutes allostery given the lack of a clear conformational change, but it was later shown that microscopic conformational changes (or subensembles) can describe this class of cooperative systems referred to as “nested allostery”.[54]

Using both X-ray crystal structures along with spectral and thermodynamic titrations, it was confirmed that this second binding site positively contributes to the cooperative binding of the primary substrate and stabilizes it for hydroxylation. Fitting of the spectral titrations and ITC binding curves revealed that neither one nor two site binding models were ideal for treating the interaction of P450terp with α-terpineol. To accommodate for this deviation, spectral titrations were fit with a binding model employing a Hill coefficient (HC) that allowed for the semi-quantitative comparison between binding affinities of the WT ($K_{D/S}$: ~2.7 μM, HC: 1.41) and a F188A mutant ($K_{D/S}$: ~36 μM, HC: 1.01) that drastically decreased affinity of α-terpineol for the second site.

Mutation of Phe188 decreased the affinity for the second site so drastically that only the proximal substrate molecule was observed in the X-ray crystal structure of the F188A mutant. This observation along with the reduction of the Hill coefficient to 1 indicates a loss of any positive cooperativity. Further, inversion of the ITC binding profile from an enthalpic to entropic binding mode corroborated these findings and is consistent with previous studies on P450cam and its

homologues that display single binding sites in X-ray structures. The excellent agreement of the K_D and K_S (~36 μM) for this variant support the assignment that these titrations are reporting the affinity for a weakened primary site adjacent to the heme. Moreover, the F188A variant not only affects the affinity of substrate for P450terp, but also alters the rate of substrate turnover and efficiency of coupling. Upon mutation of Phe188, the coupling efficiency decreases by nearly half to 51.2% and substantially slows the rate of turnover, possibly changing the nature of the rate limiting step.

Despite their differences in substrate scope and biological function, CYP3A4 exhibits an analogous critical phenylalanine at 213 to Phe188 of P450terp. Mutation of Phe213 results in significant changes to homotropic and heterotropic allosteric effects involving 3A4 substrates carbamazepine, progesterone, and α-naphthoflavone.[41] In fact, the general region of the F-F' loop, also known as substrate recognition site 2 (SRS-2), is key for the control of positive homo- and heterotropic interactions. In CYP3A4, mutations in SRS-2 have been found to alter the responsiveness to allosteric effectors, diminish the extent of homotropic allostery, and even change the regioselectivity of substrate hydroxylation.[5]

Binding of the proximal substrate in P450terp, on the other hand, is not only controlled by interactions with the second substrate residing in the upper part of the active site channel, but also through hydrogen bonding with residues next to the heme center, Ser101 and T103. Mutation of these two positions to alanine residues resulted in a loss of measurable substrate binding affinity, as ITC indicated no heat change upon titration of α-terpineol and spectral titrations were impeded by substrate solubility and lack of binding saturation. Additionally, while WT P450terp exhibits rapid turnover (670 min^{-1}) and is highly coupled (97%), removal of S101 and T103 sidechains significantly diminishes both the rate of turnover and the extent of coupling (70.6%). The triple mutant, where both the primary and secondary sites are affected, exemplifies the critical nature of these residues as both turnover and coupling efficiency are essentially abolished. The

UV-vis spectra of reduced and CO-bound S101A/T103A and the S101A/T103A/F188A variants (Figure 2-10), however, indicate these mutations may serve not only to destabilize substrate binding but also change the electronic structure the heme-cofactor. It is, therefore, possible that this is what gives rise to a decrease in the coupling efficiency and the complicated NADH consumption kinetics. Moreover, this observation may also explain, in part, the reduced spin shift observed upon addition of α-terpineol in the S101A/T103A containing-variants. Changes in the heme electronic structure (e.g. perturbations to the Fe–S bond) induced by these mutations may alter the ability of these variants to achieve the high-spin state even upon binding of substrate. Regardless, the lack of thermal changes in the ITC isotherms of the S101A/T103A titrations supports the conclusion that these mutations substantially reduce the affinity for α-terpineol in the terp1 position. This reduction in affinity could also be accompanied by a change in identity of the hydroxylated product if the substrate is more mobile within the active site and capable of reorientation.

While there are many instances of positive homotropic allostery in P450s, most do not reflect cooperative interactions with a natural substrate. This led to the hypothesis that open active sites were associated with substrate promiscuity of xenobiotic metabolizing P450s. Here, however, P450terp is believed to serve the sole purpose of hydroxylating α-terpineol and initiating the process of oxidative assimilation of α-terpineol as an alternative carbon source by its host organism. In contrast to many P450s exhibiting similar biological functions, P450terp exists in its “open” form in the presence of its natural substrate. Additionally, the occupancy of the endogenous substrate in the second site directly impacts catalytic efficiency, which has not been observed before in a Class I bacterial system. While P450terp serves the same function and displays similar efficiency to P450cam, it is unlike P450cam in several ways. It is possible that the strict regulatory elements of P450cam may represent more extreme forms of regulation, while

other bacterial systems like P450terp may display less stringent requirements, acting as a bridge for understanding substrate binding between the model system and more flexible isoforms.

This work demonstrates that this phenomenon may be a much more common than previously appreciated but hard to capture in some P450 systems due to the nature of regulatory requirements for active site rearrangement. For example, in the structure of the complex of P450cam bound to its redox partner Pdx, a well-ordered second camphor molecule is observed in 3 of the 4 asymmetric units just above the normal substrate binding site (Figure 2-3).[16] The occupation of the open active site access channel with a second molecule of camphor was suggested to confer stability to the structure while holding the primary molecule in place for oxidation similar to P450terp. This raises the interesting possibility that the closed form of P450cam with a single molecule of substrate bound is not the active form but instead, it is the more open form with two molecules of camphor bound similar to P450terp. The difference, of course, is that in P450cam the binding of its redox partner is required to shift P450cam to the more open active state.

As a result of Pdx shifting P45cam to a more open state, critical salt bridges between Asp251 on the I-helix and two residues on the F-helix/loop region, Arg186 and Lys178 are broken. The freeing of Asp251 is accompanied by a change in rotomer conformation to a position that faces the active site. This switch allows for the formation and participation of Asp251 in a proton relay network required for the controlled delivery of protons to the Fe-O_2 unit for the activation and subsequent heterolytic cleavage of the O–O bond.[17,18,56] P450terp contains an analogous aspartate (Asp270) on the I helix followed by a conserved threonine (Thr271) also critical for oxygen activation in P450cam (Thr 251).[57,58] Like Asp251 in P450cam, Asp270 in P450terp appears to be tied up in a similar but possibly weaker salt bridge with F-helix residue Gln185 as well as Lys419 which reaches over from the β5 sheet. Both interactions, however, engage the same carboxylate oxygen atom of Asp270 leaving the remaining sidechain oxygen to participate

in interactions with water molecules (Figure 2-22). While this does not preclude a redox partner induced change in conformation, it does suggest that P450terp may not require the same redox partner initiated global rearrangements to be activated for catalysis.

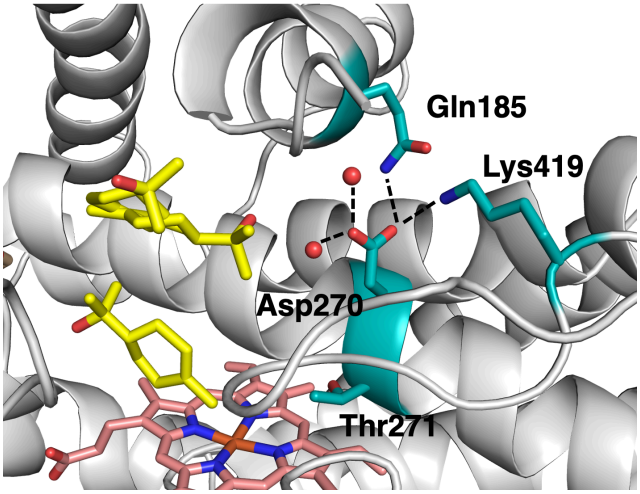

Figure 2-22. P450terp Asp270. Asp270 forms a 2.9 Å H-bond with Gln185 and a weaker 3.3 Å H-bond with Lys419. The other carboxylate oxygen is 2.5 Å and 3.3 Å from two water molecules.

Conclusion

I have solved a crystal structure of P450terp with substrate bound, wherein two substrate sites were revealed. Mutagenesis of these two sites showed a striking difference in their relative affinities for α-terpineol. Furthermore, the variants verified critical residues for substrate binding and each decreased their rates of NADH consumption as well as coupling efficiencies. Along with an X-ray crystal structure of the F188A variant and substrate titrations, the turnover assays showed that binding to the second site directly contributes to efficiency of P450 catalysis. While the presence of a second substrate molecule and its effects on reactivity may be relatively common in mammalian P450s, occurrence of this behavior in bacterial P450s with small active sites is rather surprising. This exploration raises the question of how commonly multiple molecules of substrate are present in the active site during catalysis and whether redox partner binding can initiate binding of multiple molecules when conformation changes are involved. It is quite possible

that the serendipitous capture of the second substrate *in crystallo* might represent an underappreciated but important tool in the evolution of P450 regulatory mechanisms.

Methods

Protein Expression

P450terp wild-type (WT) was encoded on a pET28a+ vector with N-terminal His6-tag (Genscript). Primers for each mutation (Genewiz) were made, and the variants with multiple mutations were created sequentially (i.e. WT to S101A to S101A/T103A to S101A/T103A/F188A) (Table 2-7). Site-directed mutagenesis was performed using standard polymerase chain reaction (PCR) protocols (Takara PrimeSTAR Max). The vector was transformed into *E. coli* C41(DE3) and plated onto Luria Broth (LB) plates containing 50 μg/mL kanamycin. Each mutation was verified by sequencing (Genewiz) after performing Minipreps (Macherey-Nagel) using standard protocols. Single colonies of each variant were taken to inoculate 100 mL LB with 50 µg/ml kanamycin and grown overnight at 37°C, 220 rotations per minute (RPM). The following day, 10 mL of the overnight starter culture were inoculated into 1 L of Terrific Broth (TB) supplemented with 50 µg/mL kanamycin. Cultures were grown at 37°C and shaken at 220 RPM until the OD_{600} = 0.8 – 1. Expression was induced with 1 mM isopropyl β-d-1-thiogalactopyranoside (IPTG) and supplemented with 0.4 mM 5-aminolevulinic acid (D-ALA). The temperature was then decreased to 25° C. After 1 hour, the speed was decreased to 100 RPM and the cells were grown for 48 hours, harvested, and then lysed or frozen, if necessary.

Table 2-7. Primers for mutagenesis.

Mutation	Primer
S101A forward	5' – gtaatcgatGCGttgACCtcgatgg – 3'
S101A reverse	5' – ccatcgaGGTcaaCGCatcgattac – 3'
S101A T103A forward	5' – gatGCGttgGCCtcgatggac – 3'
S101A T103A reverse	5' – gtccatcgaGGCcaaCGCatc – 3'
F188A forward	5' – caggatttcGCAggggtac – 3'
F188A reverse	5' – gtaccccTGCgaaatcctg – 3'

Protein Purification

Cells containing P450terp were resuspended in lysis buffer (50 mM KPi pH 7.4, 250 mM NaCl, 2 mM β-mercaptoethanol) and stirred overnight at 4° C. Cells were lysed by two passes through a microfluidizer. The lysate was centrifuged for 1 hour at 15000 RPM at 4°C (Beckman Coulter Avanti JA-17). The supernatant was loaded on to a nickel column pre-equilibrated with lysis buffer (Thermo-Fisher HisPur Ni-NTA), washed with lysis buffer for 5 column volumes (CV), then washed with lysis buffer containing 15 mM imidazole for 5 CV. The protein was then eluted with lysis buffer containing 250 mM imidazole. Fractions exhibiting red color were collected, pooled, and then dialyzed against wash buffer (50 mM KPi 7.4, 2 mM BME). Protein was removed from the dialysis bag and loaded on to a pre-equilibrated DEAE Sepharose column (Cytiva). The column was washed with 5 CV of wash buffer followed by a gradient elution from 0 to 500 mM NaCl over the course of 10 CV. Fractions with an optical purity ratio (Reinheitzahl, R/Z, A_{418}/A_{280}) > 1.2 were pooled and dialyzed against wash buffer to remove salt. The protein was then loaded on to a pre-equilibrated Q Sepharose column (Cytiva), washed, and eluted following same steps as the DEAE column. Fractions displaying an R/Z > 1.5 were pooled and concentrated to < 2 mL. The protein was then loaded on to a pre-equilibrated size-exclusion chromatography column (SEC) (Cytiva Sephacryl S-200 HR) with SEC buffer (50 mM KPi pH 7.4, 150 mM NaCl, 5 mM dithiothreitol, DTT). Fractions with R/Z > 1.8 were collected. Samples used for assays were buffer exchanged into 50 mM KPi pH 7.4 and 5 mM DTT in 30 kDa centrifugal filters (Millipore Amicon).

Samples used for crystallization were buffer exchanged into 50 mM Bis-Tris pH 7.5 and 30 mM DTT in centrifugal filters.

Crystallization

Crystals were grown from the Morpheus (MAKER) crystal screening condition (0.06 M magnesium chloride hexahydrate, 0.06 M calcium chloride dihydrate, 0.1 M sodium HEPES and MOPS pH 7.5, 20% v/v ethylene glycol, 10% v/v PEG 8000) at 4°C by hanging drop vapor diffusion. Hexagonal rods appeared within several days. Substrate-free crystals appeared bright red, while substrate-bound crystals appeared a darker reddish brown. Substrate-bound crystals were grown in the same conditions, with the addition of excess substrate in the mother liquor as well as the crystal drop. Substrate-free crystals grew significantly larger with the addition of 200 mM KCl in the mother liquor, while the same addition of KCl into the substrate-bound condition resulted in loss of crystallization. Crystals used for X-ray diffraction were grown by sitting drop vapor diffusion (2 μL:2 μL, protein:condition). Mother liquor containing 25% glycerol was used as cryoprotectant. Data were collected at the Advanced Light Source synchrotron (ALS). Data were indexed, integrated, and scaled using Mosflm and Scala.[59] Molecular replacement (MR) was performed using PHASER[60,61] by applying the substrate-free P450terp (1CPT) as the MR model. Refinement was carried out in Phenix.refine[62,63] and COOT.[64,65] Refinement was further aided by PDB_REDO.[66] Data collection and refinement statistics are listed in Table 2-1.

Spectroscopy

All ultraviolet-visible (UV-vis) spectroscopy was performed on a Cary 300 spectrophotometer. The following extinction coefficients were used: ε_{418} = 120 $mM^{-1}cm^{-1}$ for substrate-free P450terp WT and variants; ε_{396} = 96 $mM^{-1}cm^{-1}$ for substrate-bound P450terp WT only; ε_{415}=6.5 $mM^{-1}cm^{-1}$

for terpredoxin (Tdx); ε_{455} = 12.2 $mM^{-1}cm^{-1}$ for terpredoxin reductase (TdR); ε_{340} = 6.22 $mM^{-1}cm^{-1}$ for nicotinamide adenine dinucleotide (NADH).[67]

Enzyme Assays

The NADH consumption of the P450terp system was determined by monitoring the absorbance of NADH at 340 nm upon addition of substrate to a cuvette containing the catalytic components. The reconstituted systems contained 0.5 µM P450terp, 5 µM Tdx, 0.5 µM TdR and 185 µM NADH in 50 mM KPi for a final volume of 980 µL. Reactions were initiated by the addition of 20 µL of 1 mM α-terpineol, for a final volume of 1 mL and concentration of 200 µM α-terpineol. Rates were determined using the least-squares regression method.

Isothermal Titration Calorimetry

All experiments were performed on a MicroCal PEAQ-ITC instrument using a previously published protocol.[34] Concentrations of proteins and substrate were as follows: 100 µM P450terp WT in the cell and 2 mM α-terpineol in the syringe; 100 µM P450terp F188A in the cell and 2.5 mM α-terpineol in the syringe.

NADH/Substrate Coupling Assays

Each coupling reaction was run in triplicate in microcentrifuge tubes (ThermoFisher) at room temperature in 50 mM KPi pH 7.4, with the same protein concentrations as the spectral assays, and 122 μM α-terpineol. The reaction was initiated by adding 100 μM NADH. The reactions were given different end times to account for the different rates: 10 min for WT; 30 min for the S101A T103A and F188A variants; and > 1 hour for the S101A T013A F188A variant. Prior to extraction, an internal standard of camphor at 50 μM was added after the reactions were complete. Extraction was performed by addition of 500 µL of dichloromethane (DCM) to the reaction mixture and

vortexing for 30 seconds. The tubes were then centrifuged at 9000 RPM at RT for 5 minutes. The aqueous layer was removed and the extraction procedure was repeated on the aqueous layer. Then organic layers from both extractions were combined. The samples were run on a GC-MS (Thermo Fisher) and data analyzed in Chromeleon.

References:

(1) Yosca, T. H.; Ledray, A. P.; Ngo, J.; Green, M. T. A New Look at the Role of Thiolate Ligation in Cytochrome P450. *J Biol Inorg Chem* **2017**, *22* (2–3), 209–220. https://doi.org/10.1007/s00775-016-1430-3.

(2) Rittle, J.; Green, M. T. Cytochrome P450 Compound I: Capture, Characterization, and C-H Bond Activation Kinetics. *Science* **2010**, *330* (6006), 933–937. https://doi.org/10.1126/science.1193478.

(3) Yosca, T. H.; Rittle, J.; Krest, C. M.; Onderko, E. L.; Silakov, A.; Calixto, J. C.; Behan, R. K.; Green, M. T. Iron(IV)Hydroxide p K_a and the Role of Thiolate Ligation in C–H Bond Activation by Cytochrome P450. *Science* **2013**, *342* (6160), 825–829. https://doi.org/10.1126/science.1244373.

(4) Davydov, D. R.; Halpert, J. R. Allosteric P450 Mechanisms: Multiple Binding Sites, Multiple Conformers or Both? *Expert Opinion on Drug Metabolism & Toxicology* **2008**, *4* (12), 1523–1535. https://doi.org/10.1517/17425250802500028.

(5) Hlavica, P. Challenges in Assignment of Allosteric Effects in Cytochrome P450-Catalyzed Substrate Oxidations to Structural Dynamics in the Hemoprotein Architecture. *Journal of Inorganic Biochemistry* **2017**, *167*, 100–115. https://doi.org/10.1016/j.jinorgbio.2016.11.025.

(6) Denisov, I. G.; Frank, D. J.; Sligar, S. G. Cooperative Properties of Cytochromes P450. *Pharmacology & Therapeutics* **2009**, *124* (2), 151–167. https://doi.org/10.1016/j.pharmthera.2009.05.011.

(7) Poulos, T. L. Heme Enzyme Structure and Function. *Chem. Rev.* **2014**, *114* (7), 3919–3962. https://doi.org/10.1021/cr400415k.

(8) Haniu, M.; Armes, L. G.; Tanaka, M.; Yasunobu, K. T.; Shastry, B. S.; Wagner, G. C.; Gunsalus, I. C. The Primary Structure of the Monoxygenase Cytochrome P450CAM. *Biochemical and Biophysical Research Communications* **1982**, *105* (3), 889–894. https://doi.org/10.1016/0006-291X(82)91053-1.

(9) Unger, B. P.; Gunsalus, I. C.; Sligar, S. G. Nucleotide Sequence of the Pseudomonas Putida Cytochrome P-450cam Gene and Its Expression in Escherichia Coli. *Journal of Biological Chemistry* **1986**, *261* (3), 1158–1163. https://doi.org/10.1016/S0021-9258(17)36068-4.

(10) Poulos, T. L.; Finzel, B. C.; Howard, A. J. High-Resolution Crystal Structure of Cytochrome P450cam. *Journal of Molecular Biology* **1987**, *195* (3), 687–700. https://doi.org/10.1016/0022-2836(87)90190-2.

(11) Lipscomb, J. D.; Sligar, S. G.; Namtvedt, M. J.; Gunsalus, I. C. Autooxidation and Hydroxylation Reactions of Oxygenated Cytochrome P-450cam. *Journal of Biological Chemistry* **1976**, *251* (4), 1116–1124. https://doi.org/10.1016/S0021-9258(17)33808-5.

(12) Hannemann, F.; Bichet, A.; Ewen, K. M.; Bernhardt, R. Cytochrome P450 Systems—Biological Variations of Electron Transport Chains. *Biochimica et Biophysica Acta (BBA) - General Subjects* **2007**, *1770* (3), 330–344. https://doi.org/10.1016/j.bbagen.2006.07.017.

(13) Liu, X.; Li, F.; Sun, T.; Guo, J.; Zhang, X.; Zheng, X.; Du, L.; Zhang, W.; Ma, L.; Li, S. Three Pairs of Surrogate Redox Partners Comparison for Class I Cytochrome P450 Enzyme Activity Reconstitution. *Commun Biol* **2022**, *5* (1), 791. https://doi.org/10.1038/s42003-022-03764-4.
(14) Mendes, M. V.; Antón, N.; Martín, J. F.; Aparicio, J. F. Characterization of the Polyene Macrolide P450 Epoxidase from *Streptomyces Natalensis* That Converts de-Epoxypimaricin into Pimaricin. *Biochemical Journal* **2005**, *386* (1), 57–62. https://doi.org/10.1042/BJ20040490.
(15) Sawada, N.; Sakaki, T.; Yoneda, S.; Kusudo, T.; Shinkyo, R.; Ohta, M.; Inouye, K. Conversion of Vitamin D3 to 1α,25-Dihydroxyvitamin D3 by Streptomyces Griseolus Cytochrome P450SU-1. *Biochemical and Biophysical Research Communications* **2004**, *320* (1), 156–164. https://doi.org/10.1016/j.bbrc.2004.05.140.
(16) Tripathi, S.; Li, H.; Poulos, T. L. Structural Basis for Effector Control and Redox Partner Recognition in Cytochrome P450. *Science* **2013**, *340* (6137), 1227–1230. https://doi.org/10.1126/science.1235797.
(17) Follmer, A. H.; Tripathi, S.; Poulos, T. L. Ligand and Redox Partner Binding Generates a New Conformational State in Cytochrome P450cam (CYP101A1). *J. Am. Chem. Soc.* **2019**, *141* (6), 2678–2683. https://doi.org/10.1021/jacs.8b13079.
(18) Poulos, T. L.; Follmer, A. H. Updating the Paradigm: Redox Partner Binding and Conformational Dynamics in Cytochromes P450. *Acc. Chem. Res.* **2022**, *55* (3), 373–380. https://doi.org/10.1021/acs.accounts.1c00632.
(19) Follmer, A. H.; Mahomed, M.; Goodin, D. B.; Poulos, T. L. Substrate-Dependent Allosteric Regulation in Cytochrome P450cam (CYP101A1). *J. Am. Chem. Soc.* **2018**, *140* (47), 16222–16228. https://doi.org/10.1021/jacs.8b09441.
(20) Peterson, J. A.; Lu, J. Y.; Geisselsoder, J.; Graham-Lorence, S.; Carmona, C.; Witney, F.; Lorence, M. C. Cytochrome P-450terp. Isolation and Purification of the Protein and Cloning and Sequencing of Its Operon. *Journal of Biological Chemistry* **1992**, *267* (20), 14193–14203. https://doi.org/10.1016/S0021-9258(19)49697-X.
(21) Boddupalli, S. S.; Hasemann, C. A.; Ravichandran, K. G.; Lu, J. Y.; Goldsmith, E. J.; Deisenhofer, J.; Peterson, J. A. Crystallization and Preliminary X-Ray Diffraction Analysis of P450terp and the Hemoprotein Domain of P450BM-3, Enzymes Belonging to Two Distinct Classes of the Cytochrome P450 Superfamily. *Proc. Natl. Acad. Sci. U.S.A.* **1992**, *89* (12), 5567–5571. https://doi.org/10.1073/pnas.89.12.5567.
(22) Hasemann', C. A.; Ravichandran', K. G.; Peterson, J. A.; Deisenhofer', J. Crystal Structure and Reljnement of Cytochrome P450terp at 2.3 A Resolution. 17.
(23) Tuck, S. F.; Peterson, J. A.; Ortiz de Montellano, P. R. Active Site Topologies of Bacterial Cytochromes P450101 (P450cam), P450108 (P450terp), and P450102 (P450BM-3). In Situ Rearrangement of Their Phenyl-Iron Complexes. *Journal of Biological Chemistry* **1992**, *267* (8), 5614–5620. https://doi.org/10.1016/S0021-9258(18)42809-8.
(24) Fruetel, J. A.; Mackman, R. L.; Peterson, J. A.; Ortiz de Montellano, P. R. Relationship of Active Site Topology to Substrate Specificity for Cytochrome P450terp (CYP108). *Journal of Biological Chemistry* **1994**, *269* (46), 28815–28821. https://doi.org/10.1016/S0021-9258(19)61979-4.
(25) Sevrioukova, I. F.; Peterson, J. A. Reaction of Carbon-Monoxide and Molecular-Oxygen with P450terp (CYP108) and P450BM-3 (CYP102). *Archives of Biochemistry and Biophysics* **1995**, *317* (2), 397–404. https://doi.org/10.1006/abbi.1995.1180.
(26) Andersson, L. A.; Peterson, J. A. Active-Site Analysis of Ferric P450 Enzymes: Hydrogen-Bonding Effects on the Circular Dichroism Spectra. *Biochemical and Biophysical Research Communications* **1995**, *211* (2), 389–395. https://doi.org/10.1006/bbrc.1995.1826.

(27) Andersson, L. A.; Johnson, A. K.; Peterson, J. A. Active Site Analysis of P450 Enzymes: Comparative Magnetic Circular Dichroism Spectroscopy. *Archives of Biochemistry and Biophysics* **1997**, *345* (1), 79–87. https://doi.org/10.1006/abbi.1997.0248.
(28) Karplus, P. A.; Diederichs, K. Linking Crystallographic Model and Data Quality. *Science* **2012**, *336* (6084), 1030–1033. https://doi.org/10.1126/science.1218231.
(29) Alvarez, G.; Le, T.; Wong, N.; Echave, J.; Pochapsky, T. C.; Asciutto, E. K. Hydroxylation Regiochemistry Is Robust to Active Site Mutations in Cytochrome P450 $_{cam}$ (CYP101A1). *Biochemistry* **2022**, *61* (17), 1790–1800. https://doi.org/10.1021/acs.biochem.2c00233.
(30) Wells, A. V.; Li, P.; Champion, P. M.; Martinis, S. A.; Sligar, S. G. Resonance Raman Investigations of Escherichia Coli-Expressed Pseudomonas Putida Cytochrome P450 and P420. *Biochemistry* **1992**, *31* (18), 4384–4393. https://doi.org/10.1021/bi00133a002.
(31) Remba, R. D.; Champion, P. M.; Fitchen, D. B.; Chiang, R.; Hager, L. P. Resonance Raman Investigations of Chloroperoxidase, Horseradish Peroxidase, and Cytochrome c Using Soret Band Laser Excitation. *Biochemistry* **1979**, *18* (11), 2280–2290. https://doi.org/10.1021/bi00578a023.
(32) Sligar, S. G.; Egeberg, K. D.; Sage, J. T.; Morikis, D.; Champion, P. M. Alteration of Heme Axial Ligands by Site-Directed Mutagenesis: A Cytochrome Becomes a Catalytic Demethylase. *J. Am. Chem. Soc.* **1987**, *109* (25), 7896–7897. https://doi.org/10.1021/ja00259a056.
(33) Gable, J. A.; Tripathi, S.; Poulos, T. L. Structural Insights on the Conversion of Cytochrome P450 to P420. *ACS Omega* **2022**, *7* (22), 18481–18485. https://doi.org/10.1021/acsomega.2c00960.
(34) Batabyal, D.; Richards, L. S.; Poulos, T. L. Effect of Redox Partner Binding on Cytochrome P450 Conformational Dynamics. *J. Am. Chem. Soc.* **2017**, *139* (37), 13193–13199. https://doi.org/10.1021/jacs.7b07656.
(35) Batabyal, D.; Poulos, T. L. Effect of Redox Partner Binding on CYP101D1 Conformational Dynamics. *Journal of Inorganic Biochemistry* **2018**, *183*, 179–183. https://doi.org/10.1016/j.jinorgbio.2018.02.013.
(36) Murarka, V. C.; Batabyal, D.; Amaya, J. A.; Sevrioukova, I. F.; Poulos, T. L. Unexpected Differences between Two Closely Related Bacterial P450 Camphor Monooxygenases. *Biochemistry* **2020**, *59* (29), 2743–2750. https://doi.org/10.1021/acs.biochem.0c00366.
(37) Brewer, C. B.; Peterson, J. A. Single Turnover Kinetics of the Reaction between Oxycytochrome P-450cam and Reduced Putidaredoxin. *Journal of Biological Chemistry* **1988**, *263* (2), 791–798. https://doi.org/10.1016/S0021-9258(19)35424-9.
(38) Kadkhodayan, S.; Coulter, E. D.; Maryniak, D. M.; Bryson, T. A.; Dawson, J. H. Uncoupling Oxygen Transfer and Electron Transfer in the Oxygenation of Camphor Analogues by Cytochrome P450-CAM. *Journal of Biological Chemistry* **1995**, *270* (47), 28042–28048. https://doi.org/10.1074/jbc.270.47.28042.
(39) Batabyal, D.; Poulos, T. L. Crystal Structures and Functional Characterization of Wild-Type CYP101D1 and Its Active Site Mutants. *Biochemistry* **2013**, *52* (49), 8898–8906. https://doi.org/10.1021/bi401330c.
(40) Guengerich, F. P. CYTOCHROME P-450 3A4: Regulation and Role in Drug Metabolism. *Annu. Rev. Pharmacol. Toxicol.* **1999**, *39* (1), 1–17. https://doi.org/10.1146/annurev.pharmtox.39.1.1.
(41) Denisov, I. G.; Grinkova, Y. V.; Nandigrami, P.; Shekhar, M.; Tajkhorshid, E.; Sligar, S. G. Allosteric Interactions in Human Cytochrome P450 CYP3A4: The Role of Phenylalanine 213. *Biochemistry* **2019**, *58* (10), 1411–1422. https://doi.org/10.1021/acs.biochem.8b01268.
(42) Hedegaard, J.; Gunsalus, I. C. Mixed Function Oxidation. *Journal of Biological Chemistry* **1965**, *240* (10), 4038–4043. https://doi.org/10.1016/S0021-9258(18)97147-4.

(43) Katagiri, M.; Ganguli, B. N.; Gunsalus, I. C. A Soluble Cytochrome P-450 Functional in Methylene Hydroxylation. *Journal of Biological Chemistry* **1968**, *243* (12), 3543–3546. https://doi.org/10.1016/S0021-9258(18)93343-0.
(44) Peterson, J. A.; Lu, J.-Y. [60] Bacterial Cytochromes P450: Isolation and Identification. In *Methods in Enzymology*; Elsevier, 1991; Vol. 206, pp 612–620. https://doi.org/10.1016/0076-6879(91)06131-L.
(45) Madyastha, K. M.; Bhattacharyya, P. K.; Vaidyanathan, C. S. Metabolism of a Monoterpene Alcohol, Linalool, by a Soil Pseudomonad. *Can. J. Microbiol.* **1977**, *23* (3), 230–239. https://doi.org/10.1139/m77-035.
(46) Renganathan, V.; Madyastha, K. M. Linalyl Acetate Is Metabolized by *Pseudomonas Incognita* with the Acetoxy Group Intact. *Appl Environ Microbiol* **1983**, *45* (1), 6–15. https://doi.org/10.1128/aem.45.1.6-15.1983.
(47) Hawkes, D. B.; Adams, G. W.; Burlingame, A. L.; Ortiz de Montellano, P. R.; De Voss, J. J. Cytochrome P450cin (CYP176A), Isolation, Expression, and Characterization. *Journal of Biological Chemistry* **2002**, *277* (31), 27725–27732. https://doi.org/10.1074/jbc.M203382200.
(48) Frank, D. J.; Waddling, C. A.; La, M.; Ortiz de Montellano, P. R. Cytochrome P450 125A4, the Third Cholesterol C-26 Hydroxylase from *Mycobacterium Smegmatis*. *Biochemistry* **2015**, *54* (46), 6909–6916. https://doi.org/10.1021/acs.biochem.5b01029.
(49) Ikatsu, H.; Kino, Y.; Kawahara, N.; Adachi, M.; Miyoshi, S.-I.; Tomochika, K.-I.; Shinoda, S. Isolation and Characterization of Cytochrome P450-Producing Bacteria from Various Environments. *Biocontrol Sci.* **2000**, *5* (2), 111–116. https://doi.org/10.4265/bio.5.111.
(50) Balaraman, P.; Plettner, E. Chemotaxis by Pseudomonas Putida (ATCC 17453) towards Camphor Involves Cytochrome P450cam (CYP101A1). *Biochimica et Biophysica Acta (BBA) - General Subjects* **2019**, *1863* (2), 304–312. https://doi.org/10.1016/j.bbagen.2018.10.018.
(51) Fujita, M.; Aramaki, H.; Horiuchi, T.; Amemura, A. Transcription of the Cam Operon and CamR Genes in Pseudomonas Putida PpG1. *J Bacteriol* **1993**, *175* (21), 6953–6958. https://doi.org/10.1128/jb.175.21.6953-6958.1993.
(52) Aramaki, H.; Sagara, Y.; Hosoi, M.; Horiuchi, T. Evidence for Autoregulation of CamR, Which Encodes a Repressor for the Cytochrome P-450cam Hydroxylase Operon on the Pseudomonas Putida CAM Plasmid. *J Bacteriol* **1993**, *175* (24), 7828–7833. https://doi.org/10.1128/jb.175.24.7828-7833.1993.
(53) Subramanian, V.; Yadav, J. S. Regulation and Heterologous Expression of P450 Enzyme System Components of the White Rot Fungus Phanerochaete Chrysosporium. *Enzyme and Microbial Technology* **2008**, *43* (2), 205–213. https://doi.org/10.1016/j.enzmictec.2007.09.001.
(54) Skinner, S. P.; Follmer, A. H.; Ubbink, M.; Poulos, T. L.; Houwing-Duistermaat, J. J.; Paci, E. Partial Opening of Cytochrome P450cam (CYP101A1) Is Driven by Allostery and Putidaredoxin Binding. *Biochemistry* **2021**, *60* (39), 2932–2942. https://doi.org/10.1021/acs.biochem.1c00406.
(55) Cryle, M. J.; Stok, J. E.; De Voss, J. J. Reactions Catalyzed by Bacterial Cytochromes P450. *Aust. J. Chem.* **2003**, *56* (8), 749. https://doi.org/10.1071/CH03040.
(56) Amaya, J. A.; Batabyal, D.; Poulos, T. L. Proton Relay Network in the Bacterial P450s: CYP101A1 and CYP101D1. *Biochemistry* **2020**, *59* (31), 2896–2902. https://doi.org/10.1021/acs.biochem.0c00329.
(57) Martinis, S. A.; Atkins, W. M.; Stayton, P. S.; Sligar, S. G. A Conserved Residue of Cytochrome P-450 Is Involved in Heme-Oxygen Stability and Activation. *J. Am. Chem. Soc.* **1989**, *111* (26), 9252–9253. https://doi.org/10.1021/ja00208a031.

(58) Gerber, N. C.; Sligar, S. G. A Role for Asp-251 in Cytochrome P-450cam Oxygen Activation. *Journal of Biological Chemistry* **1994**, *269* (6), 4260–4266. https://doi.org/10.1016/S0021-9258(17)41772-8.
(59) Battye, T. G. G.; Kontogiannis, L.; Johnson, O.; Powell, H. R.; Leslie, A. G. W. *IMOSFLM*: A New Graphical Interface for Diffraction-Image Processing with *MOSFLM*. *Acta Crystallogr D Biol Crystallogr* **2011**, *67* (4), 271–281. https://doi.org/10.1107/S0907444910048675.
(60) McCoy, A. J. Solving Structures of Protein Complexes by Molecular Replacement with *Phaser*. *Acta Crystallogr D Biol Crystallogr* **2007**, *63* (1), 32–41. https://doi.org/10.1107/S0907444906045975.
(61) McCoy, A. J.; Grosse-Kunstleve, R. W.; Adams, P. D.; Winn, M. D.; Storoni, L. C.; Read, R. J. *Phaser* Crystallographic Software. *J Appl Crystallogr* **2007**, *40* (4), 658–674. https://doi.org/10.1107/S0021889807021206.
(62) Adams, P. D.; Afonine, P. V.; Bunkóczi, G.; Chen, V. B.; Echols, N.; Headd, J. J.; Hung, L.-W.; Jain, S.; Kapral, G. J.; Grosse Kunstleve, R. W.; McCoy, A. J.; Moriarty, N. W.; Oeffner, R. D.; Read, R. J.; Richardson, D. C.; Richardson, J. S.; Terwilliger, T. C.; Zwart, P. H. The Phenix Software for Automated Determination of Macromolecular Structures. *Methods* **2011**, *55* (1), 94–106. https://doi.org/10.1016/j.ymeth.2011.07.005.
(63) Echols, N.; Grosse-Kunstleve, R. W.; Afonine, P. V.; Bunkóczi, G.; Chen, V. B.; Headd, J. J.; McCoy, A. J.; Moriarty, N. W.; Read, R. J.; Richardson, D. C.; Richardson, J. S.; Terwilliger, T. C.; Adams, P. D. Graphical Tools for Macromolecular Crystallography in *PHENIX*. *J Appl Crystallogr* **2012**, *45* (3), 581–586. https://doi.org/10.1107/S0021889812017293.
(64) Emsley, P.; Cowtan, K. *Coot*: Model-Building Tools for Molecular Graphics. *Acta Crystallogr D Biol Crystallogr* **2004**, *60* (12), 2126–2132. https://doi.org/10.1107/S0907444904019158.
(65) Emsley, P.; Lohkamp, B.; Scott, W. G.; Cowtan, K. Features and Development of *Coot*. *Acta Crystallogr D Biol Crystallogr* **2010**, *66* (4), 486–501. https://doi.org/10.1107/S0907444910007493.
(66) Joosten, R. P.; Long, F.; Murshudov, G. N.; Perrakis, A. The *PDB_REDO* Server for Macromolecular Structure Model Optimization. *IUCrJ* **2014**, *1* (4), 213–220. https://doi.org/10.1107/S2052252514009324.
(67) Follmer, A. H. Cytochrome P450: Nature's Aircraft Carrier. Ph.D., University of California, Irvine, Ann Arbor, 2019. https://www.proquest.com/dissertations-theses/cytochrome-p450-natures-aircraft-carrier/docview/2275957801/se-2?accountid=14509.

Chapter 3

Redox Partner Recognition and Selectivity of Cytochrome P450lin (CYP111A1)

Introduction

As discussed in chapter 1, we are also interested in the regulation of the delivery of the second electron in catalysis by a protein redox partner. The cofactors and arrangements of electron transfer proteins utilized for P450 activity are diverse and often related to the biological purpose they serve, which has led to a classification scheme based on their composition. Many microbial P450s fall into Class I, which means they are powered by two soluble electron transfer proteins: a Fe_2S_2-ferredoxin that shuttles electrons to the P450 and a flavin-containing reductase that reduces the ferredoxin. These P450s often perform the initial oxidation in the metabolism of alternative carbon sources that allow the host organism to survive on unusual substrates. In fact, a common method of isolating microbial P450s is by the enrichment of the host media with potential substrates.

One such P450 isolated by this method was P450cam, which despite its significance as a model system, exhibits an uniquely strict requirement for its native electron transfer partner, putidaredoxin (Pdx), during the hydroxylation reaction of its substrate, camphor.[1] Over several decades, it was demonstrated that this specificity arises from a conformational change induced by the binding of Pdx necessary for initiating O_2 activation and formation of the active oxidant, Compound I.[2,3] The requirement for Pdx sets P450cam apart from other Class I P450s, which are often capable of turnover with non-native redox partners.[4–7] This specificity raises the question of whether it is related to either its biological role in the detoxification and oxidative metabolism of camphor or its origin as a plasmid-borne P450 from *Pseudomonads*.

Strict redox partner selectivity is shared by one P450cam homologue, P450tcu, which also originates from a *Pseudomonad* host, *Pseudomonas* sp. strain TCU-HL1, and performs the same stereoselective hydroxylation chemistry as P450cam.[8,9] The associated ferredoxins of P450tcu and P450cam, Pdx_{tcu} and Pdx, respectively, can be interchanged for camphor turnover between the homologous systems.[8] However, the same cannot be said of the redox partner of another Class I P450cam homologue, CYP101D1 from *Novosphingobium aromaticivorans* DSM12444.[10] CYP101D1 utilizes a ferredoxin redox partner known as Arx to support catalysis. While Pdx can support CYP101D1 catalysis, Arx can support neither P450cam nor P450tcu turnover.

The electron transfer proteins of P450cam and P450tcu originate from the same gene cluster as the P450s themselves.[9,11] In contrast, Arx and the associated ferredoxin reductase, ArR, are genetically associated with another P450, CYP101D2, but service as many as five related P450s from the host organism.[12,13] It is, therefore, reasonable to hypothesize that *Pseudomonad* P450s may exhibit greater selectivity for their redox partners and perhaps that the conformational changes associated with Pdx binding to P450cam may not be required in systems serviced by ferredoxins that support several P450s.

As such, our lab has focused on understanding the molecular origins of redox-partner specificity as well as examining other similar P450-redox partner interactions for insights. Like P450cam, P450lin (CYP111A1) is a plasmid-borne Class I P450 derived from *Pseudomonas incognita* and was the second bacterial P450 to be expressed and characterized. P450lin catalyzes the conversion of linalool to 8-hydroxylinolool (Scheme 3-1) and is expressed along with its redox partners, linredoxin reductase (LdR) and linredoxin (Ldx).[14–16] The sequence for Ldx is known, but the sequence of LdR is incomplete since a region of about 140 amino acids is missing from the initial sequence determination.[15] Ldx was unable to be recombinantly expressed, so I mutated Pdx at key amino acid residues to resemble Ldx, as the expression and purification protocols for Pdx are robust. I modified Pdx at several key positions (Figure 3-1) by removing the

terminal tryptophan (W106 → Δ106) and changing Asp38 to Leu (D38L) to resemble P450lin's native redox partner and reconstitute activity. Here, the interaction between P450lin and several ferredoxin-type redox partners was examined, including Pdx and Arx, and the impact of these redox partners on the stability of the oxycomplex (Fe^{II}–O_2) were assessed.

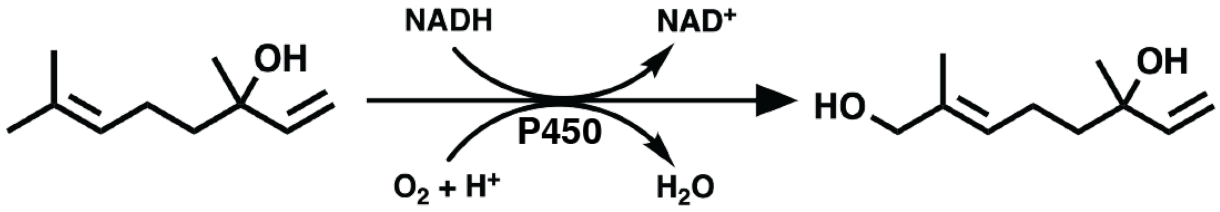

Scheme 3-1. The hydroxylation of linalool to 8-oxo-linalool as catalyzed by the P450lin system.

Results

The specificity of P450lin for non-native redox partners was determined by NADH consumption assays. The NADH consumption assay is a simple technique for testing redox partner selectivity. Based on the behavior of P450cam and other Class I P450s, the first electron transfer from the ferredoxin to the P450 is assumed to be the rate-limiting step.[17] Therefore, substrate-initiated NADH consumption is an indirect reporter of the turnover rate. If the ferredoxin is not compatible with the P450, there will be negligible NADH consumption upon addition of substrate.

P450lin was capable of turnover with non-native redox partners Pdx and Arx (Table 3-1, Figure 3-2) in contrast to the selectivity exhibited by P450cam. However, neither of these rates are as fast as the previously published rate using the native LdR and Ldx from the host *Pseudomonas incognita*,[14] which I was unable to recombinantly express. The native turnover rate of P450lin with Ldx and LdR was similar to that of P450cam, around 1000 min^{-1}. Of the non-native ferredoxins tested, Arx displayed the highest turnover rate. Examination of the sequence similarity

between Ldx, Arx, and Pdx revealed that a critical residue for the P450cam-Pdx interaction, Asp38,[18] is a leucine in both Ldx and Arx (Figure 3-1). Furthermore, the C-terminal residue of Pdx, Trp106, which also plays an important role in P450cam-Pdx binding and electron transfer,[18,19] is not present in either of the other redoxins. Pdx was therefore mutated to resemble Ldx and Arx by changing Asp38 to a leucine in both WT and a tryptophan knockout variant, Δ106. While both the D38L and Δ106 variants increased NADH consumption slightly over WT Pdx, the D38L/Δ106 double mutant enabled the highest rate of turnover of the ferredoxins with P450lin. Additionally, as expected, the single and double mutants of Pdx did not exhibit turnover with P450cam.

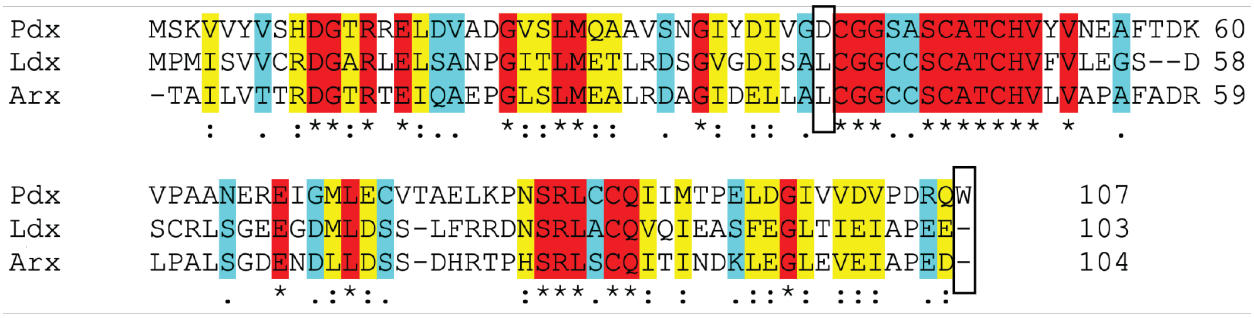

Figure 3-1. Ferredoxin sequence alignment. Conserved residues are highlighted in red and are marked with an asterisk. Highly similar residues are highlighted in yellow and are marked with two dots. Similar residues are highlighted in cyan and are marked with one dot. The residues mutated in this study are shown in a black box. Ldx and Pdx have 33.98% identity. Ldx and Arx have 54.90% identity.

Table 3-1. NADH consumption assay rates for P450lin and P450cam. Rates are given in mM^{-1} NADH μM^{-1} P450 min^{-1}.

P450	Redox Partner	NADH Consumption Rate	Coupling Efficiency
lin	Arx	179 ± 17	95.6 ± 0.9 %
	Pdx WT	5.44 ± 0.45	53.8 ± 1.9 %
	Pdx Δ106	8.67 ± 0.17	44.0 ± 3.6 %
	Pdx D38L	40.3 ± 3.3	83.4 ± 1.1 %
	Pdx D38L/Δ106	198 ± 1	97.5 ± 0.8 %
cam	Arx	– [10]	–
	Pdx WT	~1000 [20]	95% [21]
	Pdx Δ106	– [18]	–
	Pdx D38L	–	–
	Pdx D38L/Δ106	–	–

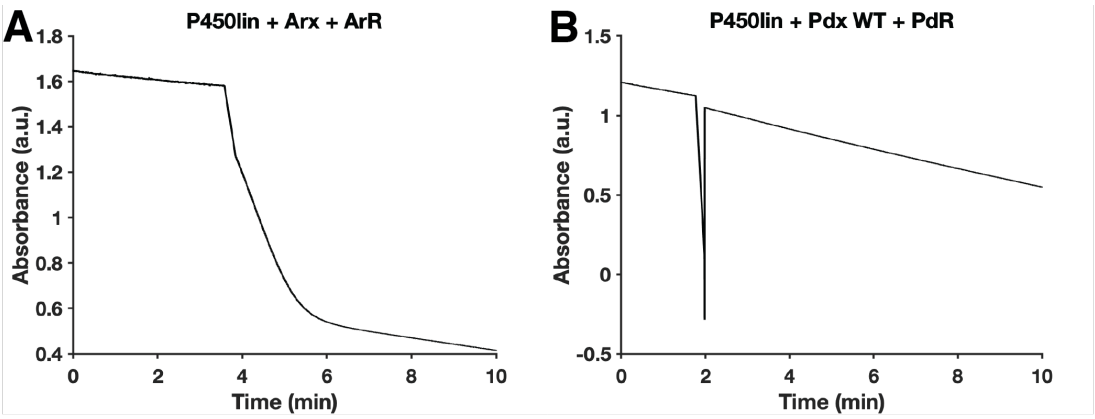
A
P450lin + Arx + ArR
Absorbance (a.u.)
Time (min)
B
P450lin + Pdx WT + PdR
Absorbance (a.u.)
Time (min)

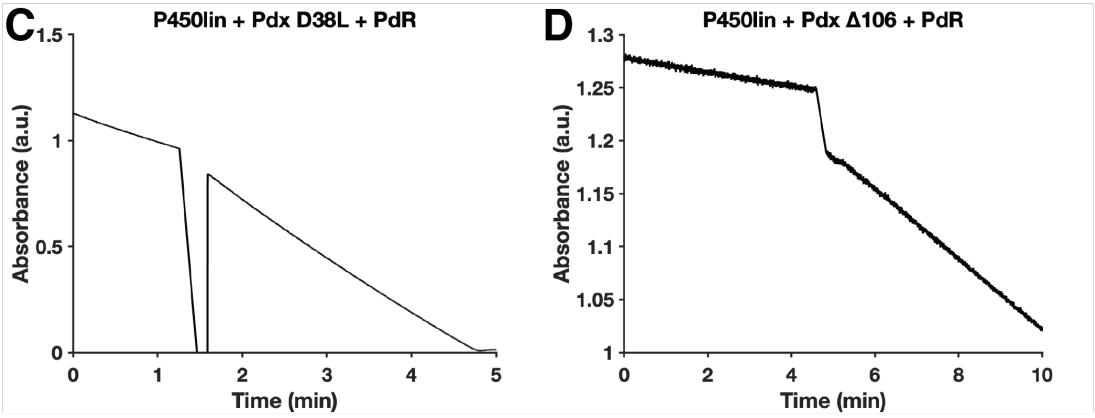
C
P450lin + Pdx D38L + PdR
Absorbance (a.u.)
Time (min)
D
P450lin + Pdx Δ106 + PdR
Absorbance (a.u.)
Time (min)

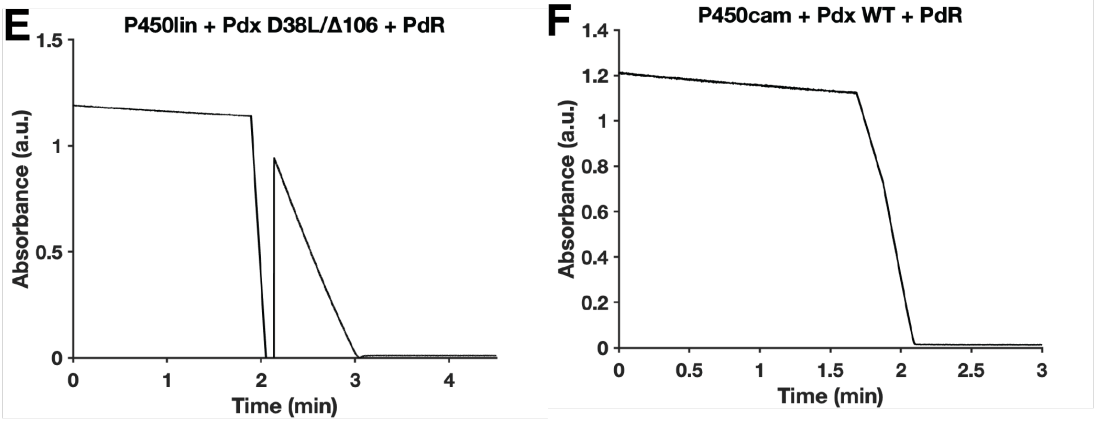
E
P450lin + Pdx D38L/Δ106 + PdR
Absorbance (a.u.)
Time (min)
F
P450cam + Pdx WT + PdR
Absorbance (a.u.)
Time (min)

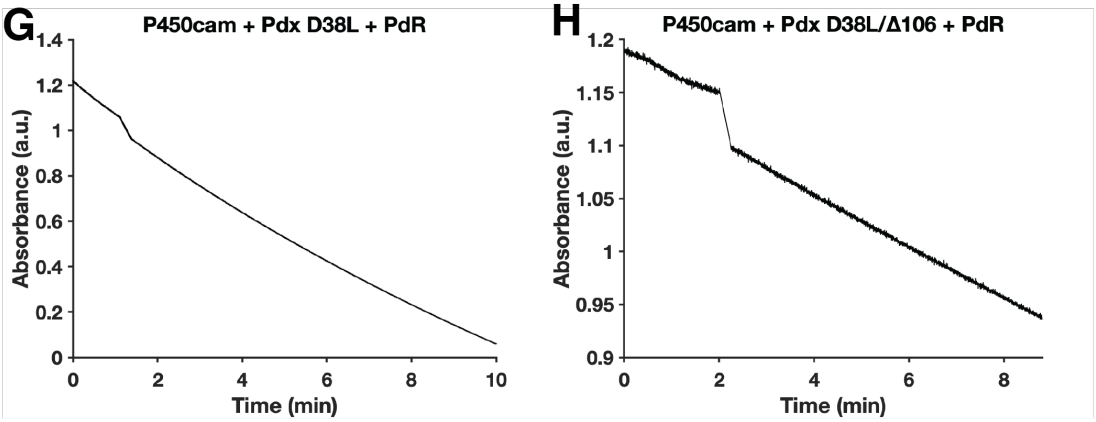
G
P450cam + Pdx D38L + PdR
Absorbance (a.u.)
Time (min)
H
P450cam + Pdx D38L/Δ106 + PdR
Absorbance (a.u.)
Time (min)

Figure 3-2. NADH traces at 340 nm for the consumption assays. (A) P450lin with Arx and ArR. Background rate is from 0-3 minutes, and rate of turnover is the linear slope from 4-5 minutes. (B) P450lin with Pdx WT and PdR. Background rate is from 0-1.5 minutes, and rate of turnover is from 3-10 minutes. (C) P450lin with Pdx D38L and PdR. Background rate is from 0-1 minutes, and rate of turnover is from 2-4 minutes. (D) P450lin with Pdx Δ106 and PdR. Background rate is from 0-4 minutes, and rate of turnover is from 6-10 minutes. (E) P450lin with Pdx D38L/Δ106 and PdR. Background rate is from 0-1.5 minutes, and rate of turnover is from 2.3-2.8 minutes. (F) P450cam with Pdx WT and PdR. Background rate is from 0-1.5 minutes, and rate of turnover is from 1.8-2 minutes. (G) P450cam with Pdx D38L and PdR. Background rate is from 0-1 minutes, and rate of turnover is from 2-10 minutes. (H) P450cam with Pdx D38L/Δ106 and PdR. Background rate is from 0-2 minutes, and rate of turnover is from 3-8 minutes.

To test whether the consumption of NADH leads to a productive consumption of substrate, the coupling efficiency of P450lin was determined with each of the redox partners. In a completely coupled system, one molecule of NADH leads to the consumption of one molecule of substrate and the formation of one molecule of product. The use of plastic centrifuge tubes led to contamination in the extractions using DCM (Figure 3-3). However, there is minimal overlap of contamination peaks (Figure 3-3, black line) with the peaks of interest in our reaction mixture (blue line). The peaks for linalool (substrate), camphor (internal standard), and product are clearly visible. Linalool and camphor were identified by their respective mass spectra (Figure 3-5). Identification of the product isomer was not possible with GC/MS by NIST database search, but instead gave molecules with the expected masses for product. Qualitatively, there was a linear relationship between the decrease in substrate and an increase in product.

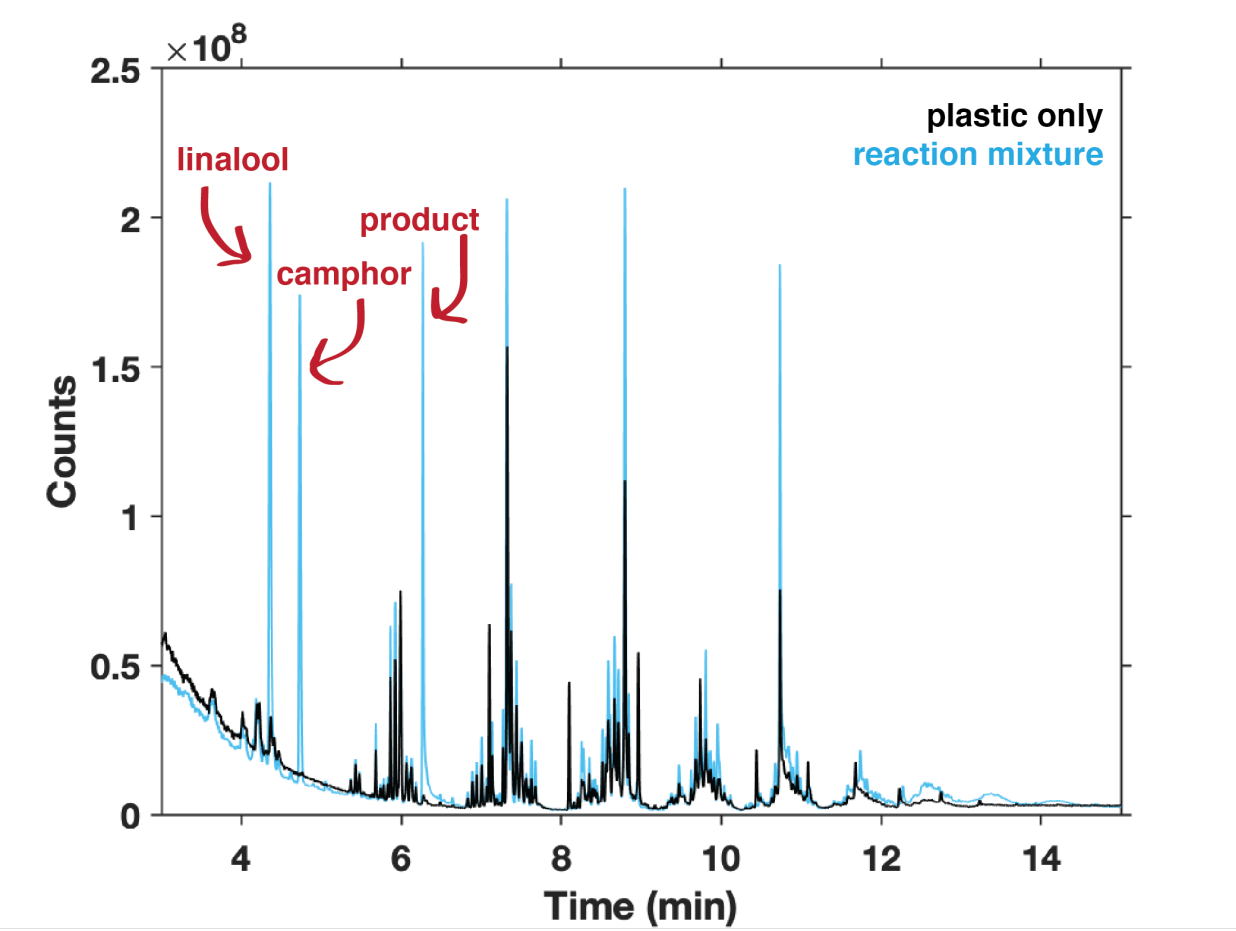

Figure 3-3. Chromatogram of DCM in plastic and extraction of reaction mixture in DCM in plastic.

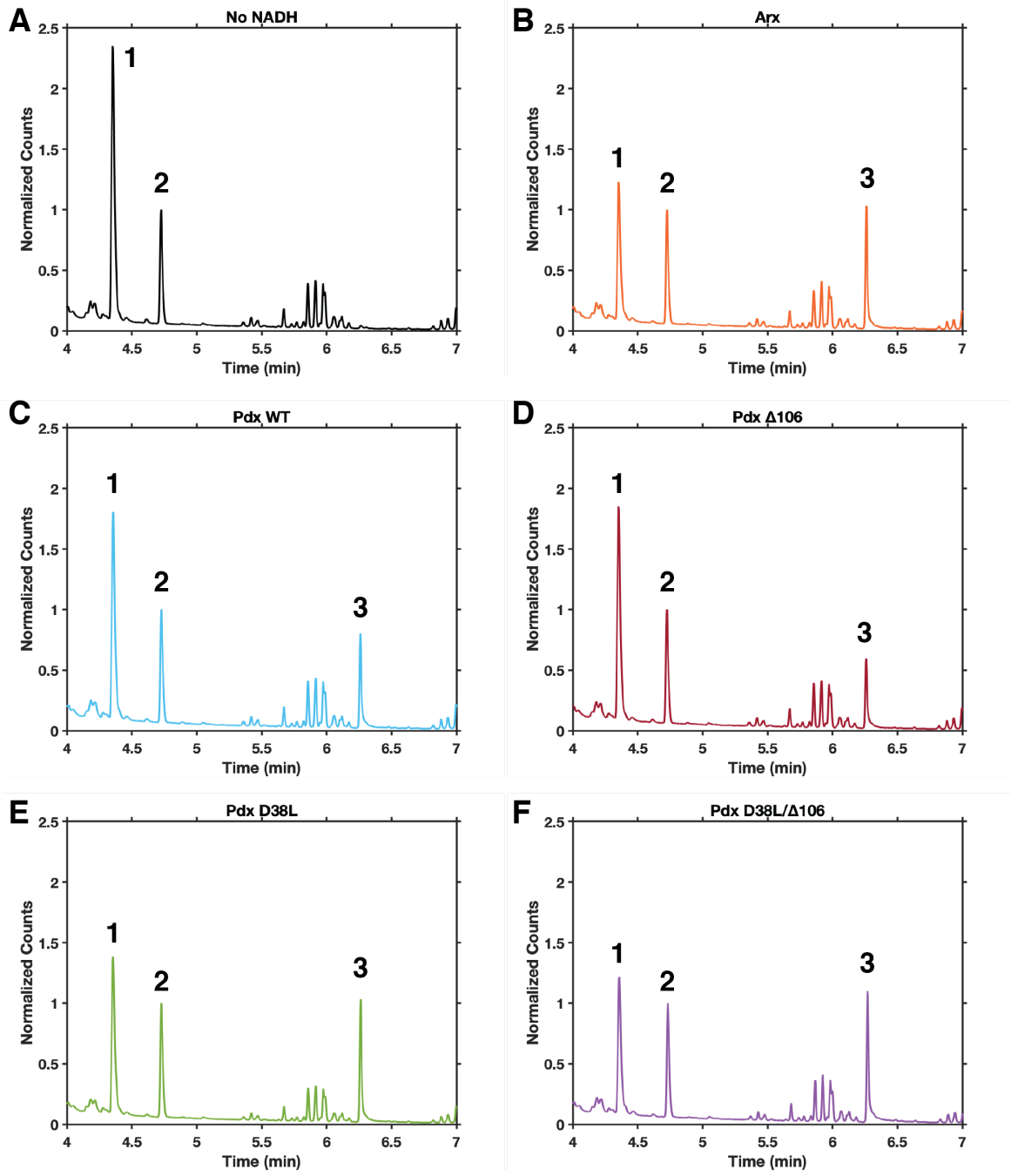

Figure 3-4. Chromatograms of reaction extractions. Each reaction contained 0.5 μM P450lin, 5 μM ferredoxin, and 0.5 μM ferredoxin reductase. The ferredoxin and reductase partners in the reaction mixtures were (A) Pdx D38L/Δ106 and PdR but no NADH added as a control, (B) Arx and ArR, (C) Pdx WT and PdR, (D) Pdx Δ106 and PdR, (E) Pdx D38L and PdR, and (F) Pdx D38L/Δ106 and PdR. Linalool (200 μM) was added to each reaction, followed by 100 μM NADH, with the exception of (A) the control. After the reaction completed, an internal standard of 50 μM camphor was added. The linalool peak (1) is around 4.4 min; the camphor peak (2) is around 4.7 min, and the product peak (3) is around 6.3 min.

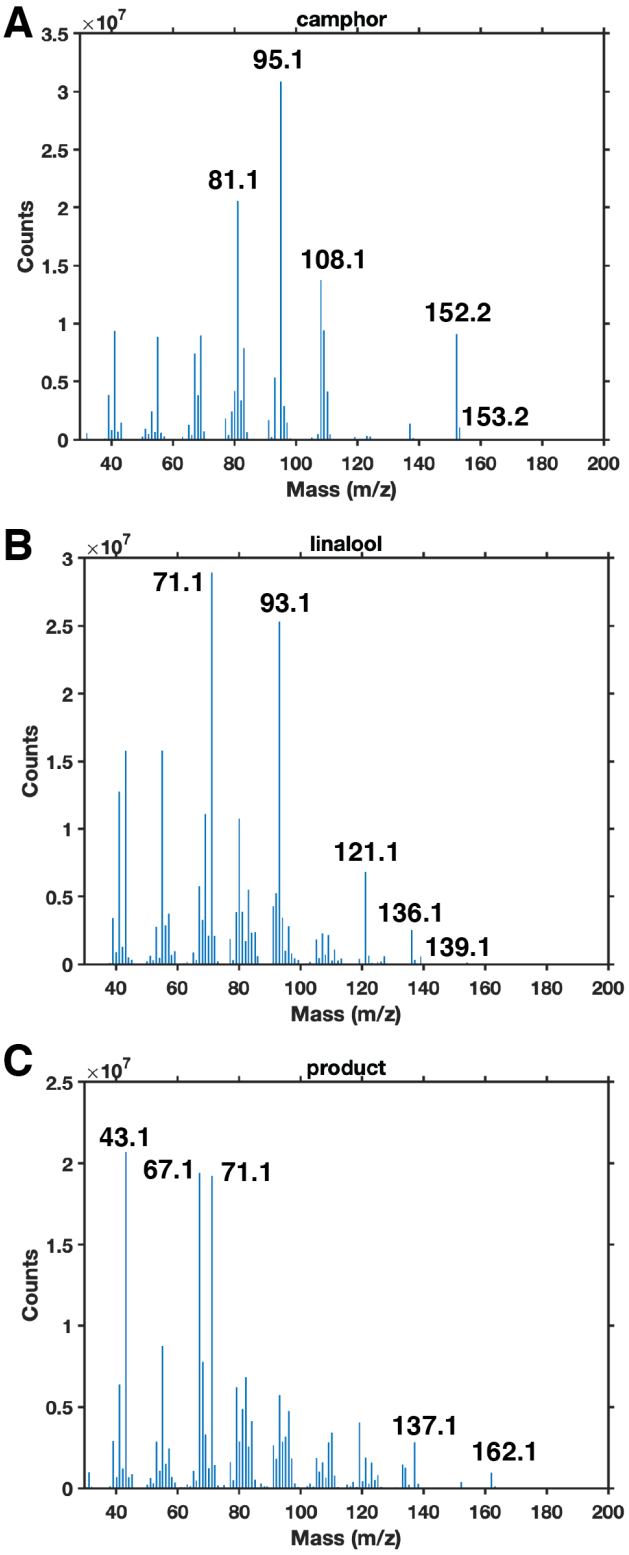

Figure 3-5. Mass spectra of camphor, linalool, and product from reaction mixtures.

Both Arx and Pdx D38L/Δ106 were almost perfectly coupled at 95.6 and 97.5%, respectively (Table 3-1, Figure 3-4). Pdx D38L exhibits a coupling efficiency of 83.4% while Pdx WT and Pdx Δ106 display nearly half the efficiency of Arx and Pdx D38L/Δ106 at 44.0 and 53.8%, respectively. These data reveal that minimal alteration of Pdx can result in near perfect coupling efficiency between a P450 and a non-native redox partner. More specifically, it highlights the importance of the leucine residue in retaining the coupling efficiency between P450lin and its redox partner.

The redox partner selectivity of P450cam is also associated with a spectral shift towards a low-spin state upon the binding of Pdx in the presence of high concentrations of camphor (Figure 3-6).[22–25] Therefore, P450lin was examined to see if it undergoes similar changes in its UV-vis spectral profile upon association with the Pdx D38L/Δ106 variant that supports catalysis. However, in contrast to P450cam, a shift towards a low-spin population of P450lin in the presence of linalool and Pdx D38L/Δ106 was not observed despite its appreciable turnover rate. I was unable to test whether the native redox partner of P450lin shifts the spectrum accordingly due to challenges in the recombinant expression of Ldx. As such, Ldx might still induce the low-spin spectral shift. Regardless, these results indicate that the residues that allow Ldx, Arx, and Pdx D38L/Δ106 to support P450lin turnover are distinct from those that may induce a spin-state change in P450lin's active site.

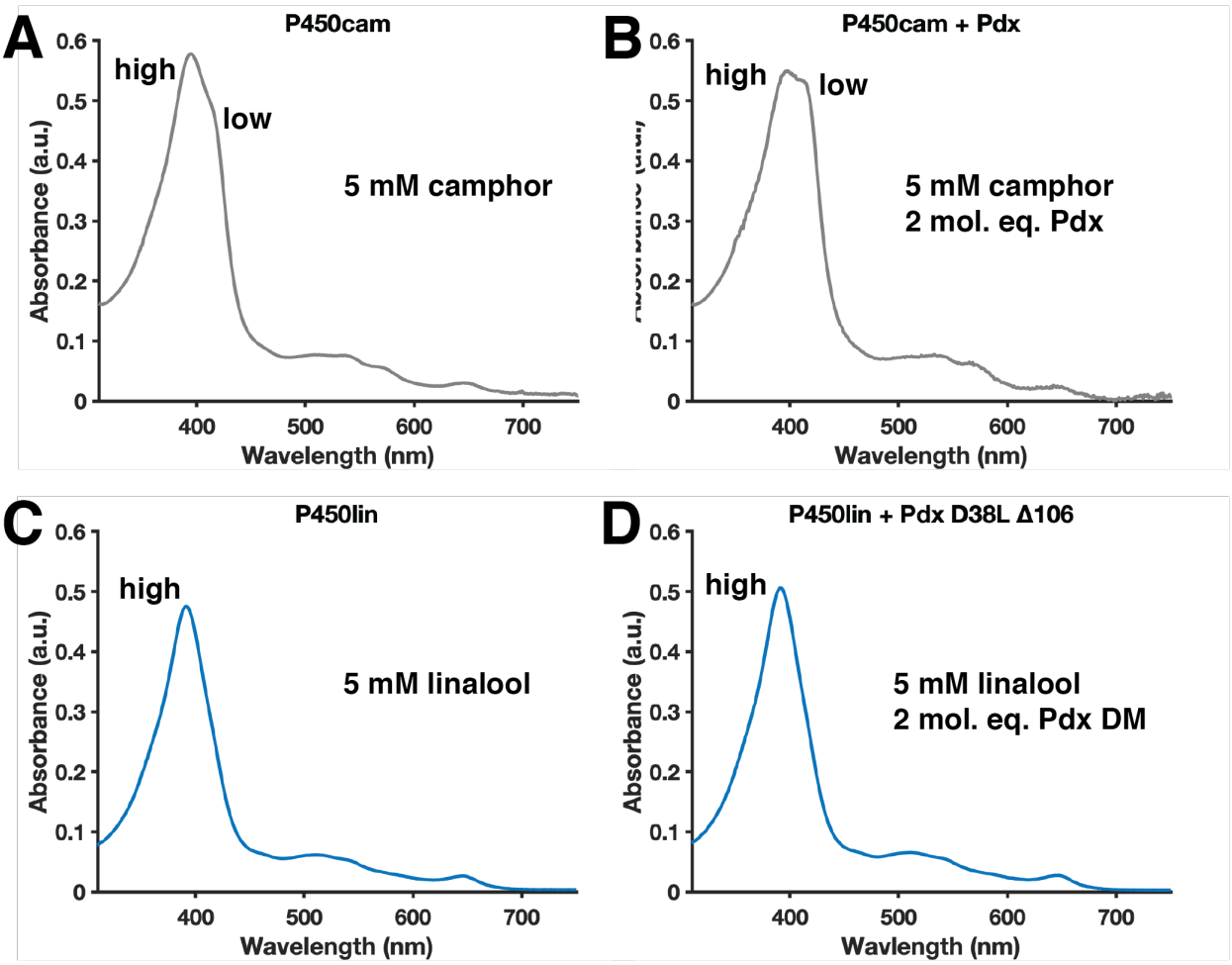

Figure 3-6. UV-vis spectra of the P450 spin-shift in presence of redox partner. P450cam was in 10 mM KPi pH 7.4 containing 5 mM camphor in the (A) absence and (B) presence of 2 molar equivalents of Pdx. P450lin was in 10 mM KPi pH 7.4 with 5 mM linalool in the (C) absence and (D) presence of 2 molar equivalents of Pdx double mutant (DM, D38L/Δ106). The low-spin population of P450cam in the presence of high-concentrations of camphor is attributed to the binding of a second substrate in an allosteric site.[22,26,27]

It is now known that the connection between a P450's spin-state and its global conformation is much more complicated than previously thought.[22,27,28] This observation means that while there is no apparent spin shift upon addition of Pdx D38L/Δ106 to substrate bound P450lin, a change in conformation cannot be ruled out. Since the selectivity of P450cam for Pdx is, in part, due to a conformational change driven by Pdx binding, I sought to determine whether alternative redox partners could induce a similar structural change in P450lin. In the absence of

direct structural information, the stability of the reduced oxygen bound P450 or “oxycomplex” has been used to provide insight into redox partner induced conformational changes.[29,30] As Pdx binding pushes P450cam towards a more open conformation, it was reasoned that redox partner induced structural changes would destabilize the oxycomplex resulting in a faster decay compared to the rate of auto-oxidation in the absence of a redox partner. Accordingly, the addition of Pdx increases the rate of oxycomplex decay by ~150 fold over the auto-oxidation rate (Scheme 3-2).[31]

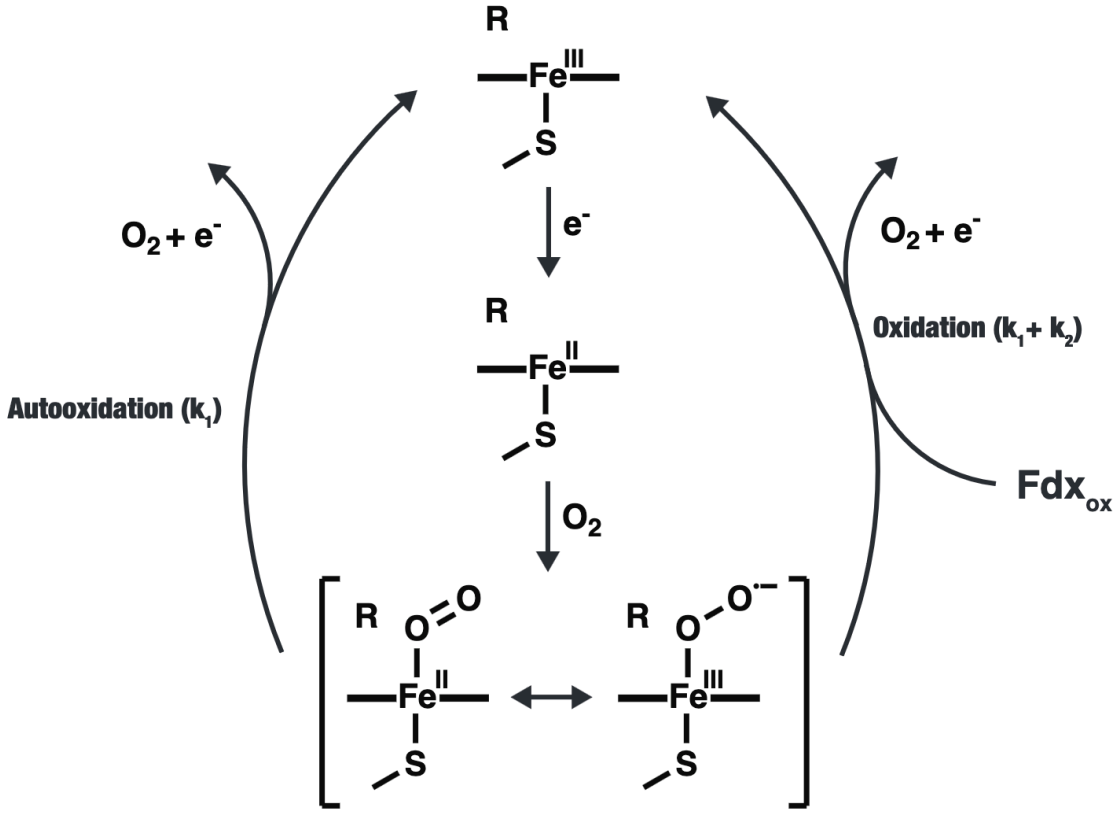

Scheme 3-2. Preparation and oxidation of the ferrous-O_2, oxycomplex. Substrate-bound high-spin ferric iron (Fe^{3+}) is reduced by dithionite, which provides 1 electron to produce the ferrous state (Fe^{2+}). Dioxygen then binds to form the oxycomplex. The reduced spectra and the oxycomplex exhibit Soret maximum at ~410 nm and ~422 nm, respectively. Without the delivery of a second electron to initiate the heterolytic cleavage of oxygen, the oxycomplex decomposes or auto-oxidizes, releasing a superoxide equivalent returning to high-spin Fe^{3+} state. In the presence of oxidized ferredoxin (Fdx), the complexation of the P450-oxycomplex and the ferredoxin results in an increase in the decay rate of the oxycomplex.

In P450lin, the decay of the oxycomplex was monitored with stopped-flow kinetics by the decrease in absorption at 431.5 nm and the growth of the ferric substrate-bound Soret at 388.8 nm (Scheme 3-2). The rate of autooxidation of the P450lin oxycomplex in the absence of redox partner was fit to a monoexponential (Equation 3-1) with both wavelengths exhibiting similar rates of decay and growth (Table 3-2, Figure 3-7, Figure 3-8), where *a* is the amplitude, *k* is the rate constant, and *c* is a constant. Differences in these two values, particularly in the case of Arx, could be attributed to the residual dithionite peak at ~350nm contributing to noise in the 388.8nm trace. In the presence of redox partner, the rates for P450lin were best fit to a biexponential model (Equation 3-2) where the first component is attributed to the decay of the oxycomplex or growth of the oxidized ferric species (Table 3-2, Figure 3-7, Figure 3-8). Consistent with the NADH consumption assays, Pdx D38L/Δ106 displayed the highest oxycomplex decay rate, at ~150x, remarkably similar to P450cam with Pdx. Arx had a similar effect on the oxycomplex, with a decay rate ~50x. Pdx WT had the lowest impact on the oxycomplex, with ~5x increase in decay rate. These values are consistent with the trend in NADH consumption rates.

Table 3-2. P450lin oxycomplex decay rates from stopped-flow kinetics.

Wavelength (nm)	Ferredoxin	k_1 (s^{-1})	k_2 (s^{-1})	Fold Increase
431.5	–	0.0584 ± 0.0007	–	1
431.5	Pdx WT	0.274 ± 0.007	0.0663 ± 0.001	4.69
431.5	Arx	4.15 ± 0.02	0.645 ± 0.010	71.1
431.5	Pdx D38L/Δ106	9.61 ± 0.14	1.28 ± 0.07	165
388.8	–	0.0590 ± 0.0005	–	1
388.8	Pdx WT	0.310 ± 0.005	0.0795 ± 0.0006	5.25
388.8	Arx	1.28 ± 0.01	0.0206 ± 0.0015	21.7
388.8	Pdx D38L/Δ106	9.10 ± 0.24	1.31 ± 0.09	154

$$Y = a * \exp(-kx) + c$$

Equation 3-1. Monoexponential

$$Y = a_1 * \exp(-k_1 x) + a_2 * \exp(-k_2 x) + c$$

Equation 3-2. Biexponential

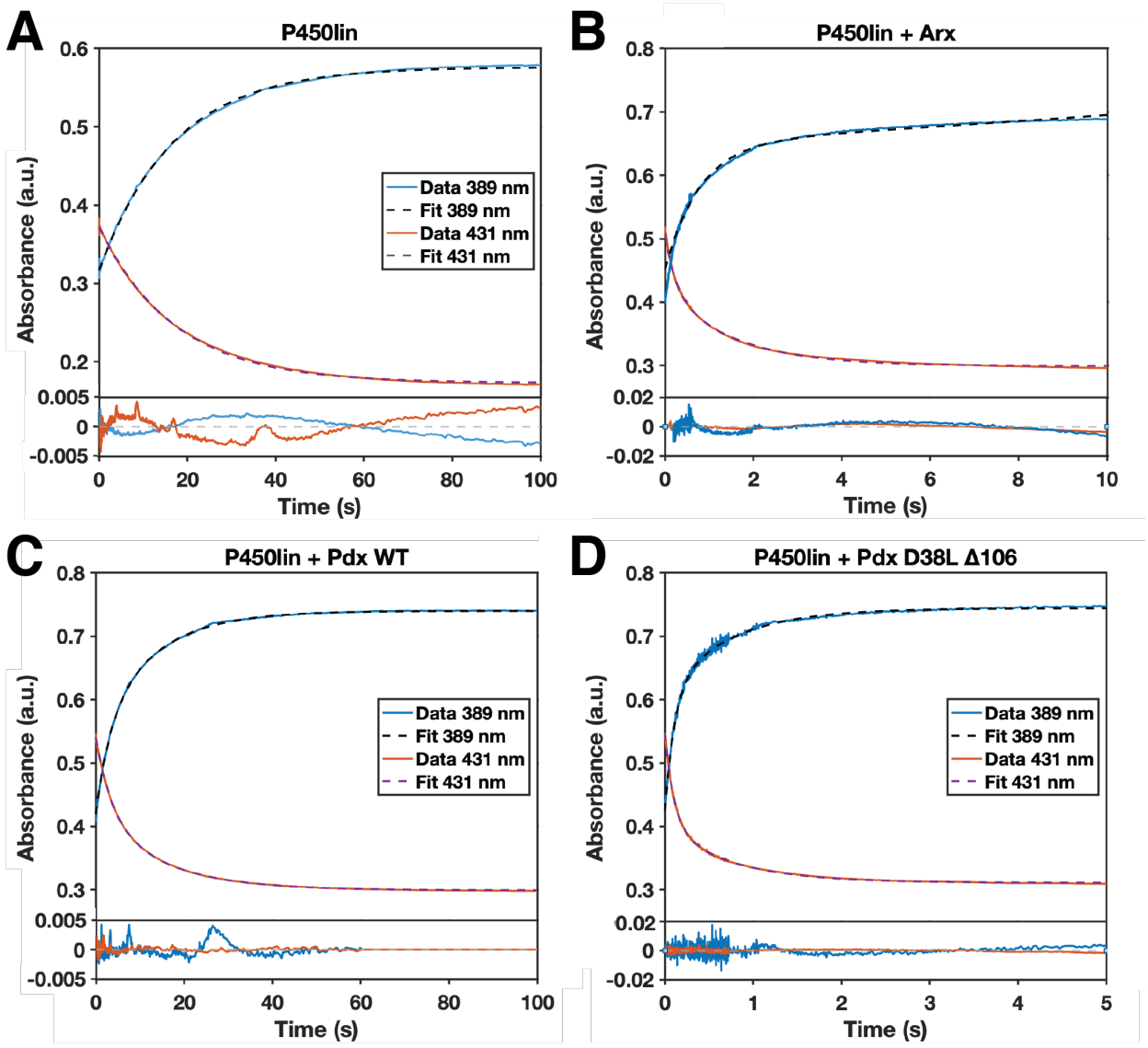

Figure 3-7. Stopped-flow kinetics of P450lin oxycomplex decay. (A) P450lin oxycomplex decay monitored at 432 nm and return to ferric at 389 nm in the (A) absence of redox partner and in the presence of (B) Arx at 2-fold concentration, or (C) Pdx at 2-fold concentration, or (D) Pdx D38L/Δ106 at 2-fold concentration. The residuals of each fit of the traces are shown in the panels underneath their respective plots.

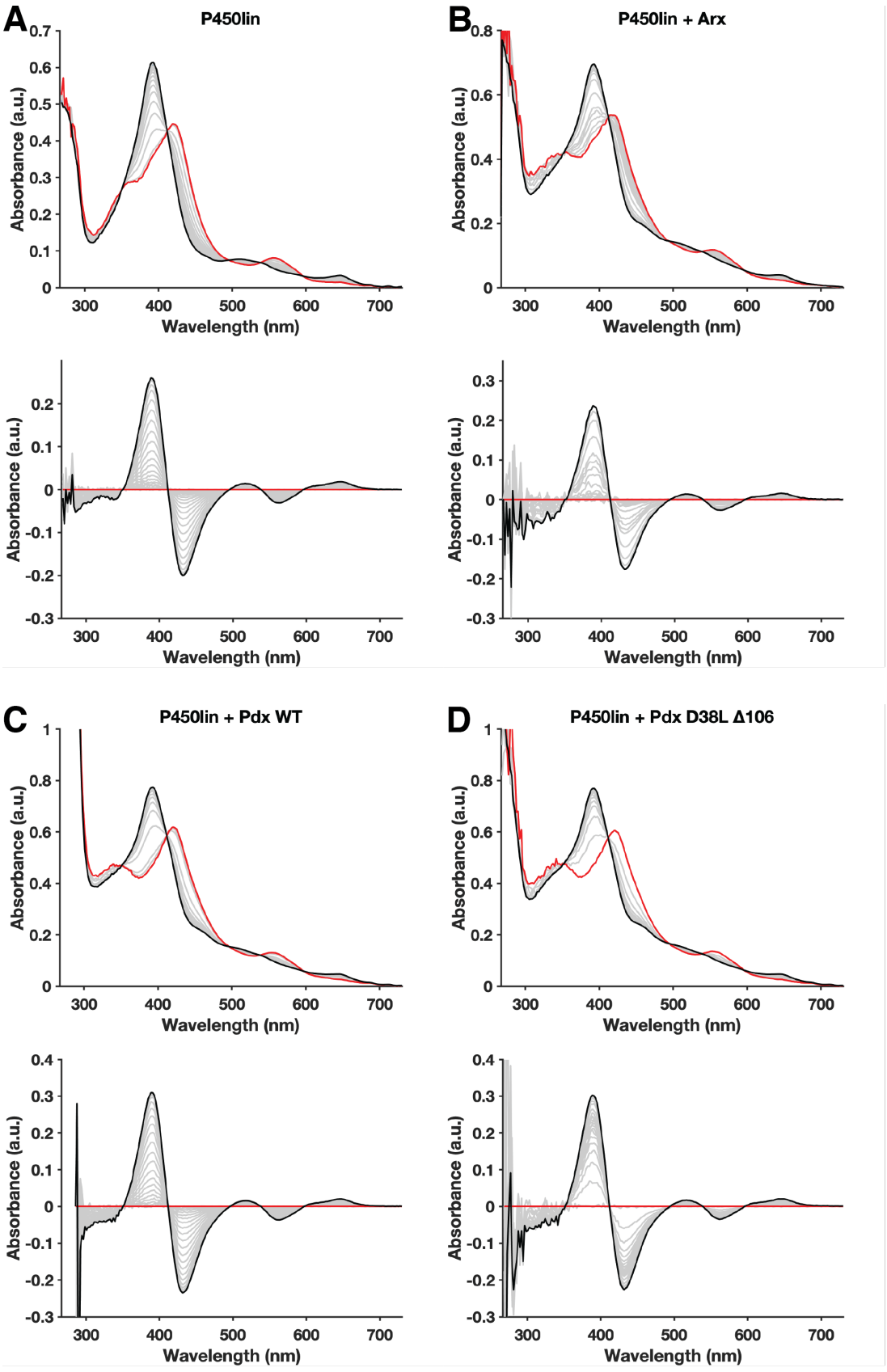
A
P450lin
B
P450lin + Arx
C
P450lin + Pdx WT
D
P450lin + Pdx D38L Δ106
Absorbance (a.u.)
Wavelength (nm)

Figure 3-8. Stopped-flow spectra and difference spectra. (A) P450lin oxycomplex decay in the absence of redox partner (top) and difference spectra (bottom). (B) P450lin oxycomplex decay in the presence of Arx (top) and difference spectra (bottom). (C) P450lin oxycomplex decay in the presence of Pdx WT (top) and difference spectra (bottom). (D) P450lin oxycomplex decay in the presence of Pdx D38L/Δ106 (top) and difference spectra (bottom). The red line is the starting spectra, the grey are the intermediate spectra, and black is the final spectra for all. All reactions were run in 50 mM KPi pH 7.4 with 1 mM linalool at room temperature. The P450 solution was degassed and anaerobically reduced with dithionite. The redox partner solution was made with buffer that had air bubbled in from an in-house air line for 10 minutes. The time scales for each are the same as its counterpart in Figure 3-8.

Discussion

The ability of redox partners to modulate the structure and activity of P450s is an active area of research, yet there is limited structural information on how these proteins associate and induce such pronounced effects.[5,32] As such, co-crystallized complexes like those of P450cam-Pdx have allowed for a deeper understanding of redox partner selectivity and the origin of induced conformational changes.[3,33] However, conservation of the selectivity of P450cam and the redox partner induced transitions across other P450s remains unclear. Based on the biological similarities between P450cam and P450lin, it was hypothesized that these two systems would behave quite similarly. When P450lin was first expressed and purified from the host *Pseudomonas incognita*, its selectivity was tested with Pdx and PdR.[14] The results with P450lin with Pdx and PdR showed selectivity on par with the previous report, albeit at slightly different rates of turnover. The scope of redox partners tested for activity were expanded to investigate the origin of selectivity and efficiency of electron transfer.

The native redox partner of CYP101D1, Arx, is more promiscuous than Pdx as it services many P450s in its native organism.[12,13] This fact could explain why CYP101D1, while tightly coupled, is less selective with respect to a redox partner for supplying electrons to oxidize substrate. On the other hand, P450s that initiate the metabolism of unusual carbon sources in *Pseudomonads* serve a critical role in assimilating their substrates as alternative energy sources, suggesting Class I systems from these organisms may be more selective and sensitive to redox

partners. Clearly this is not the case since Arx can support P450lin catalysis since NADH consumption assays revealed that Arx enables significant turnover rates in P450lin.

A sequence alignment of Pdx, Arx, and Ldx revealed high degrees of similarity between Ldx and Arx (54.90% identity) and moderate conservation between Ldx and Pdx (33.98% identity) (Figure 3-1). There are several important differences between the three ferredoxins including a critical aspartate in Pdx, Asp38, that forms an interfacial ion pair with Arg112 of P450cam.[3] Mutation of D38 in Pdx kills P450cam turnover activity.[18] In the analogous position of Arx and Ldx, there is a leucine residue. Therefore, Asp38 of Pdx was mutated to leucine which resulted in a slight increase in NADH consumption activity. Additionally, both Arx and Ldx lack a terminal tryptophan that has been identified as essential for Pdx to bind and transfer electrons to P450cam (Figure 3-1). Using a C-terminal tryptophan knockout variant of Pdx, Δ106, a double mutant was created including the D38L substitution. While Δ106 itself allowed for only slight improvement in turnover compared to Pdx (8.67 min^{-1}), the D38L/Δ106 variant displayed a substantial increase in activity (198 min^{-1}) over both WT ferredoxins and the single mutant. The ~5 and ~20-fold increase in activity of D38L/Δ106 compared to the single mutant D38L and knockout, respectively, highlights how sensitive the interfacial interactions are between P450s and their redox partners. The coupling efficiency of the Pdx variants follow a similar trend as the turnover assays with Pdx D38L/Δ106 display almost complete substrate conversion.

Based on these mutations, it appears that P450lin and Ldx likely share a similar interface to those found in other Class I systems like P450cam. As there is no crystal structure of P450lin, we utilized the Alphafold predicted structure for P450lin to analyze the potential interfacial interactions with Ldx (Figure 3-9).[34,35] The predicted structure exhibits the expected conserved P450 triangular fold. The areas of lowest confidence are also coincidentally the areas that vary the most from P450cam and likely participate in substrate binding. The Alphafold structure appears in an open conformation and while it is not known whether P450lin exhibits an open-to-

close transition upon substrate binding, the P450cam-Pdx complexes are found in a slightly open conformations even in the presence of substrate, allowing for a reasonable comparison.

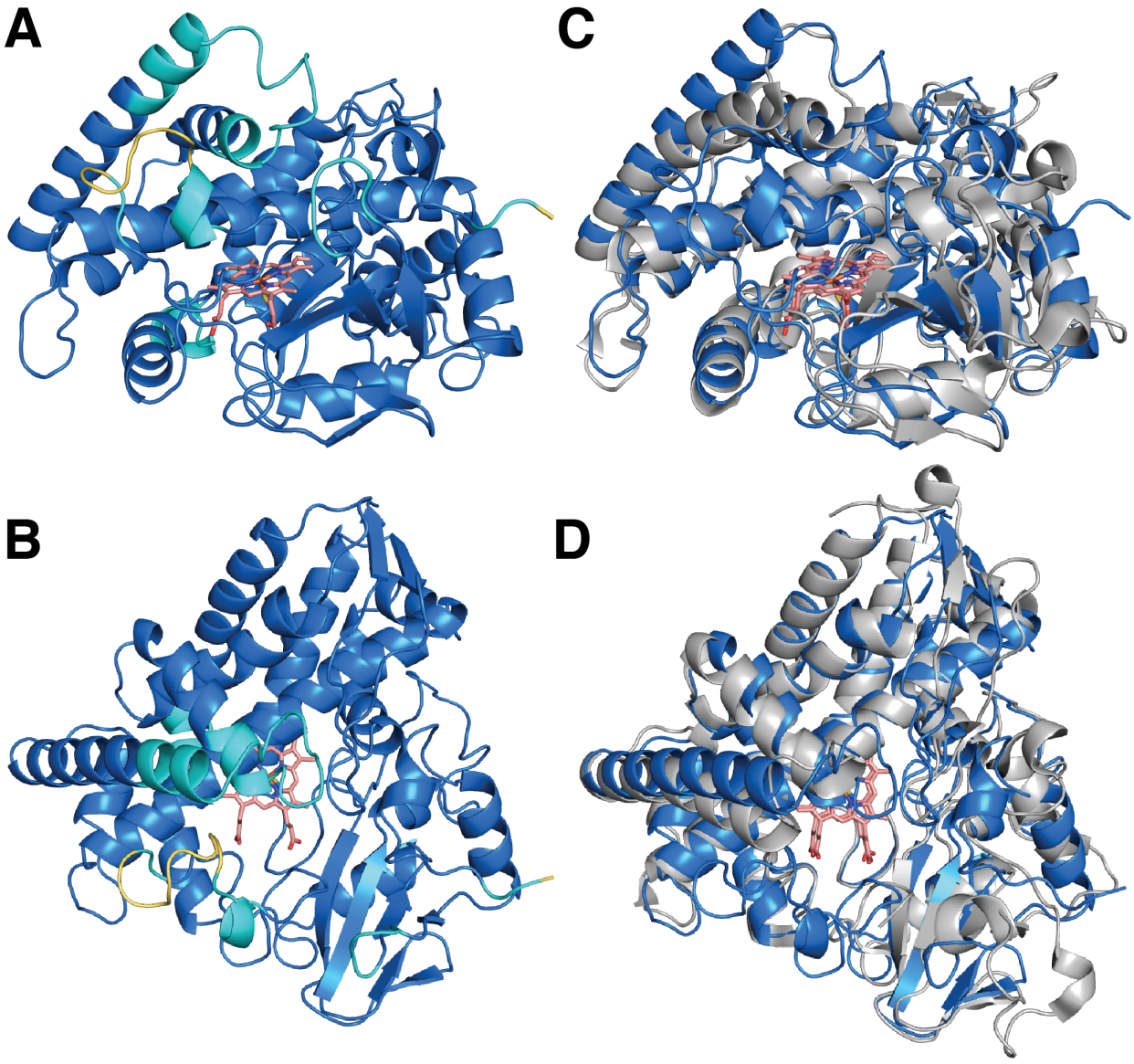

Figure 3-9. Structural alignment of P450cam in grey (PDB code: 3L62) and P450lin in blue (AlphaFold). (A) P450lin Alphafold structure. Regions of high confidence are shown in blue, average confidence shown in cyan, and low confidence shown in yellow. The heme of the Alphafold structure was added in Coot based on the structure of P450terp (PDB code: 1CPT) and is shown in pink. The heme of P450terp was chosen as the orientations of the heme propionates are more common than those found in P450cam. (B) P450lin Alphafold structure rotated ~ 60°. (C) P450lin Alphafold structure aligned to P450cam open structure and (D) rotated ~ 60°.

Many of the crucial P450cam residues that interact with Pdx originate from the C helix.[3,36,37] Overlaying the C helix from the P450cam-Pdx complex structure (PDB code: 4JWU) with the Alphafold structure of P450lin (Figure 3-10) reveals that the structural alignment correlates well with the sequence alignment (Figure 3-11) for this structural element. In P450cam, there are several residues that point towards Pdx, namely Arg109, Arg112, Ala113, and Asn116 and the corresponding residues of P450lin are Thr100, Arg104, Lys105, and Met107. Only one of these residues is conserved, Arg104, corresponding to Arg112 in P450cam, which is essential for electron transfer and forms a hydrogen bond with one of the heme propionates.[37] The retention of this residue and its role in electron transfer makes the results of our selectivity experiments quite surprising as D38 in Pdx interacts with Arg112 and its mutation to a leucine in Ldx and Arx would likely weaken the strength of this contact, but instead enhances the rate of NADH consumption and substantially improves the degree of coupling. Such a result points to the possibility that, while the surfaces P450lin and its redox partner that interact are conserved, the specific interactions and possibly the orientation of the protein-protein interface is not. Additionally, the single mutant, Δ106, that removes an interfacial tryptophan, increases the turnover frequency but decreases the coupling efficiency compared to Pdx WT. This behavior suggests that while the removal of the C-terminal tryptophan allows for more rapid electron transfer due to improved interactions with P450lin, the leucine mutation is necessary to ensure coupling for productive turnover.

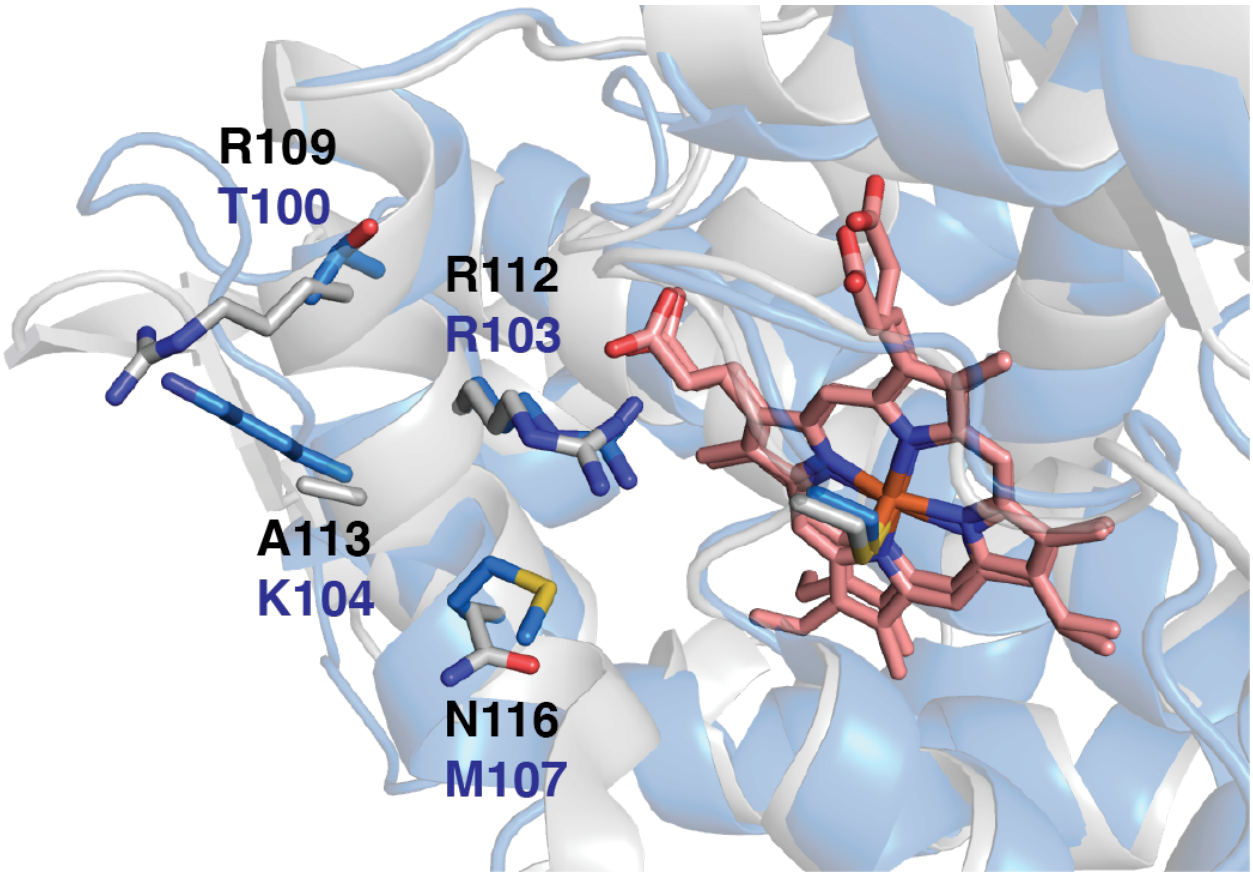

Figure 3-10. Structural alignment of residues involved in ferredoxin binding on C helices of P450cam (grey) and P450lin (blue). The heme is shown in pink. Residue labels are shown in black for P450cam and blue for P450lin.

```
P450cam MTTETIQSNANLAPLPPHVPEHLVFDFD-----MYNPSNLSAGVQEAWAVLQESNVPDLV 55
P450lin MERPDLKNP---DLYTQQVPHDIFARLRREEPVYWNPES---DGSGFWAVLRHKDIIEVS 54
        *    ::.         :**..:.  :       :**..   . .  ****:..:: ::

P450cam WTRCNGGHWIATRGQLIREAYEDYRH--FSSECPFIPREAGEAYDFIPTSMDPPEQRQFR 113
P450lin R-----------QPLLFSSAYENGGHRIFNENEVGLTNAGEAAVGVPFISLDPPVHTQYR 103
                   :  *: .***:  *  *..:   : . .  * ..   *:*** : *:*

P450cam ALANQVVGMPVVDKLENRIQELACSLIESLRPQGQCNFTEDYAEPFPIRIFMLLAGLPEE 173
P450lin KVIMPALSPARLGDIEQRIRVRAEALIERIPLGEEVDLVPLLSAPLPLLTLAELLGLDPD 163
         :   .:.   :..:*:**:  * :*** :    : ::.   : *:*:  :  * **  :

P450cam DIPHLKYLTDQMTRPD------GSMTFAEAKEALYDYLIPIIEQRRQKPGTDAISIVANG 227
P450lin CWYELYNWTNAFVGEDDPEFRKSPEDMAKVLGEFMGFCQELFESRRANPGPDIATLLANA 223
           .*   *: :.  *      .   :*:.   : .:   ::*.** :** *  :::**.

P450cam QVNGRPITSDEAKRMCGLLLVGGLDTVVNFLSFSMEFLAKSPEHRQELIERPERIPAACE 287
P450lin EINGQPVALRDFIGNLTLTLVGGNETTRNSISHTIVTLSQQPDQWDILRQRPELLKTATA 283
        ::**:*::  :      * **** :*. * :*.::  *::.*:: : * :*** : :*

P450cam ELLRRFSLVAD-GRILTSDYEFHGVQLKKGDQILLPQMLSGLDERENACPMHVDFSRQKV 346
P450lin EMVRHASPVLHMRRTAMEDTEIGGQAIAKGDKVVLWYASGNRDESVFSDADRFDVTRTGV 343
        *::*: * * .  *   .* *: *  : ***:::*    .. **   :   :.*.:*  *

P450cam SHTTFGHGSHLCLGQHLARREIIVTLKEWLTRIPDFSIAPGAQIQHKSGIVSGVQALPLV 406
P450lin QHVGFGSGQHVCVGSRLAEMQLRVVFEILSTRVKRFELCSKSR-RFRSNFLNGLKNLNVV 402
        .*. ** *.*:*:*.:**. :: *.::   **:  *.:.  :: :.:*.::.*:: * :*

P450cam WDPATTKAV      415
P450lin LVPK-----      406
```

Figure 3-11. P450 sequence alignment. P450lin and P450cam have 25.26% identity.

P450lin is highly sensitive to the nature of the residues that form the interface with its redox partner as changing only two residues of Pdx to be more like Ldx results in restored activity and improved coupling efficiency. The drastic changes in turnover rate and coupling efficiency from the subtle changes to the interface may suggest that a conformation change of P450lin may be occurring upon redox partner binding. However, more experiments are needed to demonstrate this effect. The conformational change in P450cam-Pdx complex is supported by the observation that Pdx pushes P450cam towards a low spin state,[38] however the Pdx D38L/Δ106 mutant that allows for the highest rate of NADH consumption and degree of coupling does not induce a similar

shift in the UV-vis spectrum of linalool-bound P450lin. There is, however, one feature shared by several bacterial P450s including P450lin.[29,31,39] The productive binding of a redox partner results in destabilization of the P450 oxycomplex. This could be due to back electron transfer from the ferrous oxycomplex to iron-sulfur cluster of the redox partner. Alternatively, there is the functionally much more interesting possibility that redox partner binding in all these P450s results in similar protein conformational changes or more subtle changes in the heme and ligands required for activation of the oxycomplex. If so, then redox partner binding serving an effector role in the activation of the P450 oxycomplex may be a general feature in P450 catalysis.

Beyond its role in electron transfer, Pdx induces structural changes that allow for the formation of a proton relay network in P450cam. Without crystallographic or NMR structural information, it is difficult to assess whether similar changes occur in P450lin upon redox partner binding. P450lin has a conserved Thr at position 248 that, in other P450s, provides a hydrogen bond to stabilize the oxycomplex and promotes the heterolytic cleavage of the iron-linked oxygen molecule.[40] It also displays an adjacent glutamate at position 247 where P450cam employs a similar Asp251. This distinction is subtle but important because when D251 is changed to a Glu in P450cam, activity is completely lost and Pdx loses its ability to shift P450cam toward low-spin.[41] CYP101D1, however, also has the corresponding Asp but it is tied up in fewer salt bridges than P450cam. The D259E variant retains partial activity and displays a large kinetic isotope effect (KSIE) indicating a similar importance to D251 in P450cam for the formation of a proton relay network.[41] The two residues that form the ion pair with D251 in P450cam are Arg186 which is conserved in CYP101D1 and Lys176 which is a glycine that is unable to form the second ion-pair. The lack of a second ion-pair in CYP101D1 is what allows for the retention of activity in the D259E variant. The D259E P450cam mutant is inactive as the more flexible Glu cannot be freed from the strong local H-bonding interactions upon Pdx binding, while in D251E CYP101D1 is able to break the single R186 contact. In P450lin, the alignments suggest no analogous ion-pairing for E247.

Although the Alphafold structure indicates this area of the F-helix is of moderate confidence, the corresponding residues of P450lin are Y168 and G176, which may account for why P450lin exhibits less selectivity for its redox partner.

Conclusion

P450lin is less selective for its redox partner than P450cam despite originating from a highly homologous system. P450lin exhibits almost complete coupling with non-native redox partner Arx, while WT Pdx retains ~54% coupling, the turnover rate is dramatically reduced. The removal of W106 and mutation of Asp38 to Leu remarkably recovers both the turnover rate and coupling efficiency. Like other P450s, the interaction of P450lin with its redox partner does result in a change upon redox partner binding that leads to a destabilization of the iron-linked O_2 unit. Although the selectivity of P450cam is so far unique, the influences of redox partner binding on the stability of the oxycomplex, and its important role in activation of O_2, may be conserved in many P450s.

Future Prospects

One of the initial steps in this project was the crystallization of P450lin. Crystals were obtained in two conditions: one with sodium thiocyanate and PEG 3350, and another with potassium iodide and PEG 3350 (Figure 3-12). These conditions yielded thin plates that did not diffract well. Crystallization was improved with streak seeding with a whisker, but the crystals still diffracted poorly. There is also a published account of crystals with a preliminary space group.[42] However, there was no follow-up paper and any attempts to replicate these conditions did not yield crystals. As such, the crystal structure of P450lin remained elusive. Similarly, the recombinant expression of Ldx never was successful. Attempts to perform a BLAST search the three proteins of the P450lin system yielded too many results that would be difficult to narrow

down to pursue meaningfully. However, I did discover a potential new P450lin system that might fill some of the holes in the existing P450lin system.

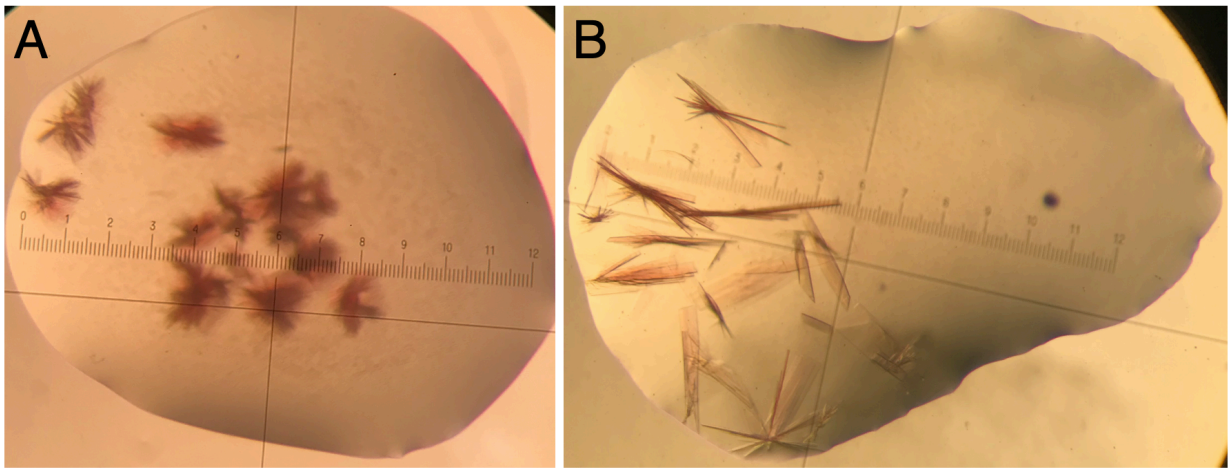

Figure 3-12. Crystals of P450lin. (A) The protein condition was 27 mg/mL P450lin in 50 mM Tris pH 7.4 and 15 mM DTT. The well condition was 0.2 KSCN and 25% v/v PEG 3350. (B) The protein condition was 25 mg/mL P450lin in 25 mM KPi pH 7.4 and 15 mM DTT. The well condition was 0.2 M KI and 25% v/v PEG 3350. The drop ratio was 1:1, protein:well for both.

When searching for the Alphafold structure for P450lin in the Alphafold database, two results were presented: P450lin from *Pseudomonas putida* and one from *Acinetobacter baylyi* (strain ATCC 33305 / BD413 / ADP1). The *Psuedomonas putida* P450lin sequence was identical to the one of P450lin I had been using.[15] A sequence alignment of the two P450lin sequences gave a sequence identity of 77% (Figure 3-13). When looking back at the BLAST search results for P450lin, this “new” P450lin sequence was one of the top results. Since the sequence identity was so high, and there was a proposed structure from Alphafold, I searched the genome from this *Acinetobacter* strain[43] for the operon, and possible ferredoxin and reductase genes. There is only one P450 in the in the entire genome, and the operon is very similar to that of the *Pseudomonad* system. The *Pseudomonad* system has an order of a hydratase, P450lin, a regulatory protein, an aldehyde dehydrogenase, an alcohol dehydrogenase, Ldx, and then LdR. Similarly, the *Acinetobacter* operon has a hydratase-related protein, an acyl-CoA synthase, a

transporter, P450lin, a regulatory protein, an aldehyde dehydrogenase an alcohol dehydrogenase, Ldx, and then LdR. There are two additional putative proteins, but the similar organization of the operon is further evidence that these P450lin systems are homologs. The sequence identity of the two Ldx's is 58% (Figure 3-14) – not as high as that of the P450lins, but given that the Pseudomonad Ldx could not be expressed, maybe a change in sequence could lead to expression. The new LdR sequence was 56% identical to the existing Pseudomonad LdR sequences (Figure 3-15). All of these sequences were above 40% identity, which means that they probably share similar functions. In fact, the sequence identity of P450s can be much lower and still retain P450 functionality. Also, the differences could be explained by the different bacterial strains over the years.

Given the promising similarities, the 3 genes were ordered in pet28a with an N-terminal H6-tag. The P450 was expressed identically to P450lin (described below), and the redoxin and reductase were expressed as reported previously.[44] The cells for the P450 appeared a red color, and the cells for the reductase appeared a yellow color, indicating that they had both expressed. The new Ldx did not express with a histag, but redoxins expressed with a histag have a long history of not being successful. Therefore, the new Ldx was cloned into the same vector used for Pdx, Tdx, and Arx, without a histag. Ldx did express recombinantly, which was personally fantastic, as I had struggled for quite a time with the *Pseudomonad* Ldx expression. This new *Acinetobacter* system has provided two proteins that were unable to be obtained from the *Pseudomonad* system, and perhaps this new P450lin protein will crystallize well.

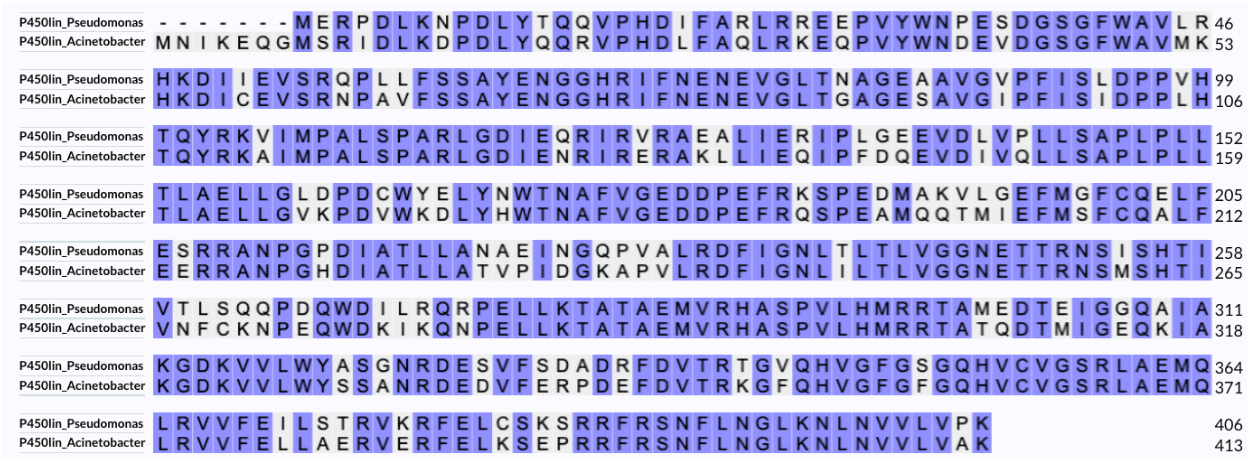

Figure 3-13. Sequence alignment of the P450lins from *Pseudomonad* and *Acinetobacter*.

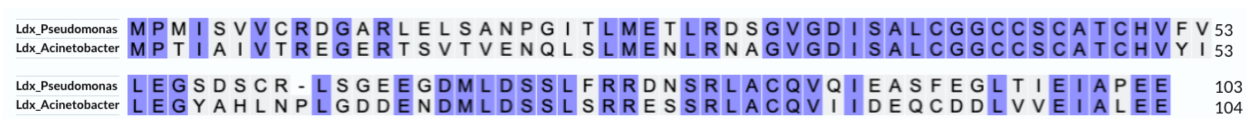

Figure 3-14. Sequence alignment of the Ldxs from *Pseudomonad* and *Acinetobacter*.

Figure 3-15. Sequence alignment of the LdRs from *Pseudomonad* and *Acinetobacter*.

Materials and Methods

Protein Expression and Purification

P450lin was encoded on a pET28a+ vector with N-terminal His6-tag (Genscript). *E. coli* BL21(DE3) cells were grown in Luria Broth (LB) overnight culture of 100 ml with 50 mg/L kanamycin. 10 mL of overnight culture were inoculated into 7 flasks each containing 1 L of Terrific Broth with 50 mg/L kanamycin. Cells were grown at 37 °C and 220 RPM until OD_{600} = 0.8 – 1. Expression was induced by addition of 1 mM isopropyl β-d-1-thiogalactopyranoside (IPTG) and supplemented with 0.4 mM 5-aminolevulinic acid (D-ALA) The shaker conditions were turned down to 25°C and 100 RPM. Protein was expressed over 48 hours, and then the cells were harvested. Cells were resuspended in lysis buffer (50 mM KPi pH 7.4, 250 mM NaCl, 2 mM BME) and lysed by two passes through a microfluidizer. The cell lysate was centrifuged at 15,000 RPM (~31,000 RCF) for 1 hour at 4°C (Beckman Coulter Avanti JA-17). The supernatant was loaded onto a NiNTA column (ThermoFisher, 50 mL) pre-equilibrated with lysis buffer. After washing with 3-5 column volumes (CVs) of lysis buffer, the protein was eluted with 1 CV of lysis buffer containing 250 mM imidazole. Fractions containing the red-colored protein were pooled. A few granules of thrombin (ThermoFisher) were added into the pooled solution. The protein solution was then dialyzed against lysis buffer overnight at 4°C. The dialyzed protein was loaded and passed through a second NiNTA column (20 mL) pre-equilibrated with lysis buffer to remove any residual protein retaining a His-tag. Protein was buffer exchanged into wash buffer (50 mM KPi pH 7.4, 2 mM BME) by several rounds of centrifugation in 30 kDa centrifugal filters (Millipore Amicon), then loaded onto a pre-equilibrated Q Sepharose column (Cytiva, 50 mL). The column was washed with 5 CVs of wash buffer followed by a gradient elution of the protein with 0 – 600 mM NaCl in wash buffer. Collected fractions with an optical purity ratio (Reinheitzahl, R/Z, A_{417}/A_{280}) > 1.4 were pooled and concentrated to less than 2 mL. The protein was then loaded onto a size exclusion column (SEC) (Cytiva Sephacryl S-200 HR, 180 mL) equilibrated with SEC

buffer (50 mM KPi pH 7.4, 5 mM DTT). Fractions with R/Z > 1.6 were collected, concentrated, and flash frozen for storage at -80°C.

P450cam, Pdx, PdR, Arx, ArR, were purified according to previously published procedures.[10,45,46] Several unsuccessful attempts were made to express and purify the natural P450lin redox partner, Ldx. I therefore generated mutants of Pdx that converted the expected binding interface to that of Ldx. The two most important differences at the binding interface are Asp38 in Pdx which is a leucine in Ldx and Trp106 of Pdx is missing in Ldx. The D38L mutation was made using by standard polymerase chain reaction protocols (Takara PrimeSTAR Max). The vector was transformed into *E. coli* C41(DE3) stock and plated onto ampilcillin-supplemented LB plates. Successful mutation was verified by miniprep (Macherey-Nagel) and sequencing (Genewiz) using standard protocols. The gene sequence for Ldx is known[15]; however, expression of the ferredoxin has proven elusive despite many attempts in different vectors, cell lines, and expression protocols.

Spectroscopy

The NADH consumption assays were run using a Cary Series 300 UV-Vis Spectrophotometer by monitoring the absorbance at 340 nm. The reaction mixtures contained 0.5 µM P450, 0.5 µM reductase, 5 µM ferredoxin in 1 ml of 50 mM KPi pH 7.4. PdR was used with all Pdx proteins, and ArR was used with Arx. The reaction was blanked, and then 2 μL of 185 mM NADH was added (for a final concentration of 370 μM) to collect the background oxidation rate. Substrate solution (20 μl) was then added to initiate the reaction. Reactions with P450cam and P450lin used 8 mM camphor and 10 mM linalool, respectively. Rates were calculated using a least-squares regression method.

NADH/Substrate Coupling Assays

Each coupling reaction was run in triplicate in microcentrifuge tubes (ThermoFisher) at room temperature in 50 mM KPi pH 7.4, with the same protein concentrations as the spectral assays, and 200 μM linalool. The reaction was initiated upon addition of 100 μM NADH. After the reactions were run to completion, an internal standard of camphor at 50 μM was added. An extraction was performed on the reaction mixture by the addition of 500 µL of dichloromethane (DCM) to the reaction mixture. The solutions were vortexed for 30 seconds and then the aqueous and organic layers were separated by centrifugation at 9000 RPM for 3 minutes at room temperature. The aqueous layer was removed and the extraction was repeated. Then organic layers from both extractions were combined. The samples were separated and analyzed by gas chromatography-mass spectrometry (GC-MS) (Thermo Fisher) and data analyzed in Chromeleon software. The concentration of substrate after the reaction was determined using a standard curve of linalool, where GC peaks corresponding to linalool were integrated.

Stopped-flow Kinetics

Stopped-flow experiments were performed using an Applied Photophysics SX18 stopped-flow spectrophotometer. Spectra were acquired using photodiode array (PDA) detection at room temperature. The P450 concentration was 15 µM, and the redoxin concentration was 30 µM, both in 50 mM KPi pH 7.4 with 1 mM linalool. The P450 was reduced with dithionite in degassed buffer. The experiments were performed in a single mix injection, where reduced P450 was mixed in equal volumes with the redoxin in oxygenated buffer. The data were fit to exponential models (Equations 4-1 and 4-2) using the ProData SX software. In some cases, the initial data points were removed to allow for convergence of the fit due to noise contributions at early times.

References:

(1) Lipscomb, J. D.; Sligar, S. G.; Namtvedt, M. J.; Gunsalus, I. C. Autooxidation and Hydroxylation Reactions of Oxygenated Cytochrome P-450cam. *Journal of Biological Chemistry* **1976**, *251* (4), 1116–1124. https://doi.org/10.1016/S0021-9258(17)33808-5.

(2) Pochapsky, T. C.; Lyons, T. A.; Kazanis, S.; Arakaki, T.; Ratnaswamy, G. A Structure-Based Model for Cytochrome P450cam-Putidaredoxin Interactions. *Biochimie* **1996**, *78* (8–9), 723–733. https://doi.org/10.1016/S0300-9084(97)82530-8.

(3) Tripathi, S.; Li, H.; Poulos, T. L. Structural Basis for Effector Control and Redox Partner Recognition in Cytochrome P450. *Science* **2013**, *340* (6137), 1227–1230. https://doi.org/10.1126/science.1235797.

(4) Hannemann, F.; Bichet, A.; Ewen, K. M.; Bernhardt, R. Cytochrome P450 Systems—Biological Variations of Electron Transport Chains. *Biochimica et Biophysica Acta (BBA) - General Subjects* **2007**, *1770* (3), 330–344. https://doi.org/10.1016/j.bbagen.2006.07.017.

(5) Liu, X.; Li, F.; Sun, T.; Guo, J.; Zhang, X.; Zheng, X.; Du, L.; Zhang, W.; Ma, L.; Li, S. Three Pairs of Surrogate Redox Partners Comparison for Class I Cytochrome P450 Enzyme Activity Reconstitution. *Commun Biol* **2022**, *5* (1), 791. https://doi.org/10.1038/s42003-022-03764-4.

(6) Mendes, M. V.; Antón, N.; Martín, J. F.; Aparicio, J. F. Characterization of the Polyene Macrolide P450 Epoxidase from *Streptomyces Natalensis* That Converts de-Epoxypimaricin into Pimaricin. *Biochemical Journal* **2005**, *386* (1), 57–62. https://doi.org/10.1042/BJ20040490.

(7) Sawada, N.; Sakaki, T.; Yoneda, S.; Kusudo, T.; Shinkyo, R.; Ohta, M.; Inouye, K. Conversion of Vitamin D3 to 1α,25-Dihydroxyvitamin D3 by Streptomyces Griseolus Cytochrome P450SU-1. *Biochemical and Biophysical Research Communications* **2004**, *320* (1), 156–164. https://doi.org/10.1016/j.bbrc.2004.05.140.

(8) Murarka, V. C.; Batabyal, D.; Amaya, J. A.; Sevrioukova, I. F.; Poulos, T. L. Unexpected Differences between Two Closely Related Bacterial P450 Camphor Monooxygenases. *Biochemistry* **2020**, *59* (29), 2743–2750. https://doi.org/10.1021/acs.biochem.0c00366.

(9) Tsang, H.-L.; Huang, J.-L.; Lin, Y.-H.; Huang, K.-F.; Lu, P.-L.; Lin, G.-H.; Khine, A. A.; Hu, A.; Chen, H.-P. Borneol Dehydrogenase from Pseudomonas Sp. Strain TCU-HL1 Catalyzes the Oxidation of (+)-Borneol and Its Isomers to Camphor. *Appl Environ Microbiol* **2016**, *82* (21), 6378–6385. https://doi.org/10.1128/AEM.01789-16.

(10) Batabyal, D.; Poulos, T. L. Crystal Structures and Functional Characterization of Wild-Type CYP101D1 and Its Active Site Mutants. *Biochemistry* **2013**, *52* (49), 8898–8906. https://doi.org/10.1021/bi401330c.

(11) Gunsalus, I. C.; Pederson, T. C.; Sligar, S. G. Oxygenase-Catalyzed Biological Hydroxylations. *Annual Review of Biochemistry* **1975**, *44* (1), 377–407. https://doi.org/10.1146/annurev.bi.44.070175.002113.

(12) Bell, S. G.; Wong, L.-L. P450 Enzymes from the Bacterium Novosphingobium Aromaticivorans. *Biochemical and Biophysical Research Communications* **2007**, *360* (3), 666–672. https://doi.org/10.1016/j.bbrc.2007.06.119.

(13) Yang, W.; Bell, S. G.; Wang, H.; Zhou, W.; Hoskins, N.; Dale, A.; Bartlam, M.; Wong, L.-L.; Rao, Z. Molecular Characterization of a Class I P450 Electron Transfer System from Novosphingobium Aromaticivorans DSM12444. *Journal of Biological Chemistry* **2010**, *285* (35), 27372–27384. https://doi.org/10.1074/jbc.M110.118349.

(14) Ullah, A. J.; Murray, R. I.; Bhattacharyya, P. K.; Wagner, G. C.; Gunsalus, I. C. Protein Components of a Cytochrome P-450 Linalool 8-Methyl Hydroxylase. *Journal of Biological Chemistry* **1990**, *265* (3), 1345–1351. https://doi.org/10.1016/S0021-9258(19)40020-3.

(15) Ropp, J. D.; Gunsalus, I. C.; Sligar, S. G. Cloning and Expression of a Member of a New Cytochrome P-450 Family: Cytochrome P-450lin (CYP111) from Pseudomonas Incognita. *J Bacteriol* **1993**, *175* (18), 6028–6037. https://doi.org/10.1128/jb.175.18.6028-6037.1993.
(16) Hui Bon Hoa, G.; Di Primo, C.; Dondaine, I.; Sligar, S. G.; Gunsalus, I. C.; Douzou, P. Conformational Changes of Cytochromes P-450cam and P-450lin Induced by High Pressure. *Biochemistry* **1989**, *28* (2), 651–656. https://doi.org/10.1021/bi00428a035.
(17) Brewer, C. B.; Peterson, J. A. Single Turnover Kinetics of the Reaction between Oxycytochrome P-450cam and Reduced Putidaredoxin. *Journal of Biological Chemistry* **1988**, *263* (2), 791–798. https://doi.org/10.1016/S0021-9258(19)35424-9.
(18) Kuznetsov, V. Yu.; Poulos, T. L.; Sevrioukova, I. F. Putidaredoxin-to-Cytochrome P450cam Electron Transfer: Differences between the Two Reductive Steps Required for Catalysis. *Biochemistry* **2006**, *45* (39), 11934–11944. https://doi.org/10.1021/bi0611154.
(19) Sligar, S. G.; Debrunner, P. G.; Lipscomb, J. D.; Namtvedt, M. J.; Gunsalus, I. C. A Role of the Putidaredoxin COOH-Terminus in *P* -450 $_{cam}$ (Cytochrome *m*) Hydroxylations. *Proc. Natl. Acad. Sci. U.S.A.* **1974**, *71* (10), 3906–3910. https://doi.org/10.1073/pnas.71.10.3906.
(20) Kadkhodayan, S.; Coulter, E. D.; Maryniak, D. M.; Bryson, T. A.; Dawson, J. H. Uncoupling Oxygen Transfer and Electron Transfer in the Oxygenation of Camphor Analogues by Cytochrome P450-CAM. *Journal of Biological Chemistry* **1995**, *270* (47), 28042–28048. https://doi.org/10.1074/jbc.270.47.28042.
(21) Batabyal, D.; Richards, L. S.; Poulos, T. L. Effect of Redox Partner Binding on Cytochrome P450 Conformational Dynamics. *J. Am. Chem. Soc.* **2017**, *139* (37), 13193–13199. https://doi.org/10.1021/jacs.7b07656.
(22) Lipscomb, J. D. Electron Paramagnetic Resonance Detectable States of Cytochrome P-450cam. *Biochemistry* **1980**, *19* (15), 3590–3599. https://doi.org/10.1021/bi00556a027.
(23) Lange, R.; Bonfils, C.; Debey, P. The Low-Spin High-Spin Transition of Camphor-Bound Cytochrome P-450. Effects of Medium and Temperature on Equilibrium Data. *Eur J Biochem* **1977**, *79* (2), 623–628. https://doi.org/10.1111/j.1432-1033.1977.tb11847.x.
(24) Marden, M. C.; Hui Bon Hoa, G. P-450 Binding to Substrates Camphor and Linalool versus Pressure. *Archives of Biochemistry and Biophysics* **1987**, *253* (1), 100–107. https://doi.org/10.1016/0003-9861(87)90642-4.
(25) Narasimhulu, S.; Havran, L. M.; Axelsen, P. H.; Winkler, J. D. Interactions of Substrate and Product with Cytochrome P450: P4502B4versus P450cam. *Archives of Biochemistry and Biophysics* **1998**, *353* (2), 228–238. https://doi.org/10.1006/abbi.1998.0650.
(26) Marden, M. C.; Hui Bon Hoa, G. P-450 Binding to Substrates Camphor and Linalool versus Pressure. *Archives of Biochemistry and Biophysics* **1987**, *253* (1), 100–107. https://doi.org/10.1016/0003-9861(87)90642-4.
(27) Follmer, A. H.; Mahomed, M.; Goodin, D. B.; Poulos, T. L. Substrate-Dependent Allosteric Regulation in Cytochrome P450cam (CYP101A1). *J. Am. Chem. Soc.* **2018**, *140* (47), 16222–16228. https://doi.org/10.1021/jacs.8b09441.
(28) Wagner, G. C.; Gunsalus, I. C.; Wang, M. Y.; Hoffman, B. M. Cobalt-Substituted Cytochrome P-450cam. *Journal of Biological Chemistry* **1981**, *256* (12), 6266–6273. https://doi.org/10.1016/S0021-9258(19)69158-1.
(29) Batabyal, D.; Lewis-Ballester, A.; Yeh, S.-R.; Poulos, T. L. A Comparative Analysis of the Effector Role of Redox Partner Binding in Bacterial P450s. *Biochemistry* **2016**, *55* (47), 6517–6523. https://doi.org/10.1021/acs.biochem.6b00913.
(30) Sevrioukova, I. F.; Peterson, J. A. Reaction of Carbon-Monoxide and Molecular-Oxygen with P450terp (CYP108) and P450BM-3 (CYP102). *Archives of Biochemistry and Biophysics* **1995**, *317* (2), 397–404. https://doi.org/10.1006/abbi.1995.1180.

(31) Glascock, M. C.; Ballou, D. P.; Dawson, J. H. Direct Observation of a Novel Perturbed Oxyferrous Catalytic Intermediate during Reduced Putidaredoxin-Initiated Turnover of Cytochrome P-450-CAM. *Journal of Biological Chemistry* **2005**, *280* (51), 42134–42141. https://doi.org/10.1074/jbc.M505426200.
(32) Sagadin, T.; Riehm, J. L.; Milhim, M.; Hutter, M. C.; Bernhardt, R. Binding Modes of CYP106A2 Redox Partners Determine Differences in Progesterone Hydroxylation Product Patterns. *Commun Biol* **2018**, *1* (1), 99. https://doi.org/10.1038/s42003-018-0104-9.
(33) Follmer, A. H.; Tripathi, S.; Poulos, T. L. Ligand and Redox Partner Binding Generates a New Conformational State in Cytochrome P450cam (CYP101A1). *J. Am. Chem. Soc.* **2019**, *141* (6), 2678–2683. https://doi.org/10.1021/jacs.8b13079.
(34) Jumper, J.; Evans, R.; Pritzel, A.; Green, T.; Figurnov, M.; Ronneberger, O.; Tunyasuvunakool, K.; Bates, R.; Žídek, A.; Potapenko, A.; Bridgland, A.; Meyer, C.; Kohl, S. A. A.; Ballard, A. J.; Cowie, A.; Romera-Paredes, B.; Nikolov, S.; Jain, R.; Adler, J.; Back, T.; Petersen, S.; Reiman, D.; Clancy, E.; Zielinski, M.; Steinegger, M.; Pacholska, M.; Berghammer, T.; Bodenstein, S.; Silver, D.; Vinyals, O.; Senior, A. W.; Kavukcuoglu, K.; Kohli, P.; Hassabis, D. Highly Accurate Protein Structure Prediction with AlphaFold. *Nature* **2021**, *596* (7873), 583–589. https://doi.org/10.1038/s41586-021-03819-2.
(35) Varadi, M.; Anyango, S.; Deshpande, M.; Nair, S.; Natassia, C.; Yordanova, G.; Yuan, D.; Stroe, O.; Wood, G.; Laydon, A.; Žídek, A.; Green, T.; Tunyasuvunakool, K.; Petersen, S.; Jumper, J.; Clancy, E.; Green, R.; Vora, A.; Lutfi, M.; Figurnov, M.; Cowie, A.; Hobbs, N.; Kohli, P.; Kleywegt, G.; Birney, E.; Hassabis, D.; Velankar, S. AlphaFold Protein Structure Database: Massively Expanding the Structural Coverage of Protein-Sequence Space with High-Accuracy Models. *Nucleic Acids Research* **2022**, *50* (D1), D439–D444. https://doi.org/10.1093/nar/gkab1061.
(36) Koga, H.; Sagara, Y.; Yaoi, T.; Tsujimura, M.; Nakamura, K.; Sekimizu, K.; Makino, R.; Shimada, H.; Ishimura, Y.; Yura, K.; Go, M.; Ikeguchi, M.; Horiuchi, T. Essential Role of the Arg ^{112} Residue of Cytochrome P450cam for Electron Transfer from Reduced Putidaredoxin. *FEBS Letters* **1993**, *331* (1–2), 109–113. https://doi.org/10.1016/0014-5793(93)80307-G.
(37) Nakamura, K.; Horiuchi, T.; Yasukochi, T.; Sekimizu, K.; Hara, T.; Sagara, Y. Significant Contribution of Arginine-112 and Its Positive Charge of Pseudomonas Putida Cytochrome P-450cam in the Electron Transport from Putidaredoxin. *Biochimica et Biophysica Acta (BBA) - Protein Structure and Molecular Enzymology* **1994**, *1207* (1), 40–48. https://doi.org/10.1016/0167-4838(94)90049-3.
(38) Unno, M.; Christian, J. F.; Benson, D. E.; Gerber, N. C.; Sligar, S. G.; Champion, P. M. Resonance Raman Investigations of Cytochrome P450cam Complexed with Putidaredoxin. *Journal of the American Chemical Society* **1997**, *119* (28), 6614–6620. https://doi.org/10.1021/ja963785a.
(39) Madrona, Y.; Hollingsworth, S. A.; Tripathi, S.; Fields, J. B.; Rwigema, J.-C. N.; Tobias, D. J.; Poulos, T. L. Crystal Structure of Cindoxin, the P450cin Redox Partner. *Biochemistry* **2014**, *53* (9), 1435–1446. https://doi.org/10.1021/bi500010m.
(40) Kim, D.; Heo, Y.-S.; Montellano, P. R. O. de. Efficient Catalytic Turnover of Cytochrome P450cam Is Supported by a T252N Mutation. *Archives of Biochemistry and Biophysics* **2008**, *474* (1), 150–156. https://doi.org/10.1016/j.abb.2008.02.044.
(41) Amaya, J. A.; Batabyal, D.; Poulos, T. L. Proton Relay Network in the Bacterial P450s: CYP101A1 and CYP101D1. *Biochemistry* **2020**, *59* (31), 2896–2902. https://doi.org/10.1021/acs.biochem.0c00329.
(42) Gunsalus, I. C.; Ghosh, D.; Gao, Y.-G.; Wang, A. H.-J. Cytochrome P450lin(P450111): Crystal Unit Cell, Tertiary Structure-Function Model. *Journal of Basic and Clinical Physiology and Pharmacology* **1992**, *3* (Supplement). https://doi.org/10.1515/JBCPP.1992.3.S1.55.

(43) Barbe, V. Unique Features Revealed by the Genome Sequence of Acinetobacter Sp. ADP1, a Versatile and Naturally Transformation Competent Bacterium. *Nucleic Acids Research* **2004**, *32* (19), 5766–5779. https://doi.org/10.1093/nar/gkh910.
(44) Gable, J. A.; Poulos, T. L.; Follmer, A. H. Cooperative Substrate Binding Controls Catalysis in Bacterial Cytochrome P450terp (CYP108A1). *J. Am. Chem. Soc.* **2023**, *145* (7), 4254–4265. https://doi.org/10.1021/jacs.2c12388.
(45) Sevrioukova, I. F.; Poulos, T. L. Putidaredoxin Reductase, a New Function for an Old Protein. *Journal of Biological Chemistry* **2002**, *277* (28), 25831–25839. https://doi.org/10.1074/jbc.M201110200.
(46) Sevrioukova, I. F.; Garcia, C.; Li, H.; Bhaskar, B.; Poulos, T. L. Crystal Structure of Putidaredoxin, the [2Fe–2S] Component of the P450cam Monooxygenase System from Pseudomonas Putida. *Journal of Molecular Biology* **2003**, *333* (2), 377–392. https://doi.org/10.1016/j.jmb.2003.08.028.

Chapter 4

Redox Partner Recognition and Selectivity of Cytochrome P450terp (CYP108A1)

Introduction

As I discussed in the previous chapter, our lab is interested in investigating the structure function relationships of P450s with endogenous and exogenous redox partner proteins. The first protein I worked with was P450lin, and in Chapter 3 it was established that P450lin is not as selective for its redox partner as P450cam, but the redox partner proteins that were capable of supporting turnover maintain an effector role. However, our lab is always looking to investigate other P450 systems to broaden our understanding. Within this context, we extended our investigation to P450terp with its natural redox partner protein, the Fe_2-S_2 ferredoxin terpredoxin (Tdx). This project has been ongoing for a few years, and was started by former graduate student Alec Follmer,[1] who established many of the vital expression and purification protocols, and early experiments with selectivity. P450terp provides a good comparison to P450cam because it is also a Class I *Pseudomonad* P450 that catalyzes the first step in the oxidative assimilation of a terpene as an alternative carbon and energy source.[2] The study on substrate binding (Chapter 2) has illustrated some key differences between P450terp and P450cam. With respect to redox partner interactions, the most important distinction is that P450terp exhibits an open conformation in the presence or absence of substrate.[3] This is critical because the binding of Pdx to P450cam shifts P450cam to a more open conformation,[4,5] but it is unclear if this preference carries over to other P450s, and if and/or how it may affect selectivity. First, the selectivity with native and nonnative redox partners was tested for P450terp, and then the extent of the effector role was investigated.

Unlike the P450lin system, the protein redox partners for the P450terp system have complete sequences and can be expressed. The expression and purification of the FAD-containing reductase, terpredoxin reductase (TdR) and the Fe_2-S_2 ferredoxin, Tdx, have been

previously described.[1] Tdx lacks the C-terminal tryptophan of Pdx and has Glu38 in place of the Asp38 of Pdx (Figure 4-1). Given that Tdx has a similar charged residue that is essential for Pdx function, the initial hypothesis was that P450terp would be selective, and the effector role would be similar. However, this turned out not to be the case, and once again it seems P450cam is unique.

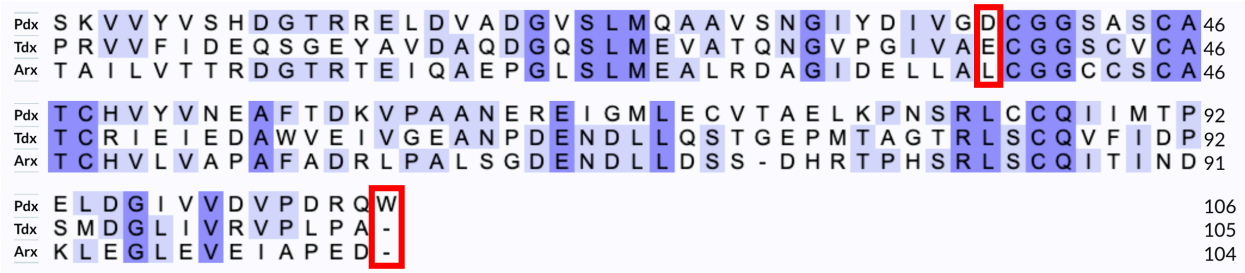

Figure 4-1. Sequence alignment of Arx, Pdx, and Tdx. Identical residues are highlighted in blue, and similar residues are highlighted in light blue. Residues that were targets for mutagenesis are boxed in red. Tdx has 32.7% identity with Arx, and 35.8% identity with Pdx.

Results and Discussion

The first goal in this project was to determine selectivity of P450terp for redox partners using an NADH consumption assay. If, upon addition of substrate, there is an increase in the rate of NADH consumption, then that ferredoxin can support turnover in P450terp (Figure 4-2). The consumption rate for Tdx with TdR has already been determined (Table 4-1)[3] providing a reference for the comparison of alternative redox partners. The redox partners from homologous systems were tested first: Pdx from the P450cam system and Arx from the CYP101D1 system.[6–8] Pdx has a very slow rate of turnover, while, surprisingly, Arx enables a high rate of turnover (Table 4-1). It was surprising that Arx supports turnover by P450terp, because the critical Glu in P450cam-Pdx complex is conserved in Tdx while in Arx this residue is a Leu. This surprise is in contrast to P450lin where both Arx and Ldx have a Leu in this interfacial position. Regardless, it is clear that P450terp, like P450lin, is not as selective for redox partner.

Given that P450terp is not as selective as P450cam, I made a series of mutations to test the degree of redox partner promiscuity. First, I mutated Tdx Glu38 to Leu to directly test if a charged residue is important in that position. While Tdx E38L enabled turnover, it occurred at a rate of 217 min^{-1} or about one third of the rate with WT Tdx (Table 4-1). This decreased rate indicates that Glu38 is moderately important but not essential for the interaction of Tdx with P450terp. In sharp contrast, mutation of Asp38 in Pdx drastically reduces activity in P450cam.[9] Furthermore, an additional surprising result is that Arx exhibits a much higher turnover rate than Tdx E39L.

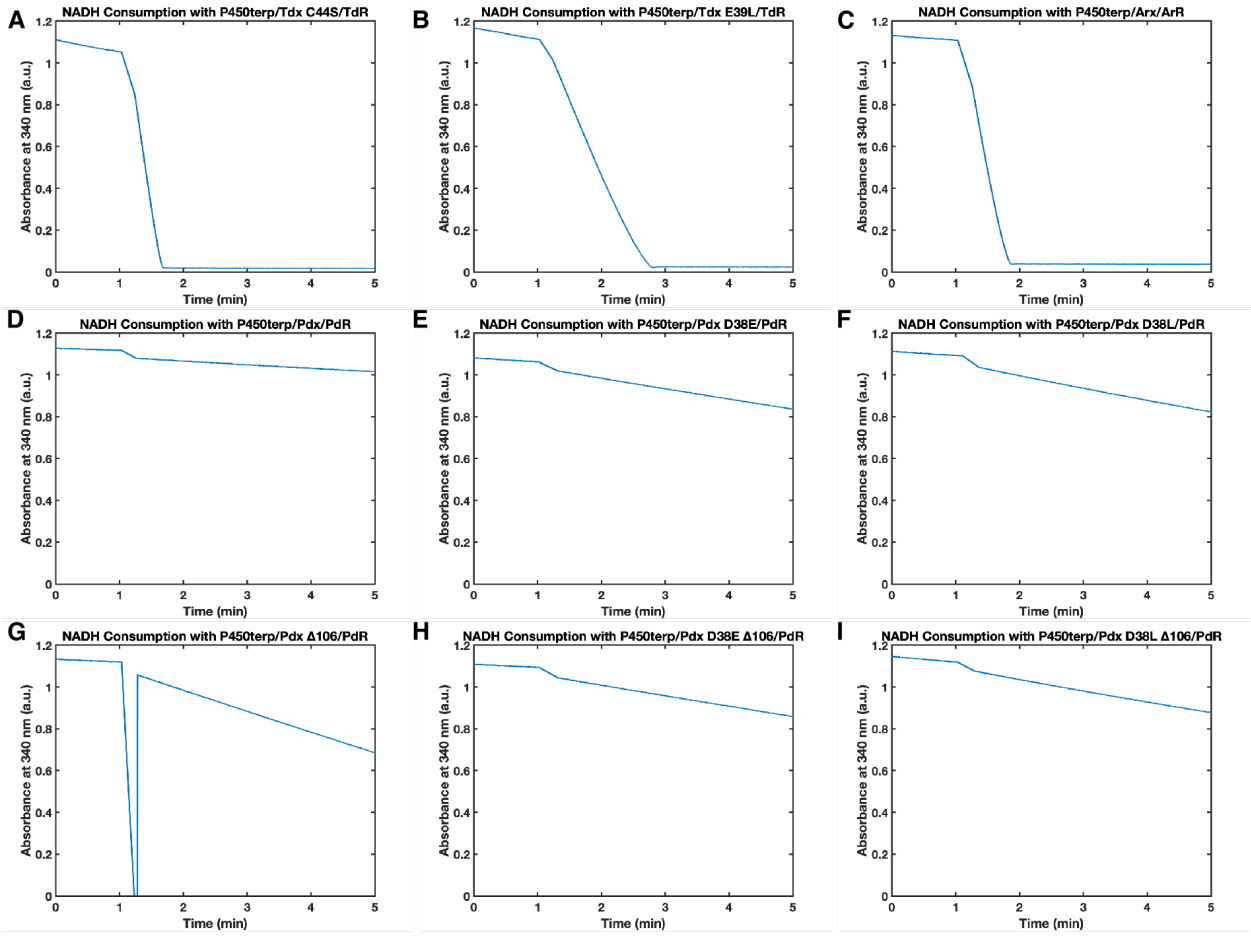

Figure 4-2. NADH consumption traces of P450terp with various redox partners monitored at 340 nm. The conditions for the experiment were 0.5 µM P450terp / 5 µM ferredoxin / 0.5 µM reductase in 50 mM KPi pH 7.4 at room temperature. NADH was added to a concentration of 185 µM, and the background rate was collected 0-1 min. Substrate (α-terpineol) was added after 1 minute to a concentration of 200 µM and the rate was determined using a fit to zero order of the resulting linear slope. P450terp selectivity was tested with (A) Tdx C44S and TdR, (B) Tdx E39L and TdR, (C) Arx and ArR (the reductase from the CYP101D1 system that corresponds to Arx), (D) Pdx and PdR, (E) Pdx D38E and PdR, (F) Pdx D38L and PdR, (G) Pdx Δ106 and PdR, (H) Pdx D38E Δ106 and PdR, and (I) Pdx D38L Δ106 and PdR. The dip in absorbance in (G) is a result of pausing the collection for substrate addition, which occasionally happens instead of the flat line as seen in the other traces.

Table 4-1. NADH turnover rates and coupling efficiencies for P450terp with various ferredoxins. The coupling efficiencies of Pdx WT and variants are works in progress.

Ferredoxin	NADH turnover (min^{-1})	Coupling Efficiency
Tdx	659 ± 8	97 ± 1[3]
Tdx C44S	646 ± 12	95.2 ± 0.2
Tdx E39L	217 ± 9	92.0 ± 1.6
Arx	510 ± 12	93.9 ± 1.0
Pdx	2.18 ± 0.46	
Pdx Δ106	28.2 ± 0.2	
Pdx D38E	9.27 ± 0.62	
Pdx D38L	11.6 ± 0.8	
Pdx D38E Δ106	11.6 ± 0.6	
Pdx D38L Δ106	8.26 ± 1.06	

Since Pdx has a very slow rate of turnover with P450terp and single mutations can exhibit substantial effects on turnover ability, I set out to alter Pdx to resemble Tdx, similar to what was done for P450lin (Chapter 3) by mutating Pdx Asp38 to Glu as well as deleting the terminal tryptophan (W106). Since Arx also supported turnover of P450terp, I used the Pdx variants from the P450lin investigation (Chapter 3) to see if they enabled catalysis. All variants displayed very slow rates and there was no discernable pattern in combining mutations like there had been with P450lin. The fastest was Pdx Δ106, and the rest displayed negligible differences in rate. The lack of a pattern indicates that the interfacial surface of Pdx is not as compatible with the surface P450terp. All of the Pdx variants displayed pseudo-zero order kinetics in their NADH consumption traces (Figure 4-2) indicating that the first electron transfer step is still rate limiting.[10]

To determine if redox partners that enable the consumption of NADH lead to productive turnover of substrate, I determined the coupling efficiency with the highest performing redox partners: Tdx E38L, Tdx C44S (used in crystallization), and Arx (Table 4-1). All redox partners tested so far had coupling efficiencies greater than 90%. Coupling efficiency was determined by tracking the depletion of substrate (Figure 4-3), as was done in Chapter 2. The high coupling efficiencies, especially that of Arx, show that external redox partners enable productive turnover yielding qualitatively similar levels of product. The coupling efficiency with the Pdx variants with

slower turnover rates will be done next to determine if very slow turnover can lead to actual product formation and substrate depletion.

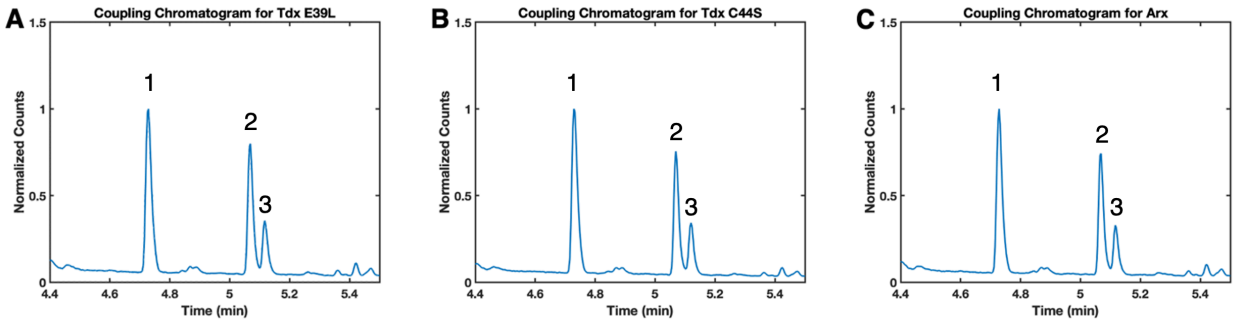

Figure 4-3. NADH coupling chromatograms with the 3 ferredoxins. All chromatograms are normalized to the camphor peak employed as an internal standard. Peak 1 is camphor (internal standard), peak 2 is α-terpineol, and peak 3 is an impurity from the α-terpineol source.

Now that it has been determined that different redox partners can enable turnover, I wanted to establish whether redox partners play an effector role in P450terp turnover by exhibiting a structural influence on the P450. One method to test this influence is by the observation of a spectral shift of the Soret in the presence of Tdx, similar to what is observed in P450cam.[11–14] However, there was no spectral change (data not shown) and while the lack of a spectral change doesn't rule out a structural change, we have shown that substrate binding in P450terp and does not adopt a closed conformation when substrate binds.[3]

Another way to probe possible structural changes upon ferredoxin binding is to monitor the decay of the oxycomplex in the presence of redox partner (Figures 4-4 through 4-8). This type of experiment has been done numerous times, with P450cam,[15] P450lin,[3] P450cin,[16] and CYP101D1[8]. The decay of the P450 oxycomplex increases in the presence of redox partner in each of these cases. The autooxidation of P450terp was previously determined,[17] but not in the presence of Tdx. Preliminary results for P450terp also indicate that redox partner binding does increase the decay of the oxycomplex. In this study, Tdx has the largest influence on P450terp, at about a 30-fold increase (Table 4-2), while Arx and Tdx E38L are closer together at about 13-

fold increase. It is interesting that although turnover rates are quite different, both ferredoxins display a similar influence on the oxycomplex decay. Pdx was used as a control, as it was the slowest redox partners, and it had an almost negligible increase on the decay of the oxycomplex at 1.5-fold increase. These results further support a seemingly common thread in P450 chemistry – binding of a redox partner induces structural changes that affect the active site and lead to an increase in the decay rate of the oxycomplex. In this case, in the absence of a second electron to proceed with catalysis, the oxycomplex decays unproductively, but in the case of catalysis under turnover conditions, the second electron would be delivered. Since all P450s studied so far all increase the rate of decay of the oxycomplex in the presence of a productive redox partner, it is tempting to suggest that whatever structural changes that result from redox partner binding are required for catalysis. If, indeed, structural changes are involved in the first electron transfer step then this could explain why the first electron transfer step is rate limiting given that structural changes are usually slow relative to the bond breaking and making reactions.

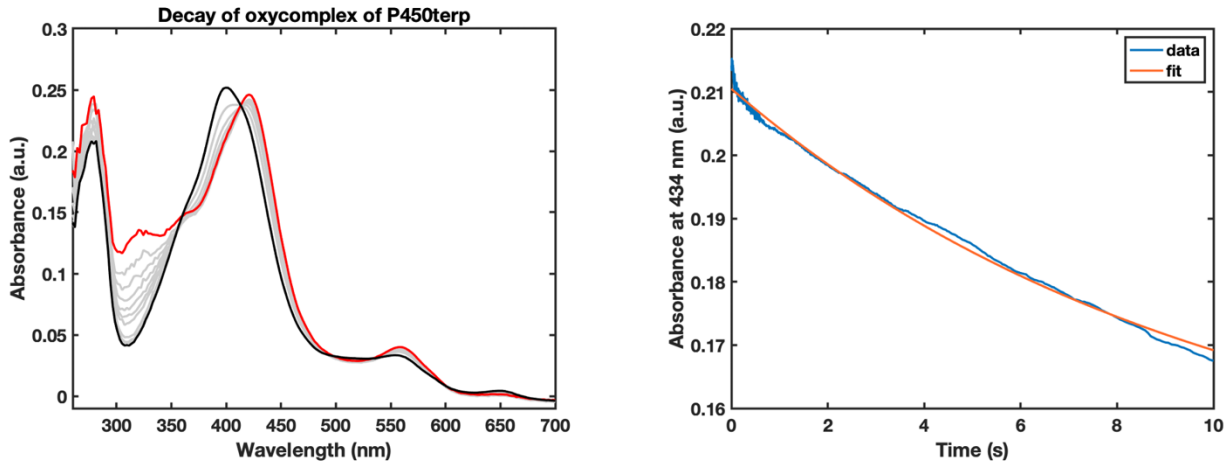

Figure 4-4. Stopped-flow spectra and kinetics of oxycomplex decay of P450terp. (Left) P450terp oxycomplex decay in the absence of redox partner. The red line is the starting spectra, the grey are the intermediate spectra, and black is the final spectra. (Right) P450terp oxycomplex decay monitored at 434 nm and fit to a single exponential.

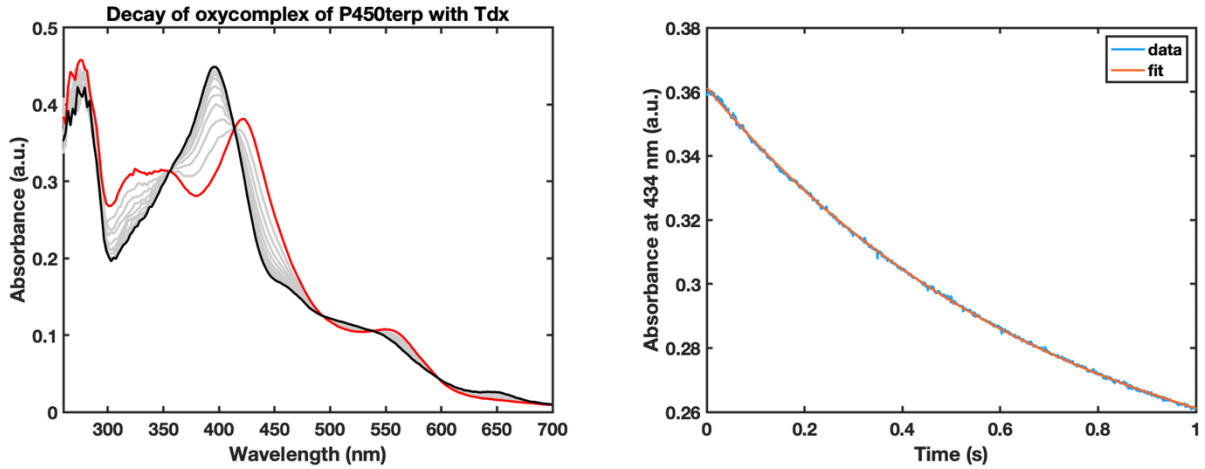

Figure 4-5. Stopped-flow spectra and kinetics of oxycomplex decay of P450terp with Tdx. (Left) P450terp oxycomplex decay in the presence of Tdx at 2-fold concentration. The red line is the starting spectra, the grey are the intermediate spectra, and black is the final spectra. (Right) P450terp oxycomplex decay monitored at 434 nm and fit to a single exponential.

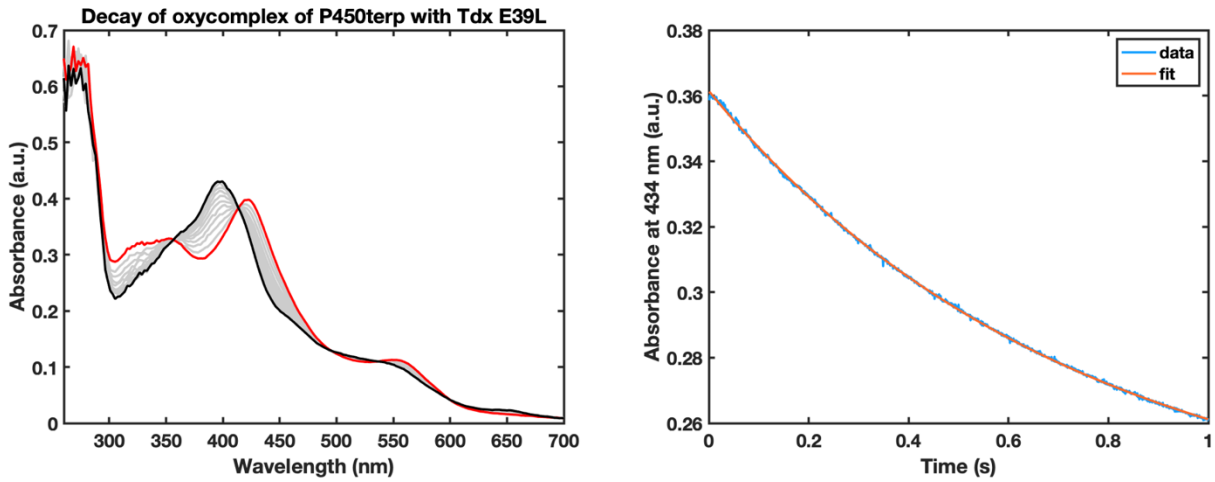

Figure 4-6. Stopped-flow spectra and kinetics of oxycomplex decay of P450terp with Tdx E39L. (Left) P450terp oxycomplex decay in the presence of Tdx E39L at 2-fold concentration. The red line is the starting spectra, the grey are the intermediate spectra, and black is the final spectra. (Right) P450terp oxycomplex decay monitored at 434 nm and fit to a single exponential.

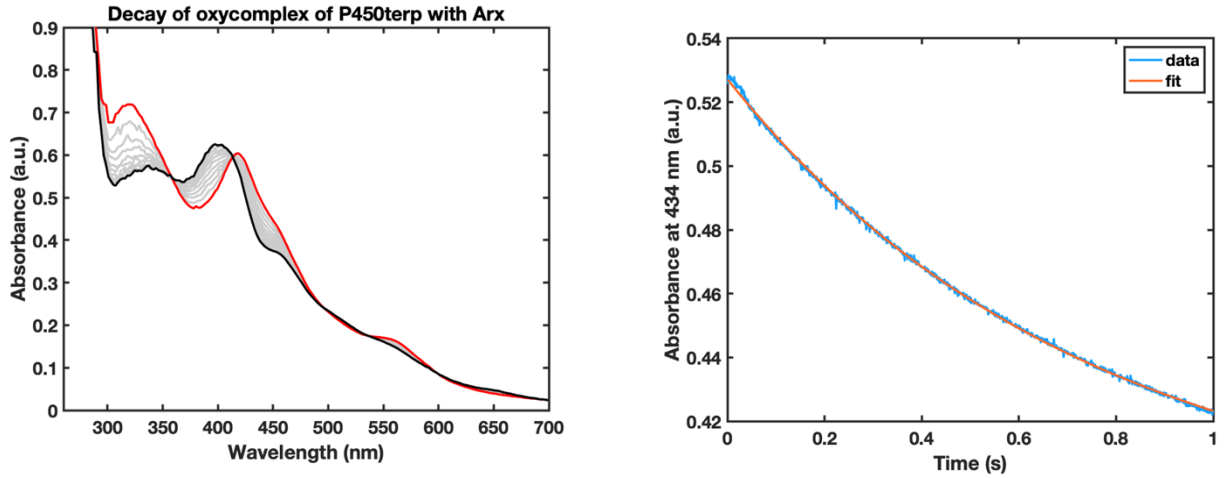

Figure 4-7. Stopped-flow spectra and kinetics of oxycomplex decay of P450terp with Arx. (Left) P450terp oxycomplex decay in the presence of Arx at 2-fold concentration. The red line is the starting spectra, the grey are the intermediate spectra, and black is the final spectra. (Right) P450terp oxycomplex decay monitored at 434 nm and fit to a single exponential.

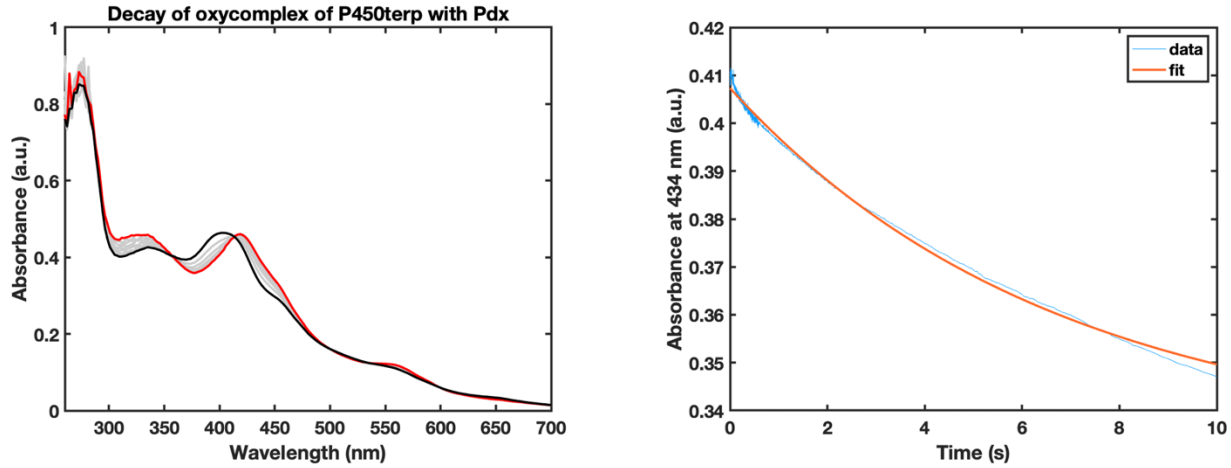

Figure 4-8. Stopped-flow spectra and kinetics of oxycomplex decay of P450terp with Pdx. (Left) P450terp oxycomplex decay in the presence of Pdx at 2-fold concentration. The red line is the starting spectra, the grey are the intermediate spectra, and black is the final spectra. (Right) P450terp oxycomplex decay monitored at 434 nm and fit to a single exponential.

Table 4-2. P450terp oxycomplex decay rates from stopped-flow kinetics.

Ferredoxin	Rate (s^{-1})	Fold Increase
–	0.101 ± 0.014	–
Tdx	3.06 ± 0.04	30.3
Tdx E39L	1.37 ± 0.02	13.5
Arx	1.28 ± 0.03	12.7
Pdx	0.151 ± 0.003	1.49

To further understand the regulatory mechanisms of the redox partner at the molecular level, a crystal structure of Tdx, the P450terp Fe_2-S_2 redox partner, was solved. First, Tdx C44S was expressed and purified, and used to set up crystal screens. This mutation was necessary to obtain good diffraction quality crystals. Fortunately, the C44S mutation did not significantly alter turnover rate or coupling efficiency (Table 4-1). Crystals were grown by hanging drop vapor diffusion at a concentration of 13 mg/mL in 1.6 M sodium citrate pH 6.5 at a protein:well drop ratio of 2:1. The crystals were harvested and sent for data collection. The structure was solved by molecular replacement using Arx (PDB ID: 3LXF) as a search model. The statistics for data collection and refinement are in Table 3-3.

Table 4-3. Statistics for data collection and refinement of Tdx C44S.

Data Collection	
Space group	P 21 21 21
Unit cell dimensions	
a, b, c (Å)	30.9699, 80.45, 86.1398
α, β, γ (°)	90, 90, 90
Resolution range (Å) (highest shell)	37.97 – 2.15 (2.227 – 2.15)
Multiplicity (outer shell)	2.0 (1.9)
Total observations	23412 (2110)
Unique reflections (outer shell)	11865 (1084)
Completeness (%) (outer shell)	96.00 (89.64)
<I/σ> (outer shell)	4.78 (0.84)
Refinement	
R_{work} %/ R_{free} % (outer shell)	0.2147/0.2680 (0.3184/0.3185)
B-factor (Wilson)	23.91
RMSD Bond length (Å)	0.01
RMSD Bond angle (°)	1.3

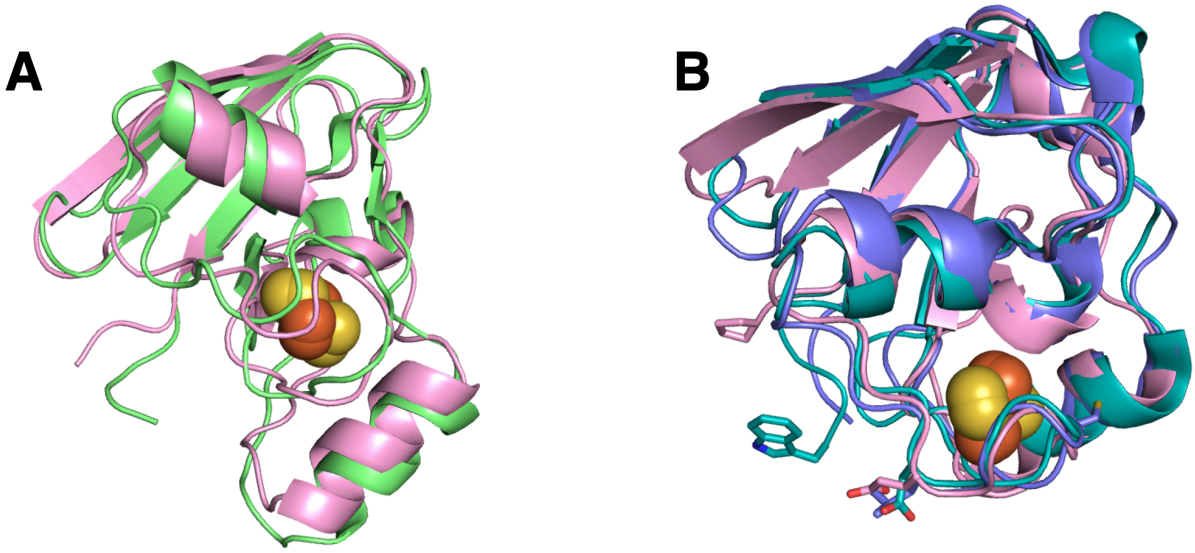

Figure 4-9. Crystal structure of Tdx C44S. (A) A ribbon representation of the crystal structure of Tdx C44S in pink and the NMR solution in green. The RMSD is 1.999 Å. (B) Crystal structures of Tdx C44S (pink), Pdx C73S (teal) (PDB ID: 1XLQ), and Arx (purple) (PDB ID: 3LXF) show a very similar fold. The C-termini of Tdx and Pdx are shown in sticks. The mutated residues of Tdx E39 and Pdx D38 are shown in sticks at the bottom, along with the corresponding L38 of Arx. The RMSD between Tdx and Pdx is 0.870 Å, and 1.069 Å between Tdx and Arx.

The NMR structure of Tdx has been solved,[18] and the comparison to the crystal structure of Tdx C44S shows that the two structures from two different methods align well (Figure 4-9A). An alignment of Tdx, Pdx, and Arx (Figure 4-9B) shows that all three ferredoxins have very similar overall folds. Their C-termini are flexible loops that end in different positions in the crystal structure, but presumably in solution would be mobile. Both Tdx and Arx are shorter by one amino acid, and lack the terminal tryptophan that is vital for the Pdx-P450cam interaction.[9,19] In the structure of Tdx C44S, the last residue from Tdx is not visible in the electron density, and so the second-to-last residue is shown (P104). The C-terminal tail is not close to the proposed interface as Pdx is, so the mechanism for inducing structural change may be different. Additionally, the residues proposed to be important at the interface are shown as sticks: D38 from Pdx, E38 from Tdx, and L38 from Arx. The mutagenesis studies show that these single residues are important, but their roles are not as clear as it is for Pdx with P450cam.[9]

In order to investigate the possible Tdx-P450terp interface, in lieu of a complex crystal structure, the two crystal structures of Tdx C44S and P450terp (PDB ID: 1CPT) were docked using two different automatic protein docking servers: ZDOCK[20] and ClusPro[21–24] (Figure 4-10A). ZDOCK is a Fast Fourier Transform based protein docking program that searches all possible binding modes in translational and rotational space between two PDB files and evaluates each using an energy-based scoring function. ClusPro is a rigid body docking followed by RMSD clustering of lowest energy structures. The selected structures are then refined using energy minimization. For both methods, the two structures are selected as inputs, and there is an option of selecting residues to include or exclude from the interface. I chose to not bias the docking results by not including or excluding any residues. Docking results are only a prediction that can aid further structural studies. In all top five results from both methods, Tdx was placed on the proximal side of the P450, with Tdx in a variety of orientations, with the iron-sulfur cluster close to the heme. The models shown above have the iron-sulfur cluster within 15 Å of the heme. As a comparison, in running Pdx and P450cam through the same methods with no bias, only three out of the top 5 predictions placed Pdx on the proximal side. Furthermore, the docking results position Tdx in a different orientation than Pdx (Figure 4-10A). The models shown are the top results that most resemble each other. In all five of the top models, Glu38 did not interact with Arg114 of P450terp. This is important because Asp38 from Pdx interacts with Arg112 from P450cam. The top predicted model for Pdx and P450cam with ZDOCK showed the Asp38-Arg112 interaction, which is known from crystallography and mutagenesis studies. The models also did not give Glu38 of Tdx a consistent interaction with P450terp, which might help to explain why the mutagenesis studies did not eliminate activity in Tdx E38L and recover activity in Pdx D38E Δ106. In the displayed models (Figure 4-10A), the docked structure indicates that Tdx E39 might hydrogen bond to P450terp H381.

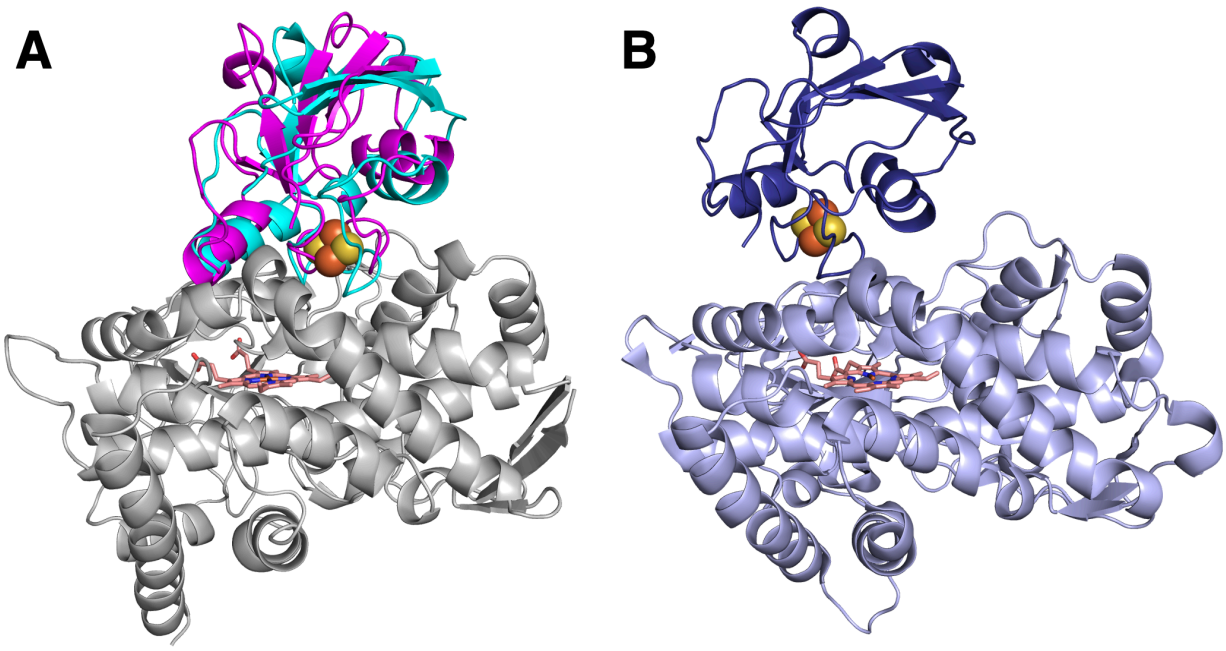

Figure 4-10. P450terp and Tdx docking results compared to the P450cam-Pdx complex. (A) The top docking results using ZDOCK (Tdx - cyan) and ClusPro (Tdx - magenta) of Tdx with P450terp (gray). Both results have < 15 Å distance between the heme of P450terp and the iron-sulfur cluster of Tdx. (B) P450cam-Pdx covalently linked complex (PDB ID: 4JWU) aligned to P450terp from (A) to show the same view. Pdx binds to P450cam differently than the docked structures predict Tdx binding to P450terp.

Future Plans

The next step is to determine the binding affinity of Tdx and P450terp, with and without substrate. This experiment has been done for P450cam, and the results show that Pdx binds tighter to an open P450cam, in the absence of substrate. Given that the substrate-bound structure of P450terp does not differ from the substrate-free structure, I do not expect a difference in binding affinities like there is for the P450cam system. However, it will be useful to compare both Tdx and Arx binding affinities to compare a natural and nonnatural redox partner that both enable turnover at the about the same magnitude.

A more difficult, but critically important pursuit is the crystallization of the P450terp-Tdx complex. There are only a handful of protein-protein redox partner complexes available and

having another one available would prove useful. To accomplish this goal, a fusion protein has been designed based on a fusion protein of CYP11A1 and Adx.[25] It is also possible to try setting up the proteins in the same crystal drop, and a covalent linker as was done for P450cam.

Materials and Methods

Tdx Protein Purification

C41 *E. coli* cells were used with a pet vector received from Dr. Irina Sevrioukova encoding the gene and grown in 2xYT media. Protein expression was allowed to start naturally. The flasks were shaken at 80 RPM for 2 days at 37 ˚C and then rested still for another 2 days at room temperature. Cells were spun down, and the cell pellet was resuspended in 20 mM KPi pH 7.5. The cells were lysed with a microfluidizer. The lysate was spun down, and then loaded onto a DE52 column and washed with wash buffer (20 mM KPi and 5 mM DTT). The red-brown colored band was excised and transferred to a clean, equilibrated DE52 column. The column was washed with wash buffer, and the protein was eluted with a gradient of 0 - 600 mM NaCl in wash buffer. The red-brown fractions were collected and dialyzed against wash buffer to remove the salt. The protein was then loaded onto a pre-equilibrated DEAE column and washed with wash buffer. The same gradient was run as the DE52 column and fractions with an R/Z (A_{415}/A_{280}) > 0.2 were collected and dialyzed against wash buffer. Tdx was then loaded onto a pre-equilibrated Q column, washed, and eluted as described. Fractions with an R/Z > 0.5 were collected and concentrated < 2mL. The protein was run on an S200 size exclusion column in SEC buffer (20 mM KPi, 250 mM NaCl, 5 mM DTT). Fractions with an R/Z > 0.6 were collected and concentrated. Concentrated protein was then aliquoted, flash frozen, and stored at -80 ˚C.

Crystallization of Tdx C44S

Tdx C44S was crystallized at 13 mg/mL in 1.6 M sodium citrate pH 6.5 in a hanging drop tray by vapor diffusion at room temperature. Crystals of Tdx C44S appeared a reddish brown, and were cryoprotected into paratone oil before flash freezing.

Data Collection and Analysis

Data were collected by Alec Follmer from single crystals at the Advanced Light Source (ALS) and the Stanford Synchrotron Radiation Laboratory (SSRL). Diffraction images were indexed, integrated, and scaled using Mosflm in the CCP4 package.[26,27] Tdx C44S was molecularly replaced with Tdx WT from Alec Follmer with Phaser[28,29] which used Arx as a search model, and there are 2 molecules in the asymmetric unit for Tdx C44S. The Phenix suite were used for structure refinement.[30,31] The structural model was revised in real space using COOT.[32,33]

Assay Protocols

NADH consumption assay, coupling by GC/MS, and stopped-flow were carried out as previously described.[3,34]

References:

(1) Follmer, A. H. Cytochrome P450: Nature's Aircraft Carrier. Ph.D., University of California, Irvine, Ann Arbor, 2019. https://www.proquest.com/dissertations-theses/cytochrome-p450-natures-aircraft-carrier/docview/2275957801/se-2?accountid=14509.

(2) Peterson, J. A.; Lu, J. Y.; Geisselsoder, J.; Graham-Lorence, S.; Carmona, C.; Witney, F.; Lorence, M. C. Cytochrome P-450terp. Isolation and Purification of the Protein and Cloning and Sequencing of Its Operon. *Journal of Biological Chemistry* **1992**, *267* (20), 14193–14203. https://doi.org/10.1016/S0021-9258(19)49697-X.

(3) Gable, J. A.; Poulos, T. L.; Follmer, A. H. Cooperative Substrate Binding Controls Catalysis in Bacterial Cytochrome P450terp (CYP108A1). *J. Am. Chem. Soc.* **2023**, *145* (7), 4254–4265. https://doi.org/10.1021/jacs.2c12388.

(4) Hollingsworth, S. A.; Batabyal, D.; Nguyen, B. D.; Poulos, T. L. Conformational Selectivity in Cytochrome P450 Redox Partner Interactions. *Proc. Natl. Acad. Sci. U.S.A.* **2016**, *113* (31), 8723–8728. https://doi.org/10.1073/pnas.1606474113.

(5) Batabyal, D.; Richards, L. S.; Poulos, T. L. Effect of Redox Partner Binding on Cytochrome P450 Conformational Dynamics. *J. Am. Chem. Soc.* **2017**, *139* (37), 13193–13199. https://doi.org/10.1021/jacs.7b07656.
(6) Yang, W.; Bell, S. G.; Wang, H.; Zhou, W.; Hoskins, N.; Dale, A.; Bartlam, M.; Wong, L.-L.; Rao, Z. Molecular Characterization of a Class I P450 Electron Transfer System from Novosphingobium Aromaticivorans DSM12444. *Journal of Biological Chemistry* **2010**, *285* (35), 27372–27384. https://doi.org/10.1074/jbc.M110.118349.
(7) Batabyal, D.; Poulos, T. L. Effect of Redox Partner Binding on CYP101D1 Conformational Dynamics. *Journal of Inorganic Biochemistry* **2018**, *183*, 179–183. https://doi.org/10.1016/j.jinorgbio.2018.02.013.
(8) Batabyal, D.; Lewis-Ballester, A.; Yeh, S.-R.; Poulos, T. L. A Comparative Analysis of the Effector Role of Redox Partner Binding in Bacterial P450s. *Biochemistry* **2016**, *55* (47), 6517–6523. https://doi.org/10.1021/acs.biochem.6b00913.
(9) Kuznetsov, V. Yu.; Poulos, T. L.; Sevrioukova, I. F. Putidaredoxin-to-Cytochrome P450cam Electron Transfer: Differences between the Two Reductive Steps Required for Catalysis. *Biochemistry* **2006**, *45* (39), 11934–11944. https://doi.org/10.1021/bi0611154.
(10) Brewer, C. B.; Peterson, J. A. Single Turnover Kinetics of the Reaction between Oxycytochrome P-450cam and Reduced Putidaredoxin. *Journal of Biological Chemistry* **1988**, *263* (2), 791–798. https://doi.org/10.1016/S0021-9258(19)35424-9.
(11) Lipscomb, J. D. Electron Paramagnetic Resonance Detectable States of Cytochrome P-450cam. *Biochemistry* **1980**, *19* (15), 3590–3599. https://doi.org/10.1021/bi00556a027.
(12) Lange, R.; Bonfils, C.; Debey, P. The Low-Spin High-Spin Transition of Camphor-Bound Cytochrome P-450. Effects of Medium and Temperature on Equilibrium Data. *Eur J Biochem* **1977**, *79* (2), 623–628. https://doi.org/10.1111/j.1432-1033.1977.tb11847.x.
(13) Marden, M. C.; Hui Bon Hoa, G. P-450 Binding to Substrates Camphor and Linalool versus Pressure. *Archives of Biochemistry and Biophysics* **1987**, *253* (1), 100–107. https://doi.org/10.1016/0003-9861(87)90642-4.
(14) Narasimhulu, S.; Havran, L. M.; Axelsen, P. H.; Winkler, J. D. Interactions of Substrate and Product with Cytochrome P450: P4502B4versus P450cam. *Archives of Biochemistry and Biophysics* **1998**, *353* (2), 228–238. https://doi.org/10.1006/abbi.1998.0650.
(15) Glascock, M. C.; Ballou, D. P.; Dawson, J. H. Direct Observation of a Novel Perturbed Oxyferrous Catalytic Intermediate during Reduced Putidaredoxin-Initiated Turnover of Cytochrome P-450-CAM. *Journal of Biological Chemistry* **2005**, *280* (51), 42134–42141. https://doi.org/10.1074/jbc.M505426200.
(16) Madrona, Y.; Hollingsworth, S. A.; Tripathi, S.; Fields, J. B.; Rwigema, J.-C. N.; Tobias, D. J.; Poulos, T. L. Crystal Structure of Cindoxin, the P450cin Redox Partner. *Biochemistry* **2014**, *53* (9), 1435–1446. https://doi.org/10.1021/bi500010m.
(17) Sevrioukova, I. F.; Peterson, J. A. Reaction of Carbon-Monoxide and Molecular-Oxygen with P450terp (CYP108) and P450BM-3 (CYP102). *Archives of Biochemistry and Biophysics* **1995**, *317* (2), 397–404. https://doi.org/10.1006/abbi.1995.1180.
(18) Mo, H.; Pochapsky, S. S.; Pochapsky, T. C. A Model for the Solution Structure of Oxidized Terpredoxin, a Fe_2S_2 Ferredoxin from *Pseudomonas* ·. *Biochemistry* **1999**, *38* (17), 5666–5675. https://doi.org/10.1021/bi983063r.
(19) Sligar, S. G.; Debrunner, P. G.; Lipscomb, J. D.; Namtvedt, M. J.; Gunsalus, I. C. A Role of the Putidaredoxin COOH-Terminus in *P* -450 $_{cam}$ (Cytochrome *m*) Hydroxylations. *Proc. Natl. Acad. Sci. U.S.A.* **1974**, *71* (10), 3906–3910. https://doi.org/10.1073/pnas.71.10.3906.
(20) Pierce, B. G.; Wiehe, K.; Hwang, H.; Kim, B.-H.; Vreven, T.; Weng, Z. ZDOCK Server: Interactive Docking Prediction of Protein–Protein Complexes and Symmetric Multimers. *Bioinformatics* **2014**, *30* (12), 1771–1773. https://doi.org/10.1093/bioinformatics/btu097.

(21) Desta, I. T.; Porter, K. A.; Xia, B.; Kozakov, D.; Vajda, S. Performance and Its Limits in Rigid Body Protein-Protein Docking. *Structure* **2020**, *28* (9), 1071-1081.e3. https://doi.org/10.1016/j.str.2020.06.006.
(22) Vajda, S.; Yueh, C.; Beglov, D.; Bohnuud, T.; Mottarella, S. E.; Xia, B.; Hall, D. R.; Kozakov, D. New Additions to the C Lus P Ro Server Motivated by CAPRI. *Proteins* **2017**, *85* (3), 435–444. https://doi.org/10.1002/prot.25219.
(23) Kozakov, D.; Hall, D. R.; Xia, B.; Porter, K. A.; Padhorny, D.; Yueh, C.; Beglov, D.; Vajda, S. The ClusPro Web Server for Protein–Protein Docking. *Nat Protoc* **2017**, *12* (2), 255–278. https://doi.org/10.1038/nprot.2016.169.
(24) Kozakov, D.; Beglov, D.; Bohnuud, T.; Mottarella, S. E.; Xia, B.; Hall, D. R.; Vajda, S. How Good Is Automated Protein Docking?: Automated Protein Docking. *Proteins* **2013**, *81* (12), 2159–2166. https://doi.org/10.1002/prot.24403.
(25) Strushkevich, N.; MacKenzie, F.; Cherkesova, T.; Grabovec, I.; Usanov, S.; Park, H.-W. Structural Basis for Pregnenolone Biosynthesis by the Mitochondrial Monooxygenase System. *Proc. Natl. Acad. Sci. U.S.A.* **2011**, *108* (25), 10139–10143. https://doi.org/10.1073/pnas.1019441108.
(26) Agirre, J.; Atanasova, M.; Bagdonas, H.; Ballard, C. B.; Baslé, A.; Beilsten-Edmands, J.; Borges, R. J.; Brown, D. G.; Burgos-Mármol, J. J.; Berrisford, J. M.; Bond, P. S.; Caballero, I.; Catapano, L.; Chojnowski, G.; Cook, A. G.; Cowtan, K. D.; Croll, T. I.; Debreczeni, J. É.; Devenish, N. E.; Dodson, E. J.; Drevon, T. R.; Emsley, P.; Evans, G.; Evans, P. R.; Fando, M.; Foadi, J.; Fuentes-Montero, L.; Garman, E. F.; Gerstel, M.; Gildea, R. J.; Hatti, K.; Hekkelman, M. L.; Heuser, P.; Hoh, S. W.; Hough, M. A.; Jenkins, H. T.; Jiménez, E.; Joosten, R. P.; Keegan, R. M.; Keep, N.; Krissinel, E. B.; Kolenko, P.; Kovalevskiy, O.; Lamzin, V. S.; Lawson, D. M.; Lebedev, A. A.; Leslie, A. G. W.; Lohkamp, B.; Long, F.; Malý, M.; McCoy, A. J.; McNicholas, S. J.; Medina, A.; Millán, C.; Murray, J. W.; Murshudov, G. N.; Nicholls, R. A.; Noble, M. E. M.; Oeffner, R.; Pannu, N. S.; Parkhurst, J. M.; Pearce, N.; Pereira, J.; Perrakis, A.; Powell, H. R.; Read, R. J.; Rigden, D. J.; Rochira, W.; Sammito, M.; Sánchez Rodríguez, F.; Sheldrick, G. M.; Shelley, K. L.; Simkovic, F.; Simpkin, A. J.; Skubak, P.; Sobolev, E.; Steiner, R. A.; Stevenson, K.; Tews, I.; Thomas, J. M. H.; Thorn, A.; Valls, J. T.; Uski, V.; Usón, I.; Vagin, A.; Velankar, S.; Vollmar, M.; Walden, H.; Waterman, D.; Wilson, K. S.; Winn, M. D.; Winter, G.; Wojdyr, M.; Yamashita, K. The *CCP* 4 Suite: Integrative Software for Macromolecular Crystallography. *Acta Crystallogr D Struct Biol* **2023**, *79* (6), 449–461. https://doi.org/10.1107/S2059798323003595.
(27) Battye, T. G. G.; Kontogiannis, L.; Johnson, O.; Powell, H. R.; Leslie, A. G. W. *IMOSFLM*: A New Graphical Interface for Diffraction-Image Processing with *MOSFLM*. *Acta Crystallogr D Biol Crystallogr* **2011**, *67* (4), 271–281. https://doi.org/10.1107/S0907444910048675.
(28) McCoy, A. J. Solving Structures of Protein Complexes by Molecular Replacement with *Phaser*. *Acta Crystallogr D Biol Crystallogr* **2007**, *63* (1), 32–41. https://doi.org/10.1107/S0907444906045975.
(29) McCoy, A. J.; Grosse-Kunstleve, R. W.; Adams, P. D.; Winn, M. D.; Storoni, L. C.; Read, R. J. *Phaser* Crystallographic Software. *J Appl Crystallogr* **2007**, *40* (4), 658–674. https://doi.org/10.1107/S0021889807021206.
(30) Adams, P. D.; Afonine, P. V.; Bunkóczi, G.; Chen, V. B.; Echols, N.; Headd, J. J.; Hung, L.-W.; Jain, S.; Kapral, G. J.; Grosse Kunstleve, R. W.; McCoy, A. J.; Moriarty, N. W.; Oeffner, R. D.; Read, R. J.; Richardson, D. C.; Richardson, J. S.; Terwilliger, T. C.; Zwart, P. H. The Phenix Software for Automated Determination of Macromolecular Structures. *Methods* **2011**, *55* (1), 94–106. https://doi.org/10.1016/j.ymeth.2011.07.005.
(31) Echols, N.; Grosse-Kunstleve, R. W.; Afonine, P. V.; Bunkóczi, G.; Chen, V. B.; Headd, J. J.; McCoy, A. J.; Moriarty, N. W.; Read, R. J.; Richardson, D. C.; Richardson, J. S.;

Terwilliger, T. C.; Adams, P. D. Graphical Tools for Macromolecular Crystallography in *PHENIX*. *J Appl Crystallogr* **2012**, *45* (3), 581–586. https://doi.org/10.1107/S0021889812017293.
(32) Emsley, P.; Cowtan, K. *Coot*: Model-Building Tools for Molecular Graphics. *Acta Crystallogr D Biol Crystallogr* **2004**, *60* (12), 2126–2132. https://doi.org/10.1107/S0907444904019158.
(33) Emsley, P.; Lohkamp, B.; Scott, W. G.; Cowtan, K. Features and Development of *Coot*. *Acta Crystallogr D Biol Crystallogr* **2010**, *66* (4), 486–501. https://doi.org/10.1107/S0907444910007493.
(34) Gable, J. A.; Poulos, T. L.; Follmer, A. H. Redox Partner Recognition and Selectivity of Cytochrome P450lin (CYP111A1). *Journal of Inorganic Biochemistry* **2023**, *244*, 112212. https://doi.org/10.1016/j.jinorgbio.2023.112212.

Chapter 5

Proximal Push of Proline in CYP158A2

Introduction

In previous chapters, I have shown the effector role of redox partner proteins on P450s and tested nonnative ferredoxins with various P450s and mutated both native and nonnative ferredoxins to interrogate their interface interactions. Despite the specific side chain interactions between the two proteins, the actual effect of redox partner binding extends beyond the interface into the active site affecting the heme pocket. Many experiments to probe the effector role of redox partner proteins have been carried out in the P450cam system with Pdx. In particular, a variant of P450cam was prepared, L358P, that replicates some of the spectral and structural effects observed upon redox partner binding.[1–5] Leu358 is the amino acid residue immediately following the cysteine ligated to the heme cofactor, and has been proposed to stabilize the negative charge on the sulfur with a hydrogen bond with the amide proton of Leu358. The change from leucine to proline results in a loss of this hydrogen bond since the proline residue does not have an amide proton. The L358P mutation in P450cam results in a similar “push effect” on the heme that was suggested to occur to P450cam in the presence of Pdx. Structural evidence for this push came from a recent crystal structure wherein cyanide-bound P450cam complexed with Pdx revealed a new rotomeric form for Leu358.[6] The sidechain of Leu358 is rotated by 90° with its δ-carbons making direct contact with the heme resulting in a distortion of the heme that is larger than what is observed in the L358P mutation (Figure 5-1). Therefore, Pdx exerts a “proximal push” on the heme that the L358P variant can somewhat replicate without the presence of redox partner. This new rotomer of Leu358 only occurs with cyanide bound, which can serve as a mimic for oxygen. Therefore, it is believed this state is catalytically relevant, at least for the oxycomplex, especially since Pdx binding and the L358P mutation decrease the stability of the oxycomplex. In

addition, the carbon monoxide complex of the L358P mutant mimics the changes that occur on the substrate binding side of the heme when oxygen binds, while carbon monoxide causes no such changes in structures of wild type P450cam.[3] These observations suggest that the proximal push effect is important for catalysis and is the primary focus of this chapter.

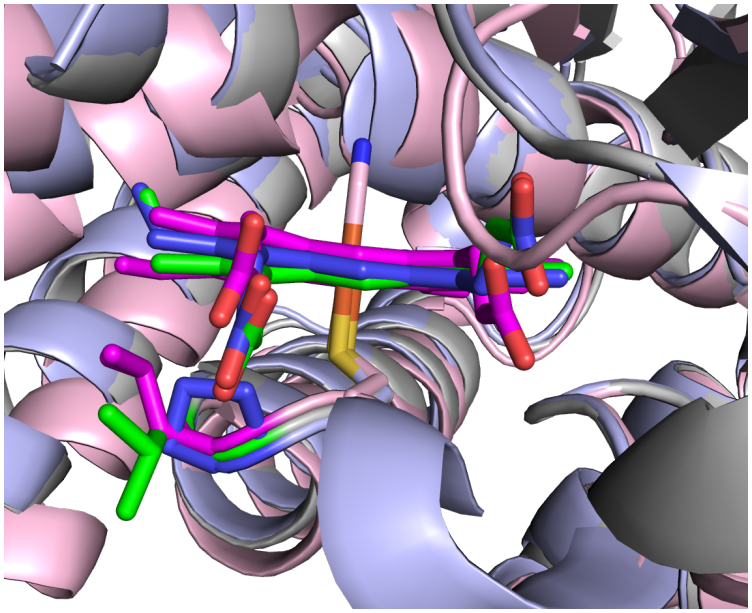

Figure 5-1. Proximal push in P450cam. Three structures of P450cam are aligned to show the push on the heme. The colors of the hemes match the side chain to which they correspond. P450cam WT backbone is shown in grey with Leu358 in green (PDB ID: 2CPP). P450cam L358P backbone is shown in periwinkle, with L358P in dark blue (PDB ID: 1T86). P450cam bound to cyanide and complexed to Pdx is shown in pink, with Leu358 shown in magenta (PDB ID: 6NBL).

Significant time and effort has gone into the isolation and characterization of the high-valent intermediates in the catalytic cycle, Compounds I and II.[7,8] When we look at the P450s initially utilized for the investigation of these intermediates, we find differences in the amino acid residues that follow the ligating cysteine. In CYP119, used to isolate and characterize Compound I, a Leu is present in the n+1 position similar to P450cam. However, CYP158A2, the P450 used for Compound II capture, a proline follows the ligating cysteine. In this regard, CYP158A2 is a naturally occurring mimic of “L358P”. Given that the generation of high-valent intermediates occurs with meta-chloroperoxybenzoic acid (mCPBA) in both P450 systems, we reasoned that

the resultant observed intermediates may be a consequence of the residue in this position. Therefore, this project has two aims: to mutate the leucine of CYP119 to proline and mutate the proline of CYP158A2 to leucine. With both of these changes, we will investigate the effect of the proline proximal push on the formation and stability of catalytic intermediates. In this chapter, I will discuss the preliminary results with CYP158A2.

CYP158A2 from *Streptomyces coelicolor* A3(2) is involved in the biosynthesis of red-brown pigments, which are predicted to protect the bacteria from physical harm, like UV damage.[9–11] This chemistry involves C-C bond formation between two or three molecules of the substrate, flaviolin, to form bi- or tri-flaviolin. Similar to P450cam and many other P450s, CYP158A2 undergoes a structural change from open to closed upon substrate binding, facilitating structural comparisons. Additionally, the intermediates investigated with CYP158A2 are the oxycomplex and Compound II.[8,11]

In this section, I will discuss our initial findings. I expressed and purified CYP158A2 WT and P354L and determined their crystal structures that provide evidence of the effect of the mutation on the heme. Additionally, UV-vis spectral data shows minor changes in the Soret. Finally, generation of Compound II in the P354L variant results in a slower rate of formation and less overall accumulation than WT. Our results support the hypothesis that the natural proline pushes on the heme relative to the P354L mutant, and that the proximal push affects the stability of the high valent intermediate, Compound II.

Results and Discussion

Crystal structures of substrate-free and substrate-bound CYP158A2 were solved to 1.88 and 2.20 Å resolutions, respectively. (Table 5-1). There were no changes to the overall fold of the P450, as expected (Figure 5-2A). Comparison of the P354L and WT substrate-free (SF) active

sites reveals that the leucine is pointed down and away from the heme, similar to what is observed in P450cam, resulting in a shift in the position of the heme compared to WT (Figure 5-1).

Table 5-1. Crystallographic data collection and refinement statistics of CYP158A2 P354L substrate-free (SF) and substrate-bound (SB).

	158A2 P354L SF	158A2 P354L SB
Resolution range	43.73 - 1.88 (1.947 - 1.88)	28.97 - 2.2 (2.279 - 2.2)
Space group	P 21 21 21	P 21 21 21
Unit cell	57.55 67.28 104.601 90 90 90	56.3 70.349 101.352 90 90 90
Total reflections	232968 (22982)	42072 (4069)
Unique reflections	33755 (3289)	21037 (2035)
Multiplicity	6.9 (7.0)	2.0 (2.0)
Completeness (%)	99.92 (99.85)	99.92 (99.80)
Mean I/sigma(I)	7.49 (4.18)	23.54 (9.83)
Wilson B-factor	13.81	15.57
R-merge	0.1744 (0.4018)	0.02484 (0.07632)
R-meas	0.1889 (0.4346)	0.03512 (0.1079)
R-pim	0.07139 (0.1638)	0.02484 (0.07632)
CC1/2	0.977 (0.913)	0.999 (0.968)
CC*	0.994 (0.977)	1 (0.992)
Reflections used in refinement	33738 (3288)	21037 (2035)
Reflections used for R-free	1677 (157)	1040 (116)
R-work	0.1569 (0.1819)	0.2162 (0.2543)
R-free	0.1940 (0.2493)	0.2615 (0.2706)
CC(work)	0.941 (0.626)	0.928 (0.744)
CC(free)	0.923 (0.700)	0.890 (0.737)

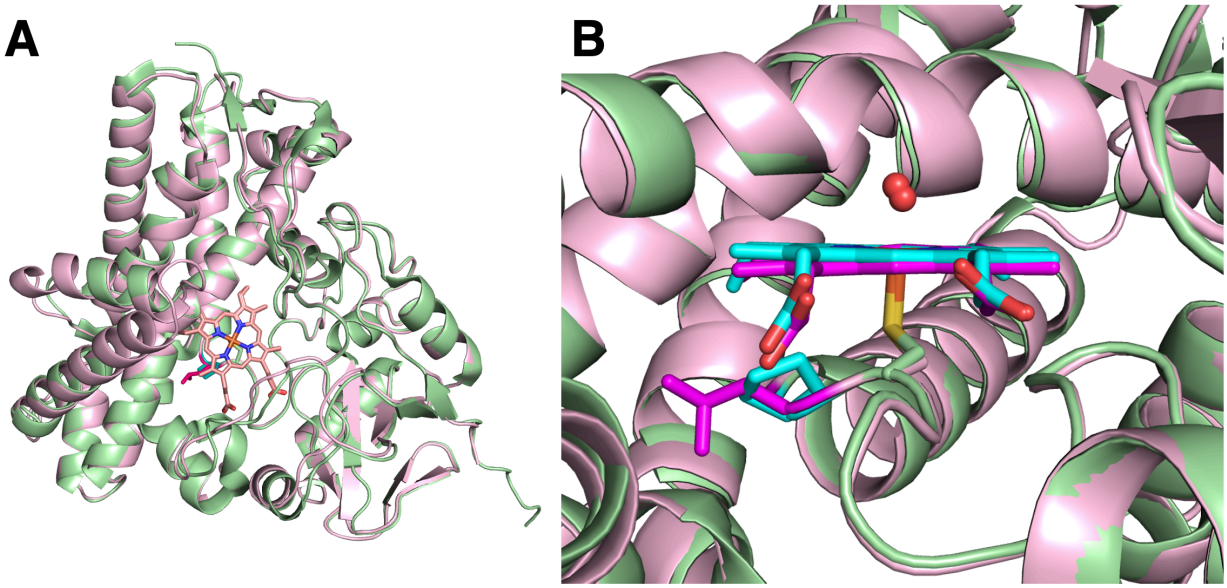

Figure 5-2. Crystal structure of 158A2 P354L substrate-free (SF). (A) Comparison of the overall structure of CYP158A2 WT (green) (PDB ID: 1SE6) and P354L (pink). (B) Comparison of the heme pocket of CYP158A2 WT and P354L. The WT proline is shown in cyan, and the mutant leucine is shown in magenta. The two red spheres are water molecules from the two structures.

The substrate-bound structure shows two molecules of substrate identical to the WT substrate-bound (SB) structure (Figure 5-3). The leucine from the P354L variant is still pointed down, similar to our SF P354L structure, but change in position of the heme is not as evident. The difference may be due to differences in resolution, as the WT structures are 1.5 Å, our P354L SF structure is 1.95 Å and our P354L SB structure is 2.20 Å. All further spectroscopic experiments are done in the absence of substrate, and we clearly see the change in the heme in the SF structure.

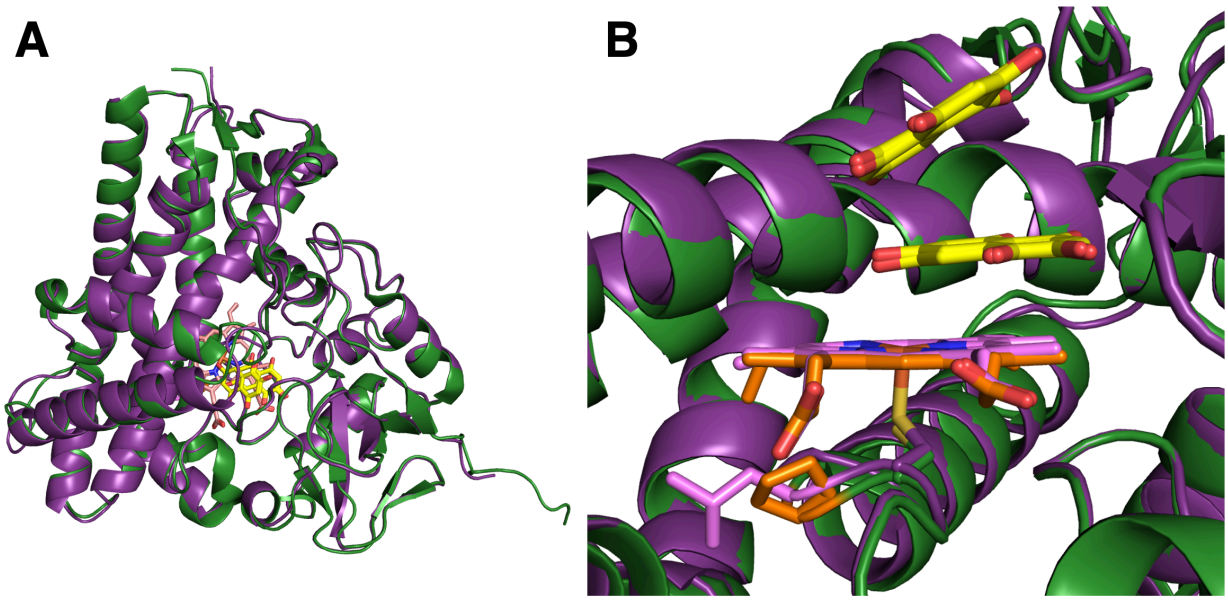

Figure 5-3. Crystal structure of 158A2 P354L substrate-bound (SB). (A) Comparison of the overall structure of CYP158A2 WT (dark green) (PDB ID: 1T93) and P354L (purple). (B) Comparison of the heme pocket of CYP158A2 WT and P354L. The WT proline is shown in orange, and the mutant leucine is shown in lilac. The two substrate molecules are shown in yellow.

The UV-vis spectra of CYP158A2 WT and P354L show small differences in the Soret and Q bands (Figure 5-4). The Soret maxima appear at 417 nm for WT and 416 nm for P354L. The ratios of the α/β bands are different as well: WT has a ratio of 1.01, and P354L has a ratio of 0.98. Additionally, the CO-bound spectra between the two variants have different λ_{max} of the Soret: WT is at 446 nm and P354L is at 449 nm. The differences observed in the UV-vis spectra support that the change in heme structure induced by the leucine mutation results in a change in electronic properties of the heme.

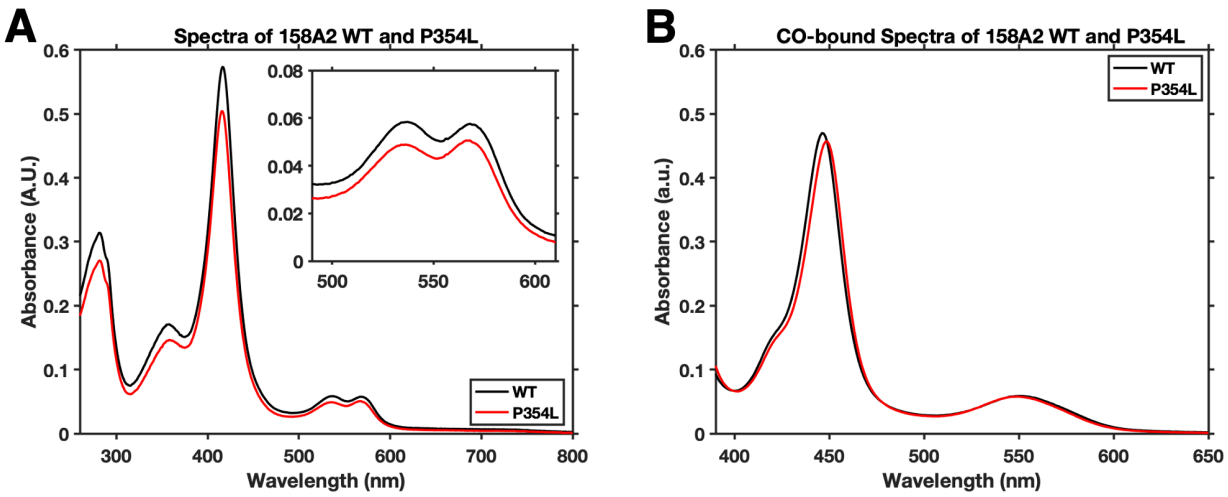

Figure 5-4. UV-vis spectra of CYP158A2 WT and P354L. (A) SF spectra of CYP158A2 WT (black) and P354L (red) in 50 mM KPi pH 7.4. The inset better shows the difference in the Q bands. (B) The CO-bound spectra of CYP158A2 WT (black) and P354L (red) in 50 mM KPi pH 7.4.

Given that the P354L mutation results in observable changes in the heme, as evidenced by the crystal structures and UV-vis spectra, we wanted to investigate whether these variations affect high valent intermediate formation. Compound II was generated for both 158A2 WT and P354L, following published procedures (Figure 5-5).[8] We found that Compound II formation is slowed by twofold in P354L compared to WT (Figure 5-6). This difference in the rate indicates that Pro354 stabilizes Compound II in CYP158A2. Additionally, the total accumulated amount of Compound II in the P354L variant is lower, as shown by the difference spectra. These data support the hypothesis that the proximal push of the proline influences the heme, and therefore affects the stability of the intermediates of the catalytic cycle.

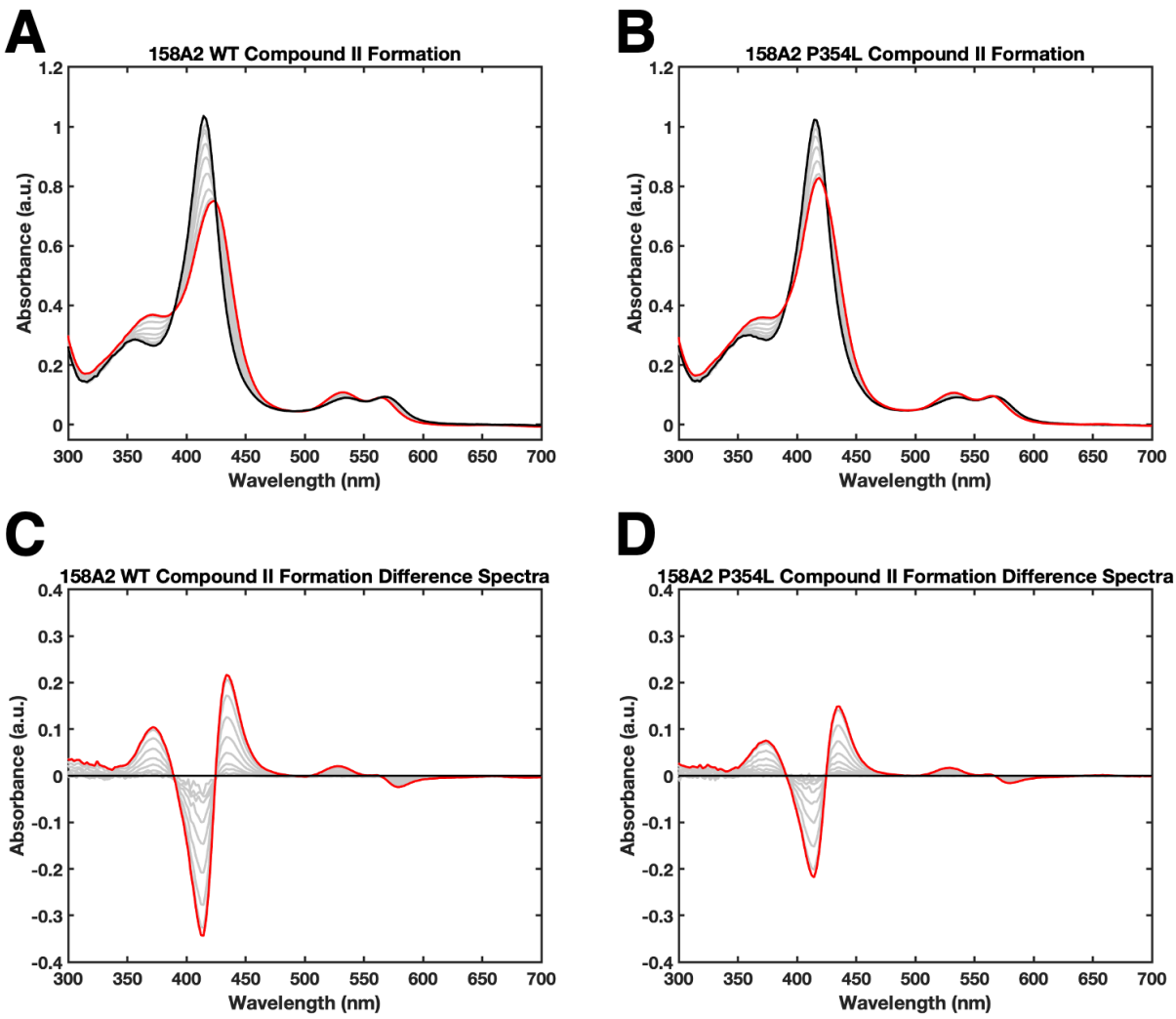

Figure 5-5. Generation of Compound II in CYP158A2. (A) UV-vis spectra of Compound II formation in CYP158A2 WT over 5 seconds. (B) UV-vis spectra of Compound II formation in CYP158A2 P354L over 10 seconds. (C) Difference spectra from the corresponding traces in (A). (D) Difference spectra from the corresponding traces in (B).

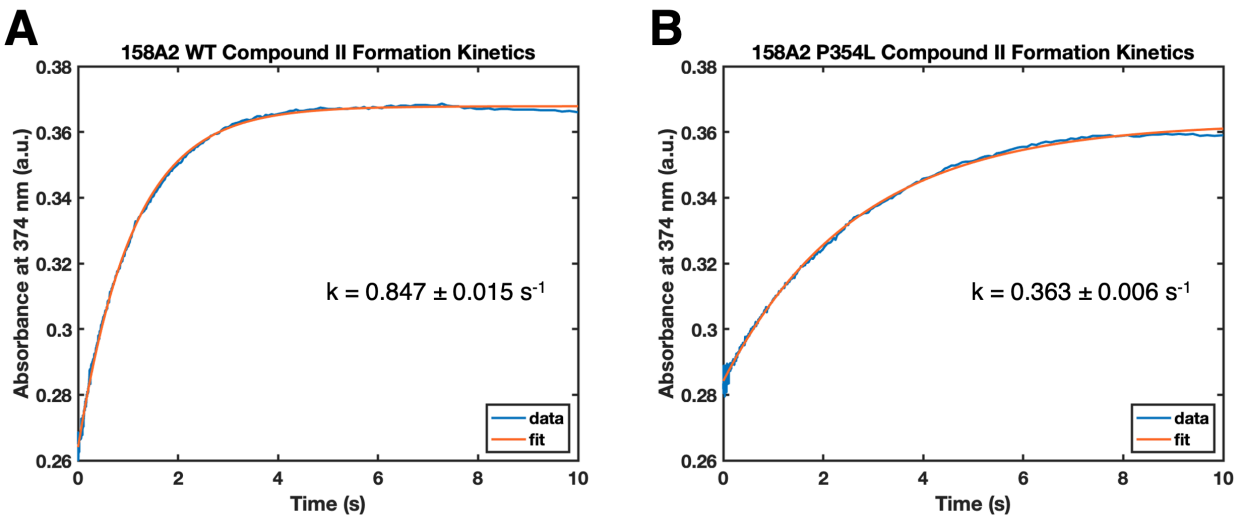

Figure 5-6. Kinetics of Compound II formation in CYP158A2. The data were fit to a single exponential from (A) 0.02 to 5 seconds in CYP158A2 WT and (B) 0.02 to 10 seconds in CYP158A2 P354L.

Future Goals

The next step is to test the decay of the oxycomplex of 158A2 WT and P354L. Since the oxycomplex is destabilized in P450cam L358P relative to P450cam WT, we predict that the mutation of P354L will stabilize the oxycomplex relative to the natural Pro354 CYP158A2. The published data for oxycomplex formation in CYP158A2 is in the presence of substrate, so we will try with and without substrate.

As mentioned in the introduction of this chapter, the other half of this project is analogous studies with CYP119, which was used to trap Compound I. CYP119 is similar to P450cam in that the residue following the ligating cysteine is leucine. Therefore, the mutation made is to proline, with L318P. The mutation of L318P has already been made, expressed and purified. Early experiments into Compound I formation are underway.

Materials and Methods

Protein Expression and Purification

CYP158A2 wild-type (WT) and P354L were encoded on a pET28a+ vector with N-terminal His6-tag (Genscript). The vector was transformed into *E. coli* C41(DE3) and plated onto Luria Broth (LB) plates containing 50 *μ*g/mL kanamycin. Single colonies of each variant were taken to inoculate 100 mL LB with 50 μg/ml kanamycin and grown overnight at 37°C, 220 rotations per minute (RPM). The following day, 10 mL of the overnight starter culture were inoculated into 1 L of Terrific Broth (TB) supplemented with 50 μg/mL kanamycin. Cultures were grown at 37°C and shaken at 220 RPM until the OD_{600} = 0.8 – 1. Expression was induced with 1 mM isopropyl β-d-1-thiogalactopyranoside (IPTG) and supplemented with 0.4 mM 5-aminolevulinic acid (D-ALA). The temperature was then decreased to 25° C. After 1 hour, the speed was decreased to 100 RPM and the cells were grown for 48 hours, harvested, and then lysed or frozen, if necessary.

Cells containing CYP158A2 were resuspended in lysis buffer (50 mM KPi pH 7.4, 250 mM NaCl, 2 mM β-mercaptoethanol) and stirred overnight at 4° C. Cells were lysed by two passes through a microfluidizer. The lysate was centrifuged for 1 hour at 15000 RPM at 4°C (Beckman Coulter Avanti JA-17). The supernatant was loaded on to a nickel column pre-equilibrated with lysis buffer (Thermo-Fisher HisPur Ni-NTA), washed with lysis buffer for 5 column volumes (CV), then washed with lysis buffer containing 15 mM imidazole for 5 CV. The protein was then eluted with lysis buffer containing 250 mM imidazole. Fractions exhibiting red color were collected, pooled, and then dialyzed against wash buffer (50 mM KPi 7.4, 2 mM BME). Protein was removed from the dialysis bag and loaded on to a pre-equilibrated Q Sepharose column (Cytiva). The column was washed with 5 CV of wash buffer followed by a gradient elution from 0 to 500 mM NaCl over

the course of 10 CV. Fractions with an optical purity ratio (Reinheitzahl, R/Z, A_{418}/A_{280}) > 1.8 were pooled and concentrated to < 2 mL. The protein was then loaded on to a pre-equilibrated size-exclusion chromatography column (SEC) (Cytiva Sephacryl S-200 HR) with SEC buffer (50 mM KPi pH 7.4, 150 mM NaCl, 5% glycerol). Fractions with R/Z > 2 were collected. Samples used for assays remained in SEC buffer. Samples used for crystallization were buffer exchanged into 20 mM Tris pH 7.5 in centrifugal filters (Millipore Amicon).

Protein Crystallization

Crystals were grown from the Index (Hampton) crystal screening condition (0.1 M Bis-Tris pH 6.5 and 25% v/v PEG 3350) at room temperature by hanging drop vapor diffusion. Crystals used for X-ray diffraction were grown by sitting drop vapor diffusion (2 μL:2 μL, protein:condition). Substrate-free protein (20 mg/mL in 20 mM Tris pH 7.4 RT) crystallized in plate clusters that appeared within a week. Substrate-bound protein was co-crystallized with 2 mM flaviolin, and the crystals were blocks that appeared in a few days. Mother liquor containing 25% glycerol was used as cryoprotectant. Data were collected at the Advanced Light Source synchrotron (ALS) for SF and on a home-source (Rigaku) for SB. Data were indexed, integrated, and scaled using Mosflm and Scala.[12] Molecular replacement (MR) was performed using PHASER[13,14] by applying the substrate-free P450terp (1CPT) as the MR model. Refinement was carried out in Phenix.refine[15,16] and COOT.[17,18]

UV-vis spectroscopy

All ultraviolet-visible (UV-vis) spectroscopy was performed on a Cary 300 spectrophotometer. The extinction coefficient used for 158A2 WT and P354L SF was ε_{416} = 100 $mM^{-1}cm^{-1}$.

Stopped-Flow Kinetics

Compound II in CYP158A2 was prepared as previously described, with the difference of a 50 mM KPi buffer and temperature of 5.5 C.[8]

References:

(1) Yoshioka, S.; Takahashi, S.; Ishimori, K.; Morishima, I. Roles of the Axial Push Effect in Cytochrome P450cam Studied with the Site-Directed Mutagenesis at the Heme Proximal Site. *Journal of Inorganic Biochemistry* **2000**, *81* (3), 141–151. https://doi.org/10.1016/S0162-0134(00)00097-0.

(2) Nagano, S.; Tosha, T.; Ishimori, K.; Morishima, I.; Poulos, T. L. Crystal Structure of the Cytochrome P450cam Mutant That Exhibits the Same Spectral Perturbations Induced by Putidaredoxin Binding. *Journal of Biological Chemistry* **2004**, *279* (41), 42844–42849. https://doi.org/10.1074/jbc.M404217200.

(3) Tosha, T.; Yoshioka, S.; Ishimori, K.; Morishima, I. L358P Mutation on Cytochrome P450cam Simulates Structural Changes upon Putidaredoxin Binding. *Journal of Biological Chemistry* **2004**, *279* (41), 42836–42843. https://doi.org/10.1074/jbc.M404216200.

(4) OuYang, B.; Pochapsky, S. S.; Pagani, G. M.; Pochapsky, T. C. Specific Effects of Potassium Ion Binding on Wild-Type and L358P Cytochrome P450cam. *Biochemistry* **2006**, *45* (48), 14379–14388. https://doi.org/10.1021/bi0617355.

(5) Karunakaran, V.; Denisov, I.; Sligar, S. G.; Champion, P. M. Investigation of the Low Frequency Dynamics of Heme Proteins: Native and Mutant Cytochrome P450 $_{cam}$ and Redox Partner Complexes. *J. Phys. Chem. B* **2011**, *115* (18), 5665–5677. https://doi.org/10.1021/jp112298y.

(6) Follmer, A. H.; Tripathi, S.; Poulos, T. L. Ligand and Redox Partner Binding Generates a New Conformational State in Cytochrome P450cam (CYP101A1). *J. Am. Chem. Soc.* **2019**, *141* (6), 2678–2683. https://doi.org/10.1021/jacs.8b13079.

(7) Rittle, J.; Green, M. T. Cytochrome P450 Compound I: Capture, Characterization, and C-H Bond Activation Kinetics. *Science* **2010**, *330* (6006), 933–937. https://doi.org/10.1126/science.1193478.

(8) Yosca, T. H.; Rittle, J.; Krest, C. M.; Onderko, E. L.; Silakov, A.; Calixto, J. C.; Behan, R. K.; Green, M. T. Iron(IV)Hydroxide p K_a and the Role of Thiolate Ligation in C–H Bond Activation by Cytochrome P450. *Science* **2013**, *342* (6160), 825–829. https://doi.org/10.1126/science.1244373.

(9) Cortés, J.; Velasco, J.; Foster, G.; Blackaby, A. P.; Rudd, B. A. M.; Wilkinson, B. Identification and Cloning of a Type III Polyketide Synthase Required for Diffusible Pigment Biosynthesis in Saccharopolyspora Erythraea‡: Biosynthesis of Diffusible Pigment in Saccharopolyspora Erythraea. *Molecular Microbiology* **2002**, *44* (5), 1213–1224. https://doi.org/10.1046/j.1365-2958.2002.02975.x.

(10) Zhao, B.; Guengerich, F. P.; Bellamine, A.; Lamb, D. C.; Izumikawa, M.; Lei, L.; Podust, L. M.; Sundaramoorthy, M.; Kalaitzis, J. A.; Reddy, L. M.; Kelly, S. L.; Moore, B. S.; Stec, D.; Voehler, M.; Falck, J. R.; Shimada, T.; Waterman, M. R. Binding of Two Flaviolin Substrate Molecules, Oxidative Coupling, and Crystal Structure of Streptomyces Coelicolor A3(2) Cytochrome P450 158A2. *Journal of Biological Chemistry* **2005**, *280* (12), 11599–11607. https://doi.org/10.1074/jbc.M410933200.

(11) Zhao, B.; Guengerich, F. P.; Voehler, M.; Waterman, M. R. Role of Active Site Water Molecules and Substrate Hydroxyl Groups in Oxygen Activation by Cytochrome P450 158A2. *Journal of Biological Chemistry* **2005**, *280* (51), 42188–42197. https://doi.org/10.1074/jbc.M509220200.
(12) Battye, T. G. G.; Kontogiannis, L.; Johnson, O.; Powell, H. R.; Leslie, A. G. W. *IMOSFLM*: A New Graphical Interface for Diffraction-Image Processing with *MOSFLM*. *Acta Crystallogr D Biol Crystallogr* **2011**, *67* (4), 271–281. https://doi.org/10.1107/S0907444910048675.
(13) McCoy, A. J. Solving Structures of Protein Complexes by Molecular Replacement with *Phaser*. *Acta Crystallogr D Biol Crystallogr* **2007**, *63* (1), 32–41. https://doi.org/10.1107/S0907444906045975.
(14) McCoy, A. J.; Grosse-Kunstleve, R. W.; Adams, P. D.; Winn, M. D.; Storoni, L. C.; Read, R. J. *Phaser* Crystallographic Software. *J Appl Crystallogr* **2007**, *40* (4), 658–674. https://doi.org/10.1107/S0021889807021206.
(15) Adams, P. D.; Afonine, P. V.; Bunkóczi, G.; Chen, V. B.; Echols, N.; Headd, J. J.; Hung, L.-W.; Jain, S.; Kapral, G. J.; Grosse Kunstleve, R. W.; McCoy, A. J.; Moriarty, N. W.; Oeffner, R. D.; Read, R. J.; Richardson, D. C.; Richardson, J. S.; Terwilliger, T. C.; Zwart, P. H. The Phenix Software for Automated Determination of Macromolecular Structures. *Methods* **2011**, *55* (1), 94–106. https://doi.org/10.1016/j.ymeth.2011.07.005.
(16) Echols, N.; Grosse-Kunstleve, R. W.; Afonine, P. V.; Bunkóczi, G.; Chen, V. B.; Headd, J. J.; McCoy, A. J.; Moriarty, N. W.; Read, R. J.; Richardson, D. C.; Richardson, J. S.; Terwilliger, T. C.; Adams, P. D. Graphical Tools for Macromolecular Crystallography in *PHENIX*. *J Appl Crystallogr* **2012**, *45* (3), 581–586. https://doi.org/10.1107/S0021889812017293.
(17) Emsley, P.; Cowtan, K. *Coot*: Model-Building Tools for Molecular Graphics. *Acta Crystallogr D Biol Crystallogr* **2004**, *60* (12), 2126–2132. https://doi.org/10.1107/S0907444904019158.
(18) Emsley, P.; Lohkamp, B.; Scott, W. G.; Cowtan, K. Features and Development of *Coot*. *Acta Crystallogr D Biol Crystallogr* **2010**, *66* (4), 486–501. https://doi.org/10.1107/S0907444910007493.

Chapter 6

Structural Insights on the Conversion of Cytochrome P450 to P420

Introduction

Cytochromes P450 (P450s) derive their name from the formation of the 450 nm Soret absorption band upon reduction and coordination of carbon monoxide (CO) to the ferrous heme iron.[1] This peak at 450 nm is unique among heme proteins where most other heme systems give a band at 420 nm upon CO ligation. This difference in Soret maxima has been attributed to the cysteine thiolate ligand that coordinates the protein to the heme iron in P450s, while other heme proteins are coordinated though a neutral ligand, such as histidine. However, harsh treatments of a P450 often result in a shift of the 450 nm reduced-CO band to 420 nm, which is associated with an inactivated or "damaged" P450, called P420.[2,3] Conversion of P420 back to P450 often is not possible. The origin of the molecular difference between P420 and P450 species has been attributed to protonation of the cysteine thiolate ligand,[4] complete dissociation of the cysteine ligand,[5] or replacement of the cysteine ligand by histidine.[5,6] Given that as little as a 0.2Å increase in S-Fe bond length[7] can lead to P420, the changes responsible for the change from P450 to P420 could be subtle, making determination of the molecular basis for inactivation challenging.

A crystal structure of a P420 would help to settle the question and, fortunately, such structures have been solved: a P450cam-Pdx complex structure and the open form of P450cam without substrate. Sarvind *et. al.*[8] solved the crystal structure of P450cam complexed to its ferredoxin Fe_2S_2 redox partner, putidaredoxin (Pdx). In order to trap the complex, a crosslinking approach was used where engineered cysteine residues were crosslinked with a homo-bifunctional maleimide. Where to place the cysteine residues to be crosslinked required some knowledge on the orientation of Pdx relative to P450cam. A model of the P450cam-Pdx complex derived from mutagenesis and NMR studies was used as a guide.[9] The resulting structure (called

complex1, PDB code: 4JWS) unexpectedly showed that His355 in P450cam crosslinked with Cys73 in Pdx (Figure 6-1). The reason His355 was crosslinked rather than the engineered cysteine residue is because Pdx in the crystal structure was oriented quite differently than the model used to engineer the crosslinking sites.

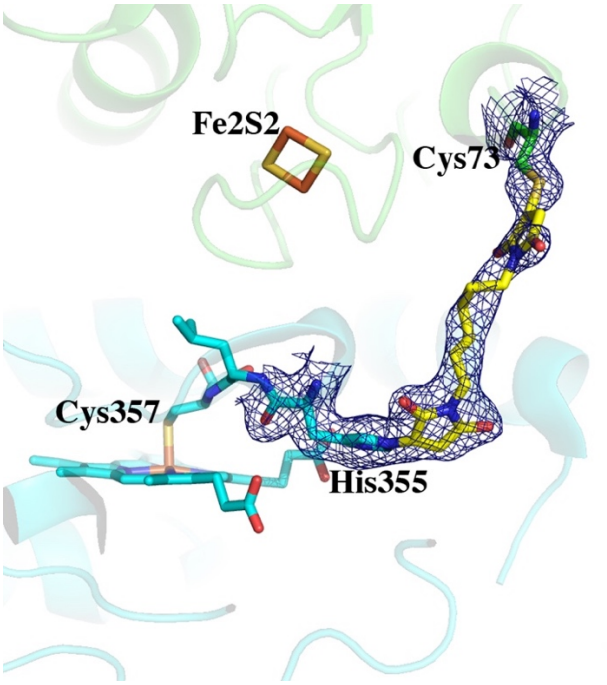

Figure 6-1. Crystal structure of the P450cam (cyan)-Pdx (green) complex1 (PDB code: 4JWS). The 2.15Å $2F_O$-F_C map is contoured at 1.0 σ. His355 in P450cam crosslinks to Cys73 in Pdx by the homo bifunctional maleimide (yellow). Very little movement of His355 is required to form the crosslink.

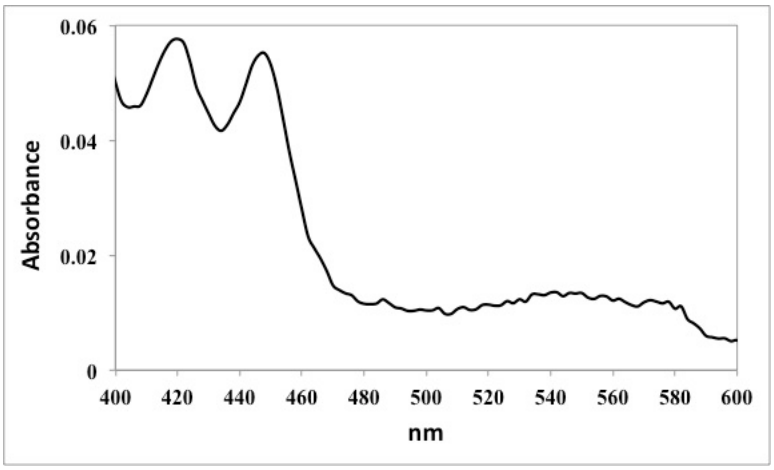

Figure 6-2. P450cam-Pdx complex1 bound to carbon monoxide. P450cam-Pdx complex1 was reduced with sodium dithionite followed by treatment with carbon monoxide. The spectrum clearly indicates a large fraction of P420.

The UV/Vis spectrum of the reduced-CO complex of complex1 clearly shows a large fraction of the crosslinked complex is P420 (Figure 6-2). At the time, there was concern that owing to the large amount of P420, the complex1 P450cam-Pdx structure does not reflect the active form of the enzyme. Therefore, cysteine residues were engineered that would place the crosslink far from the heme and avoid crosslinking His355. The resulting 2.09 Å crystal structure (PDB code: 4JWU), called complex2, shows that the engineered cysteine residues crosslinked as expected and the reduced-CO spectrum of complex2 is fully P450.[8] Although complex1 and complex2 have different crosslinking sites, Pdx binds the same in both complexes, but there are major differences in the P450. In complex2, the entire polypeptide is visible and well-ordered. Additionally, a molecule of product, 5-*exo*-hydroxycamphor, is bound in the active site, presumably because X-ray generated reducing equivalents drives O_2 activation and substrate hydroxylation *in crystallo*. However, in complex1, which gives a split P450 and P420 spectrum, the B' helix (residues 91-101) and part of the F/G loop (residues 187-188) are disordered and other helical segments such as the F, G, and I helices are displaced such that the active site is

more open (Figure 6-3). In addition, there is ill-defined density in the heme pocket that could be disordered substrate or product.

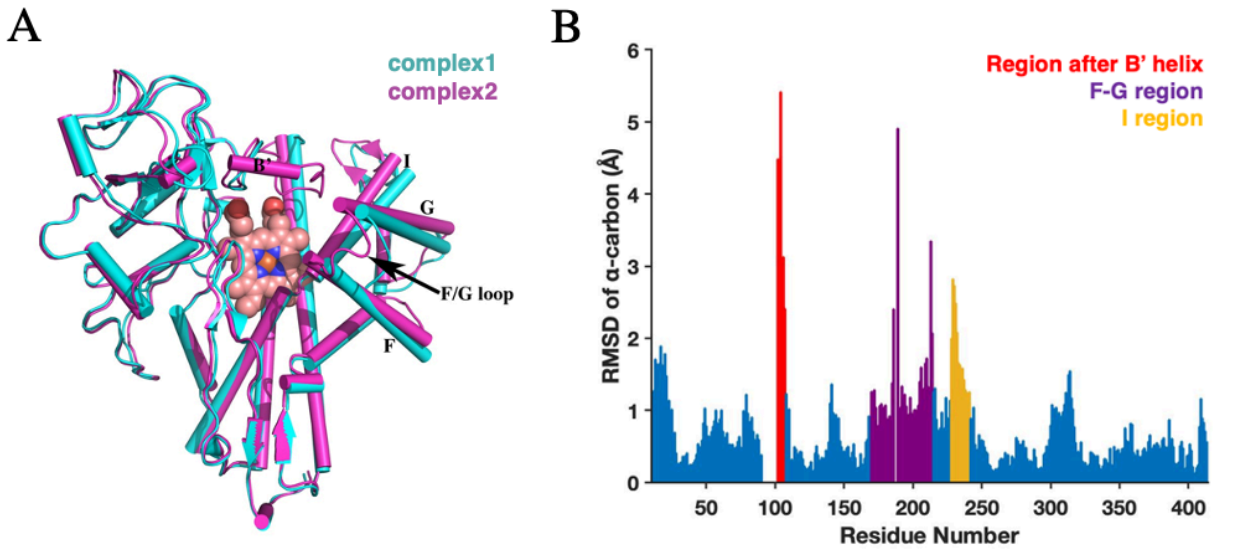

Figure 6-3. Comparison of complex1 and complex2. (A) Structural comparison of complex1 (P420, cyan) and complex2 (P450, magenta). (B) A plot of α-carbon RMSD between complex1 and complex2 vs. residue number. Regions of large changes are highlighted. The B' helix is disordered in complex1 and the F and G helices are displaced further from the main body of the protein. This displacement provides a wider opening to the active site. Part of the I helix, which runs over the surface of the heme and provides key residues for substrate binding and O_2 activation, also is displaced.

Similarly, the structure of P450cam crystallized in the absence of substrate has an active site that is partially disordered and open. This open form of P450cam also generates a large fraction of P420.[10] However, at a nominal resolution of ~2 Å, the heme and thiolate ligand environment are identical in complex1, complex2, and the open form of P450cam crystallized in the absence of substrate. These results show that P420 can be generated without ligand swapping or displacement of the cysteine thiolate ligand. In addition, treatment of P450cam with the well-known histidine modifying reagent, diethylpyrocabonate, actually promotes P420 formation suggesting that histidine ligation is not a requirement for P420 formation.[3] However,

such chemical modification results can be difficult to interpret owing to the possibility of incomplete histidine modification and/or modification of other residues. It thus remains a possibility that in some cases a switch to histidine ligand from the cysteine ligand may occur in the interconversion of P450 to P420 species. To test this possibility, we identified the three top candidates for heme ligation in P450cam as His352, 355, and 361 (Figure 6-4). We then converted these residues to glutamine to determine if the variant would still form P420. Notably, His355 is the closest to the heme (Figure 6-1) and is the most likely candidate as a P420 ligand.[6]

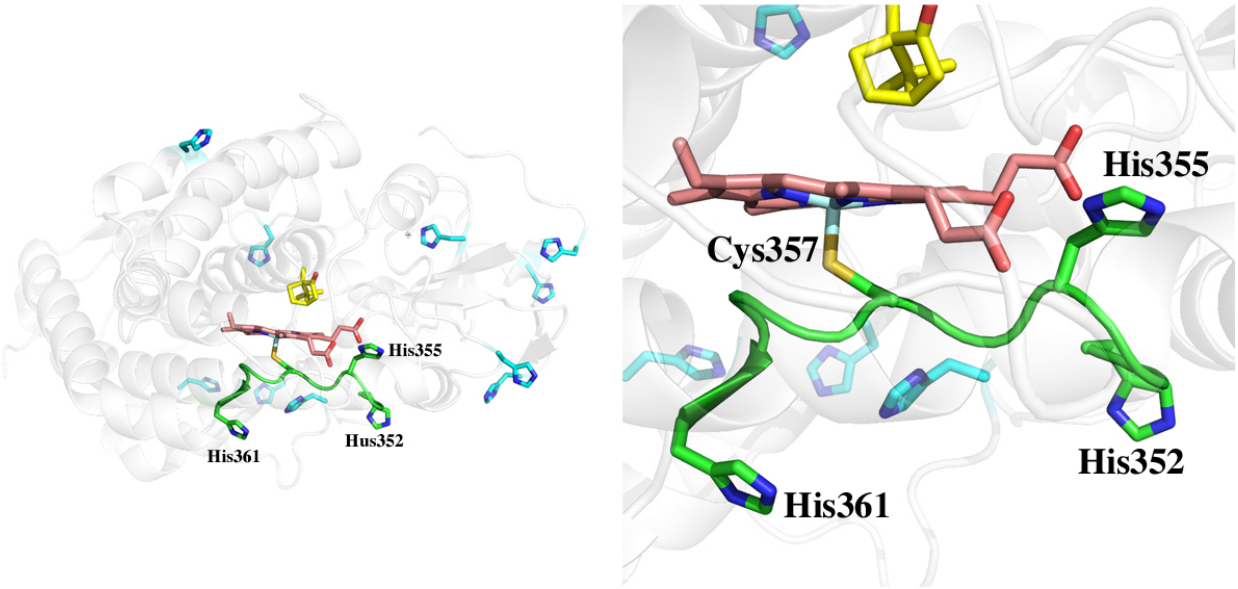

Figure 6-4. P450cam histidine residues. Location of all the histidine residues in P450cam, colored aqua. The 3 most likely candidates to switch with the cysteine ligand are His352, His355, or His 361, colored green. These histidine residues are all on the same segment of polypeptide that is not associated with any regular secondary structure and could conceivably rearrange to enable histidine coordination without too much disruption of helices or sheets. The heme is shown in pink, and the substrate, camphor, is shown in yellow.

Results and Discussion

There are 3 histidine residues on the proximal side of the heme that are the most likely candidates for a heme ligand (Figure 6-4). The H352Q/H355Q/H361Q triple variant was generated and found to exhibit a complete conversion to P420 upon reduction and incubation with

CO, while both WT and a H352Q/H361Q double variant yield complete formation of the expected 450 nm Soret band Figure 6-5(A). Treatment of WT and the double variant with acetone induces the formation of P420, ruling out the role of His352 and His361 in P420 formation Figure 6-5(B).

This lack of alteration in the spectra is not surprising given that both histidine residues are oriented toward the surface and play no direct role in stabilizing the active site (Figure 6-4). In contrast, His355 plays a significant role, as His355 forms hydrogen bonds with one of the heme propionates directly stabilizing the heme. The single variant of H355Q was not investigated in this work, but presumably it would display the same P420 results as the triple variant, as it is the only difference between the triple and double variants.

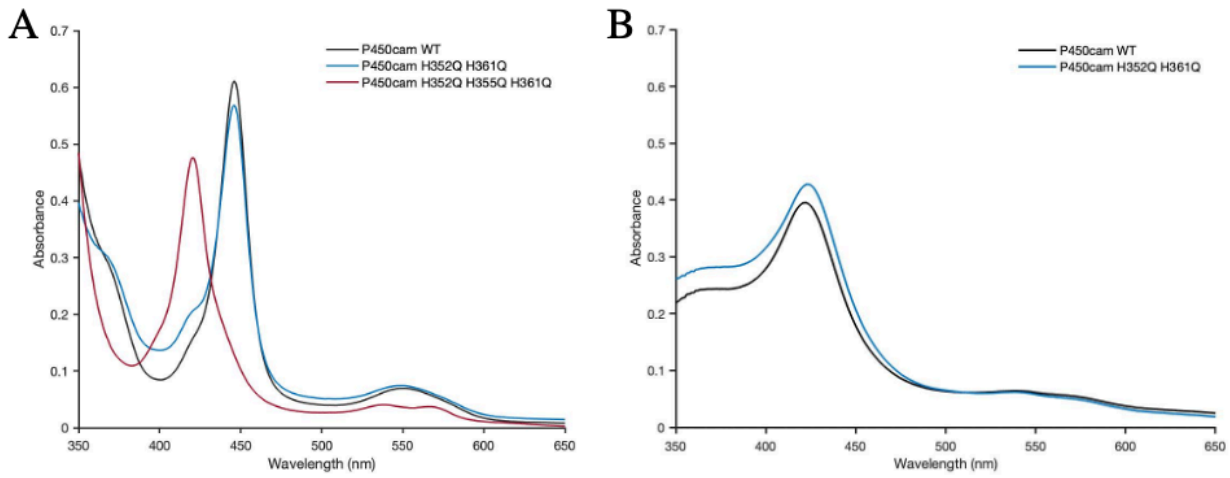

Figure 6-5. UV-vis spectrum of P450cam WT and variants in the reduced-CO form. (A) Wild type, double, and triple variants. (B) Acetone induced conversion to P420.

The generation of P420 with the alteration of His355 in P450cam WT is consistent with the complex1 crystal structure, where the His355-heme interaction is disrupted in the crosslink between His355 and Pdx, and complex1 generates a large fraction of P420. These results also clearly show that a switch from cysteine to histidine ligation is not a requirement for the P450-to-P420 conversion. Instead, the disruption of the heme pocket as evidenced in the complex1 crystal structure is the more likely reason for P420. The hypothesis that P420 is associated with a

disordered, more open active site structure is evidenced by the fact that substrate binding results in no spin shift and that CO can more readily escape the P420cam active site.[11] The crystal structures of complex1, substrate-free P450cam,[11] and P450cam-Pdx complex2 with cyanide bound (PDB code: 6NBL)[12] all show a rather dramatic restructuring around the substrate binding pocket with very little change around the cysteine ligand. Even though the results presented here indicate that ligand swapping is an unlikely reason for the P450-to-P420 switch, the results do not disprove this possibility.[5,6] Such a switch, however, would require an energetically expensive major restructuring of the proximal pocket secondary structure and breakage of an S-Fe bond. A majority of structural and biochemical data favor changes in the substrate binding pocket and not major changes in cysteine ligation that are detectable in ~ 2Å crystal structures as the source of the P450-to-P420 conversion.

Conclusion

The results presented here demonstrate that a ligand swapping of cysteine for histidine in P450cam is not necessary for conversion to P420. Instead, structural disruption of the heme pocket is the more likely cause of the shift in the spectrum where disorder can be caused by a number of alterations. Historical reasoning for P420 focused on possible changes to the cysteine ligand, as that ligand was the principal difference between P450s and previously characterized heme proteins that generate P420 with a histidine ligand. Our work presented here shows that protein scaffolds, not just ligation, can control the electronic structures of their cofactors. The presence of P420 or P450 therefore provides a good test to see if P450 enzymes have properly structured heme pocket for catalysis and further experiments.

Methods and Materials

The P450cam WT and triple mutant genes were ordered in pET28a vectors from Genscript. The triple variant (His352, 355, and 361 to Gln) gene was used as a template for generation of the double variant gene by restoring Gln355 to His355 using the Takara PrimeSTAR Max DNA Polymerase kit for PCR. All three proteins followed the same expression and purification steps. The protein was overexpressed in *E. coli* C41 cells in TB media. Protein production was induced with 1mM IPTG at an OD_{600}= 0.8-1.0, and the cells were grown at 25 °C and 80 RPM for 48 hours. The cells were harvested and resuspended in lysis buffer (50 mM KPi pH 7.4, 1 mM camphor, 250 mM NaCl, and 2 mM β-mercaptoethanol (BME)) and lysed through a microfluidizer. The protein was loaded onto a HisPur™ Ni-NTA Resin (Thermo Scientific) column and washed with 3-5 column volumes of lysis buffer, which was followed by elution with 250 mM imidazole in lysis buffer. The protein was then dialyzed against 50 mM KPi pH 7.4, 8 mM camphor (saturated), 250 mM NaCl, and 2 mM BME. The N-terminal 6-His-tag was cleaved with thrombin. The proteins were loaded back onto an Ni-NTA column to collect the His-tag cleaved sample in the flow through. The protein was dialyzed against 50 mM KPi pH 7.4, 8 mM camphor (saturated), and 5 mM BME. The protein was loaded onto a Q Sepharose (Cytiva) column and eluted with a gradient of 0-500 mM NaCl in 50 mM KPi pH 7.4, 1 mM camphor, and 5 mM BME. Finally, the protein was run on a size exclusion (S-200) chromatography (Cytiva) column in 50 mM KPi pH 7.4, 1 mM camphor, 150 mM NaCl, and 5 mM BME. The protein was concentrated, flash-frozen, and stored at -80 °C. The P450 to P420 conversion was induced by the addition of 30% v/v acetone.[10]

All UV-visible spectroscopy was performed with an Agilent Cary 300 spectrophotometer at room temperature. The following protocol was used for all three P450cam proteins. The buffer was 50 mM KPi pH 7.4 and 1 mM camphor, and had CO bubbled in the buffer for 5-10 seconds. The

protein was added to a final concentration of ~6 μM. A few granules of dithionite powder were added to the cuvette, and the solution was inverted for mixing. The P450/P420 peaks appeared immediately, and reached a maximum after ~10 min.

References:

(1) Omura, T.; Sato, R. A New Cytochrome in Liver Microsomes. *Journal of Biological Chemistry* **1962**, *237* (4), PC1375–PC1376. https://doi.org/10.1016/S0021-9258(18)60338-2.

(2) Martinis, S. A.; Blanke, S. R.; Hager, L. P.; Sligar, S. G.; Hui Bon Hoa, G.; Rux, J. J.; Dawson, J. H. Probing the Heme Iron Coordination Structure of Pressure-Induced Cytochrome P420 $_{cam}$. *Biochemistry* **1996**, *35* (46), 14530–14536. https://doi.org/10.1021/bi961511u.

(3) Lipscomb, J. D. Electron Paramagnetic Resonance Detectable States of Cytochrome P-450cam. *Biochemistry* **1980**, *19* (15), 3590–3599. https://doi.org/10.1021/bi00556a027.

(4) Perera, R.; Sono, M.; Sigman, J. A.; Pfister, T. D.; Lu, Y.; Dawson, J. H. Neutral Thiol as a Proximal Ligand to Ferrous Heme Iron: Implications for Heme Proteins That Lose Cysteine Thiolate Ligation on Reduction. *Proc. Natl. Acad. Sci. U.S.A.* **2003**, *100* (7), 3641–3646. https://doi.org/10.1073/pnas.0737142100.

(5) Wells, A. V.; Li, P.; Champion, P. M.; Martinis, S. A.; Sligar, S. G. Resonance Raman Investigations of Escherichia Coli-Expressed Pseudomonas Putida Cytochrome P450 and P420. *Biochemistry* **1992**, *31* (18), 4384–4393. https://doi.org/10.1021/bi00133a002.

(6) Sun, Y.; Zeng, W.; Benabbas, A.; Ye, X.; Denisov, I.; Sligar, S. G.; Du, J.; Dawson, J. H.; Champion, P. M. Investigations of Heme Ligation and Ligand Switching in Cytochromes P450 and P420. *Biochemistry* **2013**, *52* (34), 5941–5951. https://doi.org/10.1021/bi400541v.

(7) Jung, C.; Friedrich, J.; Ristau, O. Quantum Chemical Interpretation of the Spectral Properties of the CO and O2 Complexes of Hemoglobin and Cytochrome P-450. *Acta Biol Med Ger* **1979**, *38* (2–3), 363–377.

(8) Tripathi, S.; Li, H.; Poulos, T. L. Structural Basis for Effector Control and Redox Partner Recognition in Cytochrome P450. *Science* **2013**, *340* (6137), 1227–1230. https://doi.org/10.1126/science.1235797.

(9) Pochapsky, T. C.; Lyons, T. A.; Kazanis, S.; Arakaki, T.; Ratnaswamy, G. A Structure-Based Model for Cytochrome P450cam-Putidaredoxin Interactions. *Biochimie* **1996**, *78* (8–9), 723–733. https://doi.org/10.1016/S0300-9084(97)82530-8.

(10) Lee, Y.-T.; Wilson, R. F.; Rupniewski, I.; Goodin, D. B. P450cam Visits an Open Conformation in the Absence of Substrate ›. *Biochemistry* **2010**, *49* (16), 3412–3419. https://doi.org/10.1021/bi100183g.

(11) Tian, W. D.; Wells, A. V.; Champion, P. M.; Primo, C. D.; Gerber, N.; Sligar, S. G. Measurements of CO Geminate Recombination in Cytochromes P450 and P420. *Journal of Biological Chemistry* **1995**, *270* (15), 8673–8679. https://doi.org/10.1074/jbc.270.15.8673.

(12) Follmer, A. H.; Tripathi, S.; Poulos, T. L. Ligand and Redox Partner Binding Generates a New Conformational State in Cytochrome P450cam (CYP101A1). *J. Am. Chem. Soc.* **2019**, *141* (6), 2678–2683. https://doi.org/10.1021/jacs.8b13079.

Chapter 7

Conclusion

Together the chapters presented in my thesis have addressed a few of the ways in which the catalytic cycle of cytochromes P450 is regulated. As discussed in chapter 1, our goal is to expand our knowledge of the regulation of the catalytic cycle of P450s, starting with P450cam and expanding into the most similar bacterial systems in order to better understand if what we have learned about P450cam is shared by these other bacterial P450 systems. Surprisingly, we found that these other P450s, namely P450terp and P450lin, behave quite differently than P450cam and exhibit unique structural and mechanistic features. The differences underscore that even the “simplest” bacterial P450s can exhibit unexpectedly complex structural and mechanistic properties.

In Chapter 2, we found that P450terp demonstrates positive homotropic allostery in a Class I bacterial P450 with its natural substrate. P450terp does not adopt a closed conformation in the presence of substrate, unlike P450cam. Additionally, the crystal structure revealed that there are two molecules of substrate bound in the active site. Through substrate binding assays and NADH coupling experiments, it was shown that the second binding site is necessary for binding of substrate in the first binding site and for high coupling efficiency. The dependence of P450terp for two molecules of substrate is similar to CYP3A4, a human P450 that has been heavily studied. CYP3A4 serves a very different biological function, but the impact of different substrates on binding and catalysis has been an ongoing area of research. Given our new information about P450terp, we wondered to what extent are these substrate-driven regulations general across P450s as a whole, and not necessarily beholden to the divide between mammalian and bacterial P450s. In fact, we have observed two molecules in a bacterial P450 before under specific circumstances – in P450cam in the presence of Pdx. So, despite the many differences

between these bacterial P450s, the binding of more than one substrate may be a more general feature shared by bacterial P450.

We explored the effector role of redox partner proteins on P450s in Chapters 3 and 4. Both P450lin and P450terp are *Pseudomonad* P450s that have the same biological function in *Pseudomonad* bacteria, so we expected the specificity of each P450 for its ferredoxin redox partner to remain similar to P450cam. However, both P450lin and P450terp are able to turnover substrate with a foreign ferredoxin redox partner, and mutations to existing ferredoxins show differing degrees of change in turnover rate. Clearly, the interactions between each P450 and each ferredoxin are nuanced. Even though all ferredoxins presumably bind to the proximal side of the P450, the individual residues that dictate specific orientation are not universally important. Despite the surprising promiscuity of P450lin and P450terp toward a protein redox partner, there is a unifying theme of the effect of redox partner binding on decay of the oxycomplex. In all P450s studied thus far, redox partner proteins that can enable turnover, increase the decay rate of the oxycomplex in the P450. Beyond the simple association of ferredoxin and P450 to transfer an electron, there is a structural change in the P450 that results in destabilization of the oxycomplex. Since this effect has been consistent, it is thus tempting to suggest that redox partner binding is important in catalysis, beyond delivery of the electron.

To further investigate structural impacts on the heme, we looked at preliminary data of a proximal push in CYP158A2 in Chapter 5. This work was inspired by the mutation of L358P in P450cam, wherein the mutation of the leucine residue following the ligating cysteine residue to a proline shares some of the effects that only arise upon Pdx binding with P450cam. The idea is that Pdx exerts a “proximal push” on the P450 heme, and that the proline mutation mimics a similar push in the absence of redox partner. In this chapter, we looked at CYP158A2, which naturally contains a proline following the ligating cysteine. So far, our preliminary data shows that mutation of this proline to a leucine slows formation of Compound II and lowers the total

accumulation of Compound II. This is the first direct proof of a proximal push impacting a high-valent intermediate in the P450 catalytic cycle. We aim to further this research by testing CYP119, and investigating the role of the proximal push on Compound I.

In Chapter 6, the origin of the P420 species was investigated in P450cam. Historically, the differences between heme proteins that have a Soret at 450 or 420 is due to the differences of a cysteine or histidine ligand, respectively. Damage of a P450 protein can result in a P420 species, that is often considered inactive. Much research has gone into determination of this damaged species, with the focus being on alteration of the ligating residue to the heme. However, we posit a more nuanced explanation, and suggest that the cysteine residue need not be altered to produce a P420 species. Mutation of potentially ligating histidine residues to glutamine demonstrate that conversion to P420 does not require histidine ligation.

We often remark in the lab that P450s are the best to work with – for their beautiful, identifiable color and their relative stability and ease of purification. In short, P450s are rocks. Despite the ease of expression and purification, P450s during catalysis are anything but stagnant and unchanging. They display many forms of regulation and structural changes in a delicate balance for correctly controlling the powerful chemistry at the heart of the enzyme.